#### **INFORMATION TO USERS**

This manuscript has been reproduced from the microfilm master. UMI films the text directly from the original or copy submitted. Thus, some thesis and dissertation copies are in typewriter face, while others may be from any type of computer printer.

The quality of this reproduction is dependent upon the quality of the copy submitted. Broken or indistinct print, colored or poor quality illustrations and photographs, print bleedthrough, substandard margins, and improper alignment can adversely affect reproduction.

In the unlikely event that the author did not send UMI a complete manuscript and there are missing pages, these will be noted. Also, if unauthorized copyright material had to be removed, a note will indicate the deletion.

Oversize materials (e.g., maps, drawings, charts) are reproduced by sectioning the original, beginning at the upper left-hand comer and continuing from left to right in equal sections with small overlaps.

ProQuest Information and Learning 300 North Zeeb Road, Ann Arbor, MI 48106-1346 USA 800-521-0600



# The Transport of Radioactive Ions in a Gas Filled Radio Frequency Quadrupole Mass Filter System

by

Chantal Boudreau

A thesis submitted to the Faculty of Graduate Studies and Research in partial fulfillment of the requirements for the degree of Master of Science

Physics Department McGill University, Montreal, PQ ©August 14, 2001



National Library of Canada

Acquisitions and Bibliographic Services

395 Wellington Street Ottawa ON K1A 0N4 Canada Bibliothèque nationale du Canada

Acquisitions et services bibliographiques

395, rue Wellington Ottawa ON K1A 0N4 Ceneda

Your file Value nitionnal

Our life Natre référence

The author has granted a non-exclusive licence allowing the National Library of Canada to reproduce, loan, distribute or sell copies of this thesis in microform, paper or electronic formats.

The author retains ownership of the copyright in this thesis. Neither the thesis nor substantial extracts from it may be printed or otherwise reproduced without the author's permission.

L'auteur a accordé une licence non exclusive permettant à la Bibliothèque nationale du Canada de reproduire, prêter, distribuer ou vendre des copies de cette thèse sous la forme de microfiche/film, de reproduction sur papier ou sur format électronique.

L'auteur conserve la propriété du droit d'auteur qui protège cette thèse. Ni la thèse ni des extraits substantiels de celle-ci ne doivent être imprimés ou autrement reproduits sans son autorisation.

0-612-75289-5



To my parents, for their love and support.

#### 0.1 Abstract

The technique of ion transfer in radio frequency quadrupole (RFQ) systems is described. Computer simulations of the gas filled RFQ mass filter system located at Argonne National Laboratory (ANL) in Argonne, II. are performed and compared to data obtained from the transfer of radioactive ions produced from the fragmentation of an off-line <sup>252</sup>Cf fission source put before the system. The device is used to transport radionuclides created in on-line fusion evaporation reactions from a 150 torr helium filled gas cell to a high vacuum mass spectrometer. Operation parameters and performance results for the gas filled RFQ mass filter system are presented. In addition, the first on-line transfer of a radioisotope resulting in a precise mass measurement using the Canadian Penning Trap (CPT) mass spectrometer is discussed.

## 0.2 Résumé

Les techniques utilisées pour le transfer des ions dans un système quadrupolaire à radio-fréquences (RFQ) sont décrites. Des simulations par ordinateur du système de filtre de masse RFQ opéré avec gaz situé au Argonne National Laboratory (ANL) à Argonne, Il. sont produites et comparées aux données obtenues du transfer d'ions radioactifs provenant de la fissure d'une source de <sup>252</sup>Cf hors-ligne mise au début du système. L'appareil est utilisé pour transporter des produits radioactifs, créés dans une réaction d'évaporation de fusion, d'une cellule à gaz remplie de 150 torr d'helium jusqu'au spectromètre de masse operant à très basse pression. Les conditions d'opérations et les résultats de la performance du système de filtre de masse RFQ sont présentés. En plus, les premiers transfers en-ligne de radioisotopes résultant en la mesure précise de leurs masses avec l'aide du spectromètre de masse du Canadian Penning Trap (CPT) sont discutés.

## **0.3** Acknowledgements

I would like to sincerely thank my supervisor Jonathan P. K. Lee for his guidance, help, and patience during the course of this thesis. I am grateful for the long hours he spent reading many earlier versions of the thesis and the advice he gave me to transform it into its final readable version.

Special thanks should be given to Guy Savard at ANL. Without his help, much of this work wouldn't have been possible. I would also like to thank him for generously letting me use his office computer and parts of his simulation program, as well as for his advice on experimental and simulation procedures and thesis writing.

I would like to thank Sid Gulick for his help and suggestions throughout my stay at McGill University and for proof reading the thesis.

My research at ANL was made much more easy and enjoyable due to the help and advice of all the project's collaborators that often came to the lab to help during experimental runs. Here I thank Fritz Buchinger, John Crawford, Kumar Sharma, and Gene Sprouse. I also wish to thank the graduate and summer students that were present during my stay at ANL; Andrew Cassidy, Jason Clark, Jeff Fingler, Hiroshi Fukutani, Michael Maier, Christian Trempe, and Joe Vaz. Their help and support was more than essential to me on both scientific and personal levels.

Many thanks to all the ANL post-docs and staff members who were always more than willing to lend a hand.

Finally, I would like to thank my family for their ongoing support and to my friends, for not letting me forget that there is life outside the lab.

# **Table of Contents**

	0.1 Abstract	ii
	0.2 Résumé	iii
	0.3 Acknowledgements	iv
1	Introduction	1
2	Theory of RFQ Devices	4
	2.1 The Quadrupole Field	. <b>4</b>
	2.1.1 The Mass Filter	. 5
	2.1.2 The Resolution of a Mass Filter	10
	2.1.3 The Addition of Gas to the RFQ Mass Filter System	.11
	2.1.4 Guiding, Bunching and Ejecting Ions in a Gas Filled RFQ System	. 13
3	Experimental Apparatus	15
	3.1 The ATLAS Facility	15
	3.2 The Experimental Set-up.	16
	3.2.1 The Enge Split-Pole Magnetic Spectrograph	.18
	3.2.2 The Gas Cell	19
	3.2.3 The RFQ Mass Filter System	21
	3.2.4 The Transfer Section	21
	3.2.5 The CPT Mass Spectrometer	22
	3.3 The Gas Filled RFO Mass Filter System	24

	3.3.1	Structure and Vacuum System	.24
	3.3.2	Electrical Components of RFQ Mass Filter System	. 26
	3.4 The	Ion Detectors	30
	3.4.1	Silicon Detectors	31
	3.4.2	MCP Detectors	32
4	RFQ Sys	tem Simulations with SIMION	33
	4.1 Sect	or 1 of the Gas Filled RFQ Mass Filter System	35
	4.1.1	Ion's Initial Velocity, Pressure in Sector 1, and Distance between	
		Gas Cell Plate and Rods	37
	4.1.2	RF Potential Amplitude of Sector 1	39
	4.1.3	Effect of the DC Gradient on Transfer	40
	4.1.4	Summary of Sector 1 Tests	41
	4.2 Secto	or 2 of the Gas Filled RFQ Mass Filter System	42
	4.2.1	Effect of the DC Gradient and Gas Pressure in Sector 2	43
	4.2.2	Sector 2 Mass Filtering	46
	4.2.3	Nozzle Geometry	48
	4.2.4	Summary of Sector 2 Tests.	50
	4.3 Secto	or 3 of the Gas Filled RFQ Mass Filter System	51
	4.3.1	The Effect of the DC Gradient on Transfer	53
	4.3.2	Cooling Time of Ions in Linear Trap	54
	4.3.3	Capture and Ejection in the Linear Trap	55
	131	Summary of Sector 2 Tests	٤0

5	Off-Line	Testing of the Gas Filled RFQ Mass Filter System	60
	5.1 Sect	or 1 of the Gas Filled RFQ Mass Filter System	62
	5.1.1	The DC Potentials	63
	5.1.2	The RF Potential Amplitude	66
	5.1.3	Summary of Sector 1 Tests	68
	5.2 Secto	or 2 of the Gas Filled RFQ Mass Filter System	68
	5.2.1	Effects of DC Gradient and Pressure	69
	5.2.2	Mass Filter Calibration	72
	5.2.3	Mass Distribution of <sup>252</sup> Cf Fission Fragments	75
	5.2.4	Summary of Sector 2 Tests	77
	5.3 Secto	or 3 of the Gas Filled RFQ Mass Filter System	77
	5.3.1	DC Potential Gradient	77
	5.3.2	Linear Trapping	79
	5.3.3	Summary of Sector 3 Tests	. 83
	5.4 Conc	clusion of Gas Filled RFQ Mass Filter Tests	84
6	The On-L	ine Transfer of <sup>120</sup> Cs	86
	6.1 The I	Reaction	86
	6.2 Trans	sfer of Radioisotopes in the Gas Filled RFQ Mass Filter System	87
	6.2.1	Mass Distribution of Products	. 88
	6.2.2	Adding Mass Selectivity to Prevent Saturation on Linear Trap	<b>9</b> 0
	6.3 Trans	fer to CPT and Results	91

6.4 Conclusion of On-Line Experiments	92
7 Conclusion	93
References	96

# **List of Figures**

rigure 2.1:	quadrupole field.	5
Figure 2.2:	Graphical representation of the stable and unstable solutions of the Mathieu equation.	8
Figure 2.3:	Intersection of stable solutions in x and y.	9
Figure 2.4:	Capture and ejection potentials for linear trap.	14
Figure 3.1:	The ATLAS facility.	16
Figure 3.2:	The experimental set-up used for precise mass measurement studies at ANL.	17
Figure 3.3:	The Enge split-pole magnetic spectrograph.	18
Figure 3.4:	Gas Cell and gas filled RFQ mass filter system.	20
Figure 3.5:	Transfer line to CPT mass spectrometer.	21
Figure 3.6:	The Canadian Penning Trap mass spectrometer.	22
Figure 3.7:	Geometrical configuration of the four rods used as RFQ mass filter systems.	24
Figure 3.8:	General nozzle plate schematics.	25
Figure 3.9:	Coupling scheme of DC and RF potentials and how they are applied to the rods of RFQ mass filter system.	27
Figure 3.10:	Bloc diagram of electronics of RFQ mass filter system.	28
Figure 3.11:	General schematic diagram of the high voltage switcher logic drivers coupled to the linear trap segments of sector 3.	29
Figure 3.12:	Schematic diagram of the detector holder.	31
Figure 4.1:	Model of sector 1.	35
Figure 4.2:	Schematics of sector 1.	36

Figure 4.3:	Cross section of the 4 rod structures with equipotentials created when potentials 180° out of phase are applied to each opposite pair of rods.	36
Figure 4.4:	The ion's trajectories through sector 1 for different initial ion velocities and initial pressures at the exit aperture of the gas cell.	38
Figure 4.5:	Representation of electric field lines along the axial direction and trajectory of ions.	39
Figure 4.6:	Plot of the number of ions transmitted through sector 1 as a function of the RF amplitude applied on sector 1 rods.	40
Figure 4.7:	Model of sector 2.	42
Figure 4.8;	Schematic diagram of sector 2 simulation.	43
Figure 4.9:	Ion transmission for different pressures and DC gradients along the rods of sector 2.	44
Figure 4.10:	Ion trajectories inside the rod structures of sector 2 under different pressures as seen from xz plane.	45
Figure 4.11:	Ion trajectories under different DC gradients seen from xz-plane.	46
Figure 4.12:	Ion trajectories in xz and yz planes.	47
Figure 4.13:	Stability diagram for sector 2 mass filter.	48
Figure 4.14:	Transmission efficiency of ions injected into various nozzle geometries.	49
Figure 4.15:	Model of sector 3.	51
Figure 4.16:	Schematic diagram for the simulated sector 3.	52
Figure 4.17:	Time taken for ions in sector 3's linear trap to get cooled to a given energy.	54
Figure 4.18:	Study of the number of ions transferred into the drift tube for different ejection pulse rates.	57
Figure 5.1:	Transmission of ions through the gas filled RFQ mass filter system for various DC potential differences between the exit plate of the gas cell and the first segment of the rods of sector 1	63

Figure 5.2:	Transmission of ions through the gas filled RFQ mass filter system for various DC potential differences between the first and last segments of sector 1's rods.	1 64
Figure 5.3:	Transmission of ions through the gas filled RFQ mass filter system for various DC potential differences between the last segment of sector 1's rods and the nozzle which follows it.	1 65
Figure 5.4:	Ions transmitted through gas filled RFQ mass filter system for different RF amplitudes applied to the rods of sector 1.	66
Figure 5.5:	Ions transmitted through gas filled RFQ mass filter system for different RF amplitudes applied to the rods of sector 1. In this test the rods of sector 1 are moved 1 cm closer to the exit plate of the gas cell.	67
Figure 5.6:	Ion transmitted for different DC gradients and pressures in sector 2	?. 70
Figure 5.7:	Ion transmitted through the gas filled RFQ mass filter system for various DC potential differences from the last segment of sector 2's rods to the exit nozzle plate of sector 2.	71
Figure 5.8:	TOF spectrum of ions transferred from the gas cell to the end of the gas filled RFQ mass filter system.	73
Figure 5.9:	Stability diagram obtained with values from table 5.2.	74
Figure 5.10:	Mass distribution of fragments from <sup>252</sup> Cf source.	76
Figure 5.11:	Effect of DC gradient along sector 3 rods on ion transmission.	78
Figure 5.12:	Transmission yields for different ejection pulse widths.	80
Figure 5.13:	Transmission efficiency as a function of linear trap ejection pulse amplitude.	81
Figure 5.14:	Comparison of time-of-flight spreads of mass peaks for various pulse amplitudes as seen on the MCP at the end of the RFQ mass filter system.	82
Figure 5.15:	Effect of ejection pulse rate on transmission efficiency.	82
Figure 6.1:	TOF spectra for different DC offsets (U) on sector 2 rods.	88

Figure 6.2:	TOF spectra for different RF frequencies on sector 2 rods for a mass filter with $U = 28 \text{ V}$ and $V = 230 \text{ Vp-p}$ .	89
Figure 6.3:	Mass distribution of ions transmitted through gas filled RFQ mass filter system with $U = 32\ V$ on sector 2 rods.	90
Figure 6.4:	Ion transmitted for different U values at RF frequency of 460 kHz and 440 kHz applied to the rods of sector 2.	91

## **List of Tables**

Table 3.1:	Typical voltages applied to RFQ rod segments.	30
Table 4.1:	Summary of the range of operation for sector 1 parameters.	41
Table 4.2:	Summary of ranges of operation for sector 2's parameters.	51
Table 4.3:	Transfer efficiency, time-of-flight (TOF) spread and energy spread of ions captured and ejected from linear trap for different trap depths, pulse widths and pulse amplitudes.	57
Table 4.4:	Summary of ranges of operation for sector 3's parameters.	59
Table 5.1:	Most abundant fission products from a <sup>252</sup> Cf source.	60
Table 5.2:	RF frequencies at which half of the calibration peak's amplitude is lost for various U values and calculated $a$ and $q$ values.	74
Table 5.3:	Summary of gas filled RFQ mass filter system optimal parameters.	84
Table 6.1:	Expected reaction products from fusion evaporation of a <sup>60</sup> Ni beam on a natural Cu target.	87

# **Chapter 1**

## Introduction

Radio Frequency Quadrupole (RFQ) mass filters, ion guides, and ion traps operate on the principle that the application of a combination of DC and AC electric potentials to given electrodes can create fields to confine ions of a certain mass region in two or three dimensional space [Daw76, Gul86, Klu92, Lun99]. Once trapped, ions are more easily manipulated to suit the requirements of a given experiment.

The first quadrupole mass filters were developed in the 1950's by Paul et al. [Pau58] and have been since used in a number of applications in the atmospherical, environmental and medical sciences. For example, analytical chemistry has benefited from ion guides by using them to transport bio-molecules from atmospheric pressure ion (API) sources to mass analysers [Cap96].

More recently, these devices have gained popularity in the field of nuclear physics where they have been shown to be particularly efficient in the transfer and manipulation of ions from high pressure environments to systems such as Penning trap mass spectrometers which require near vacuum conditions to operate [He00, Kim97]. Penning trap mass spectrometers can perform accurate mass measurements on radioisotopes

delivered to them. From this measurement, the binding energy of radionuclei can be found. The study of nuclei far from stability is of particular interest since it could result in a better determination of a correct nuclear standard model. In addition, because some of these radionuclides naturally originate in the interior of exploding stars, a better knowledge of binding energies could be helpful in the understanding of these violent phenomena.

A Penning trap mass spectrometer system (ISOLTRAP) developed at ISOLDE at CERN [Bec89] has already made successful mass measurements on over 80 radionuclides with a high mass resolution and an accuracy of over a part in 10<sup>7</sup> [Klu93]. A similar system, the Canadian Penning Trap (CPT) mass spectrometer, is currently in operation at Argonne National Laboratory (ANL) in Argonne, II., U.S.A. [Sav97]. Here the measured radioactive nuclides are created from the fusion evaporation reaction of a heavy ion beam hitting a target. The products are separated with a magnetic spectrograph and enter a helium filled gas cell operating at pressures of about 150 torr. In order to deliver these products to the ultra-high vacuum Canadian Penning Trap (CPT) mass spectrometer to perform a precise mass measurement, a fast, efficient transport method is needed. The RFQ mass filter system is well suited for this task. Ions are confined in two dimensions and guided to the CPT mass spectrometer while three stages of differential pumping remove the helium gas.

The purpose of this thesis is to investigate the properties of the gas filled RFQ mass filter system located at ANL in order to better understand and improve the workings of the apparatus. The system's parameters are optimized with the help of a model

simulating the motion of the ions within the structure and by performing a number of experimental studies.

The work presented in this thesis is divided into the following chapters. Chapter 2 introduces the theory associated with RFQ mass filters operated in gas filled mode. In chapter 3, a description of the apparatus used for the work in this thesis is given. A detailed account of the computer simulations of the gas filled RFQ mass filter system is presented and results are shown in chapter 4. Chapter 5 includes the studies and results of the off-line experiments performed with the gas filled RFQ mass filter system at ANL. Finally, chapter 6 presents the results of a particular on-line experimental run to demonstrate the use of the gas filled RFQ mass filter system as a crucial part of the transfer system to the CPT mass spectrometer.

# Chapter 2

# **Theory of RFQ Devices**

This chapter introduces the theory associated with the quadrupole field and how one can be generated with the rod electrode structures of RFQ mass filter systems. It also presents the resulting behavior of ions in this system, first operating under ideal vacuum conditions, then including the effects of the addition of gas inside the device. Finally, a brief description of how the RFQ system can be used as a linear trap in the axial direction is given.

## 2.1 The Quadrupole Field

The electric potential generally associated with the quadrupole field can be given in Carthesian coordinates by

$$\Phi = \Phi_0 (\lambda x^2 + \sigma y^2 + \gamma z^2)$$
 (2.4.1)

where  $\Phi_0$  is a position independent factor and  $\lambda$ ,  $\sigma$ , and  $\gamma$  are weighting constants which must obey the equation

$$\lambda + \sigma + \gamma = 0 \tag{2.4.2}$$

in order to satisfy Laplace's equation, such that

$$\nabla \cdot \mathbf{E} = \nabla \cdot (-\nabla \Phi) = -2\Phi_{o} (\lambda + \sigma + \gamma) = 0$$
 (2.4.3)

#### 2.1.1 The Mass Filter

A quadrupole field can be obtained from various electrode geometries. For a mass filter consisting of four hyperbolic rods as seen in figure 2.1, the potential is given by setting  $\gamma = 0$  and  $\lambda = -\sigma = 1$  such that

$$\Phi = \Phi_0 (x^2 - y^2) \tag{2.4.4}$$

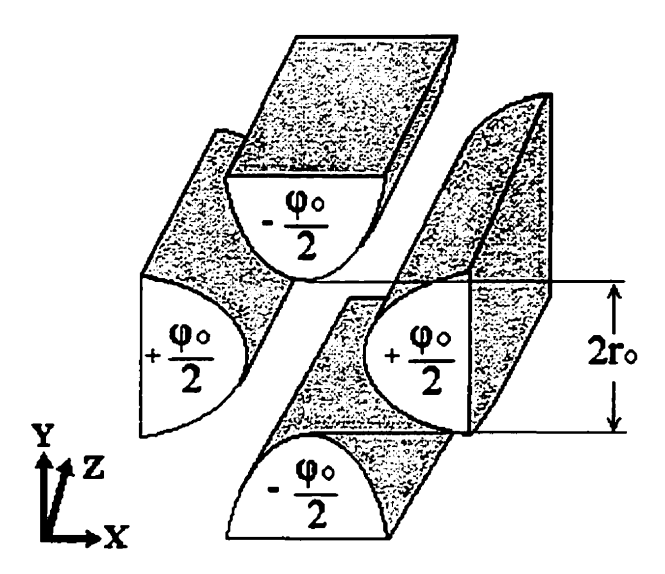


Figure 2.1: Geometry of electrodes needed to create two-dimensional quadrupole field. Four hyperbolic rods are separated by  $2r_o$ , and a potential of  $\phi_o$  is applied between each set of opposite rods.

If one now defines  $\phi_0$  as the potential difference between neighboring rods and  $r_0$  as half the distance between opposite rods of hyperbolic cross section, the potential function becomes

$$\Phi = \frac{\varphi_0}{2r_0^2} (x^2 - y^2) \tag{2.4.5}$$

Since the ions' equations of motion within the structure take the form  $m\ddot{x} = q_e E_x$ , the decoupled equations are given by

$$\ddot{x} + \frac{q_c}{mr_0^2} \phi_0 x = 0 {(2.4.6)}$$

$$\ddot{y} - \frac{q_c}{mr_0^2} \phi_0 y = 0 \tag{2.4.7}$$

$$\ddot{z} m = 0 \tag{2.4.8}$$

where q<sub>e</sub> and m are the charge and mass of the ion respectively [Daw76].

Applying a constant electric potential  $\varphi_0$  between the pairs of rods gives rise to a simple harmonic motion of the ions in the x-direction, but also results in a divergent trajectory in the y-direction. In such a case ions will eventually hit an electrode and be lost. However it is possible to find a time varying  $\varphi_0$  for which ions of a certain range of  $q_e/m$  will remain within the structure. Particularly, one can have

$$\varphi_0 = U - V \cos \omega t \tag{2.4.9}$$

where U is a DC voltage applied between the two pairs of opposite rod electrodes and Vcos $\omega$ t is a sinusoidal voltage applied to the rod electrodes with peak-to-peak amplitude V and angular frequency  $\omega = 2\pi f$ . Equations (2.4.6) and (2.4.7) now become

$$\ddot{x} + \frac{q_e}{mr_0^2} (U - V\cos\omega t)x = 0$$
 (2.4.10)

$$\ddot{y} - \frac{q_e}{m{r_0}^2} (U - V\cos\omega t)y = 0$$
 (2.4.11)

The following parameters can further be defined

$$a_{\rm u} = a_{\rm x} = -a_{\rm y} = \frac{4q_{\rm e}U}{{\rm mr_0}^2\omega^2}$$
 (2.4.12)

$$q_{\rm u} = q_{\rm x} = -q_{\rm y} = \frac{2q_{\rm e}V}{{\rm mr_0}^2\omega^2}$$
 (2.4.13)

$$\xi = \underline{\omega t} \tag{2.4.14}$$

such that one can now express both equations (2.4.10) and (2.4.11) as

$$\frac{d^2u}{d\xi^2} + (a_u - 2q_u\cos 2\xi)u = 0$$
 (2.4.15)

in which u can be substituted for either x or y. Equation (2.4.15) is the canonical form of the well-known Mathieu equation. It has stable and unstable solutions depending on  $a_u$  and  $q_u$ . The solutions are of the form

$$u(\xi) = \alpha' e^{\mu \xi} \sum_{n=-\infty}^{+\infty} C_{2n} e^{2in\xi} + \alpha'' e^{-\mu \xi} \sum_{n=-\infty}^{+\infty} C_{2n} e^{-2in\xi}$$
 (2.4.16)

where  $\alpha$ ' and  $\alpha$ '' are integration constants that are dependent on the initial conditions.  $C_{2n}$  and  $\mu$  are solely dependent on a and q. Stable solutions arise when u remains finite as  $\xi \to \infty$ . Values of a and q giving stable solutions are plotted in figure 2.2.

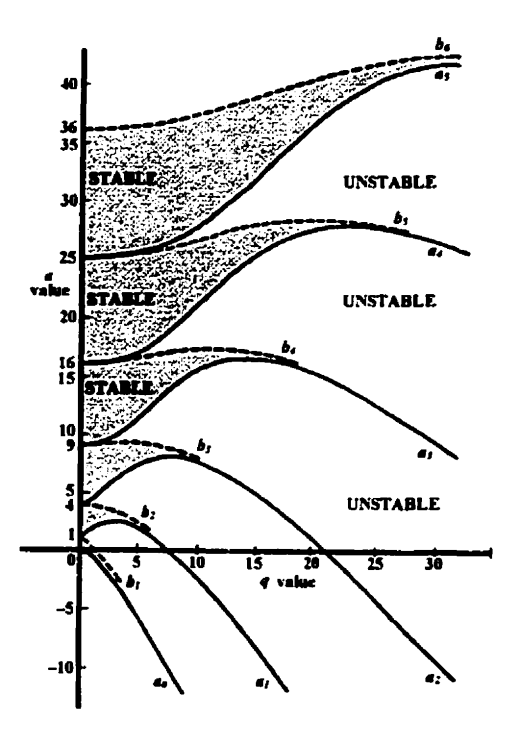


Figure 2.2: Graphical representation of the stable and unstable solutions of the Mathieu equation. The intersections of the curves  $a_0$ ,  $b_1$ ,  $a_1$ ,  $b_2$ , ... impose limits to the stability regions (shaded area). Odd-numbered curves are asymmetrical about the a value axis, but even-numbered ones are symmetrical. Both are symmetrical about the q value axis.

For a mass filter consisting of four rods as in figure 2.1, the trajectories of the ions must be stable in both xz and yz planes. The solutions to the Mathieu equation must therefore be stable in x and y. It is usually more appropriate to operate in the stable

region closer to the origin since a and q, proportional to the applied potentials U and V, are smaller and more practical to obtain. This region is seen more closely in figure 2.3, a representation of the intersecting x and y stable positive regions nearest to the origin. According to equations (2.4.13) and (2.4.14), ions having the same mass to charge ratio  $m/q_e$  hold the same operating point (a,q) if  $r_o$ ,  $\omega$ , U and V are kept constant. Alternatively, for a certain U and V, only a limited range of ions with  $m/q_e$  values will have an (a,q) point lying within the stable shaded area. Varying U or V consequently affects this range of stability. The mass scan line is designated as a line going through the origin of the stability diagram for which all points have the same a/q or equally U/V ratio. Evidently, for a particular mass scan line, only ions having a limited range of  $m/q_e$  values will lie in the stable region, from  $(m/q_e)_{low} = \frac{2V}{q_{low}r_o^2\omega^2}$  to  $(m/q_e)_{high} = \frac{2V}{q_{high}r_o^2\omega^2}$ .

This range, or mass resolution, becomes narrower as the a/q ratio increases.

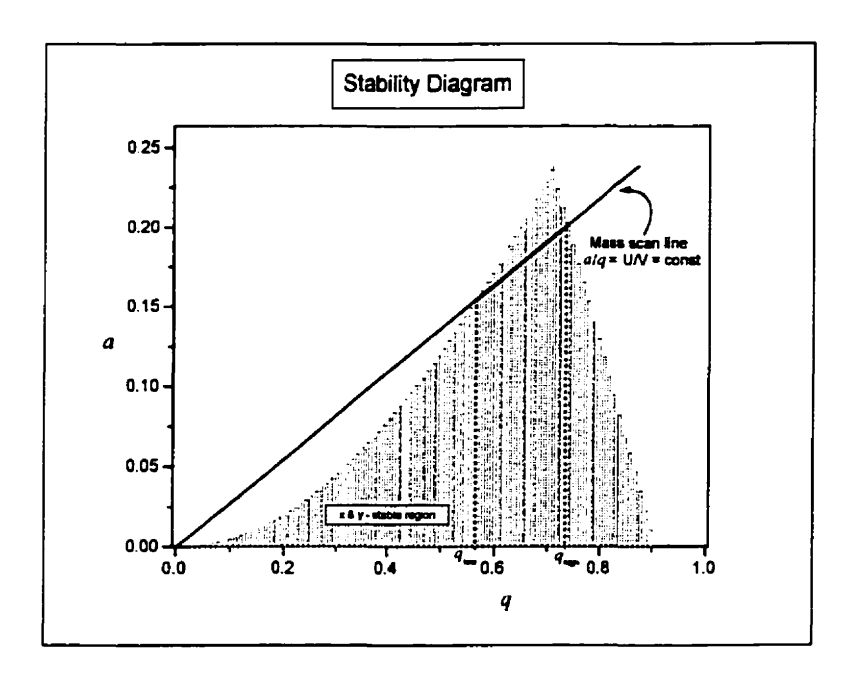


Figure 2.3: Intersection of stable solutions in x and y [Fuk00].

#### 2.1.2 The Resolution of a Mass Filter

As previously discussed, increasing the U/V ratio applied on the mass filter's electrodes increases the slope of the mass scan line on the stability diagram, making the stable mass range narrower and thus increasing the mass filter resolution. In a perfect mass filter of unlimited length the tip of the stability diagram where the resolution approaches infinity is located at an (a,q) value of (0.23699, 0.70600). The resolution of an ideal mass filter is determined by Paul et al. [Pau58] to be

$$R = \frac{0.178}{(0.23699 - a_{0.706})} \tag{2.4.17}$$

where  $a_{0.706}$  is the a value at q = 0.706, and R is determined from the width of the stable region along the mass scan line. For example, it is easy to see from the definition of a and q that the resolution of a particular mass filter can be increased by increasing the DC potential U applied on the rods if all other parameters are kept fixed.

The resolution of a real mass filter is somewhat modified since these are not infinitely long or large. In practice the most influential parameter is usually the length of the filter. Ions close to stability in a shorter mass filter are less likely to be rejected. For a mass filter of finite length L, the maximum resolution determined experimentally by von Zahn [Von56] is

$$R_{\text{max}} = \frac{n^2}{12.2} \tag{2.4.18}$$

where n is the number of field cycles the ion spends in the mass filter, defined as  $n=fL(m/2E_zq_e)^{1/2}$ . Here the ions are assumed to have an energy of  $E_zq_e$  in the z-direction.

## 2.1.3 The Addition of Gas to the RFQ Mass Filter System

The previously presented theory applies to the use of RFQ mass filter systems in perfect vacuum conditions. Adding inert gas to such a system will affect the motion of confined ions. Ions will collide with the gas particles and change trajectory with each collision. The mean free path which is the average distance between collisions can be given as

$$\lambda = (\sqrt{2} \, n\sigma)^{-1} \tag{2.4.19}$$

where n is the number of particles per unit volume and  $\sigma$  is the collision cross section [Sam71].

For ion motion in the gas filled RFQ mass filter system this effect can be approximately quantified by adding a viscous drag term  $2k\frac{du}{d\xi}$  to the Mathieu equation, which becomes

$$\frac{\mathrm{d}^2 u}{\mathrm{d}\xi^2} + 2k\underline{\mathrm{d}}\underline{u} + (a_\mathrm{u} - 2q_\mathrm{u}\cos 2\xi)u = 0 \tag{2.4.20}$$

where  $k = K/m\omega$ . K is the mobility constant, a property of the ion/gas combination. The drift velocity of the ions that are near thermal equilibrium with the gas along the field lines of a weak electric field,  $E_{\rm el}$ , is given by

$$v_{\text{drift}} = KE_{\text{el}} \tag{2.4.21}$$

The mobility constant is often described in terms of the reduced mobility  $K_o$  and is related to the pressure P and temperature T of the gas as follows [Mas88].

$$K = 3.71 \frac{K_0 T \lceil {}^{\circ}K \rceil}{P \lceil torr \rceil}$$
 (2.4.22)

With the addition of this viscous drag force and weak electric field, the equations of motion of the ions in the RFQ mass filter are modified to

$$\ddot{x} + \frac{b}{m}\dot{x} + \frac{q_c}{mr_0^2}(U - V\cos\omega t)x = 0$$
 (2.4.23)

$$\ddot{y} + \frac{b}{m} \dot{y} - \frac{q_e}{mr_o^2} (U - V\cos\omega t) y = 0$$
 (2.4.24)

$$\ddot{z} + \frac{b}{m}\dot{z} - \frac{q_c E_{cl}}{m} = 0$$
 (2.4.25)

with the newly introduced drag force constant b, related to the ion mobility by

$$b = \frac{q_c}{K} \tag{2.4.26}$$

Another effect of adding gas to the system is the resulting gas flow between sectors of the system if each sector is operated at a different pressure. Within a closed structure the product of the gas density,  $\rho$ , the flow velocity of the gas,  $\nu$ , and the cross sectional area, A, at any given point must remain constant. In equation form this is represented by

 $\nu_1 \rho_1 A_1 = \nu_2 \rho_2 A_2 \tag{2.4.27}$ 

where the subscripts 1 and 2 refer to two different locations inside the structure.

It is important to take the gas flow into account, especially in regions of the gas filled RFQ mass filter system where the pressure differential is large. The transport of the ions between two subsequent sectors is affected since the gas entering the later sector will expand in all directions, carrying the ions along with it. In addition, the relatively high pressure in certain regions leads to a large number of collisions and a strong interaction between the ions and the gas molecules. For these reasons, simulation models should include realistic gas dynamic features. The treatment of the gas flow and collisions in the simulation of the system is later described in chapter 4.

## 2.1.4 Guiding, Bunching and Ejecting Ions in a Gas Filled RFQ System

The rods of RFQ mass filter systems can be physically cut into isolated segments, electrically linked by resistors. By segmenting the rods of the structure it becomes possible to apply independent DC potentials to each set of segments. This is useful when the gas flow due to differential pressures in the system is by itself insufficient to transmit the ions forward and additional guidance is required. Applying a potential gradient along the rod segments directs the charged ions towards regions of lower potential.

This rod segmentation also allows the option of using segments as a linear trap. Consider three neighboring rod segments. If a lower potential is applied to the middle segment relative to the two neighboring segments, a potential well is created. Low energy ions fall into the well and get further cooled by collisions with neutral gas

molecules until they settle at the bottom of the potential well. This confines the ions axially. A pulsed voltage can then be applied to the segments to eject the ions out of the trap as needed. This is schematically seen in figure 2.4, a representation of the segmented rods and of the relative potential gradient in the axial or z-direction.

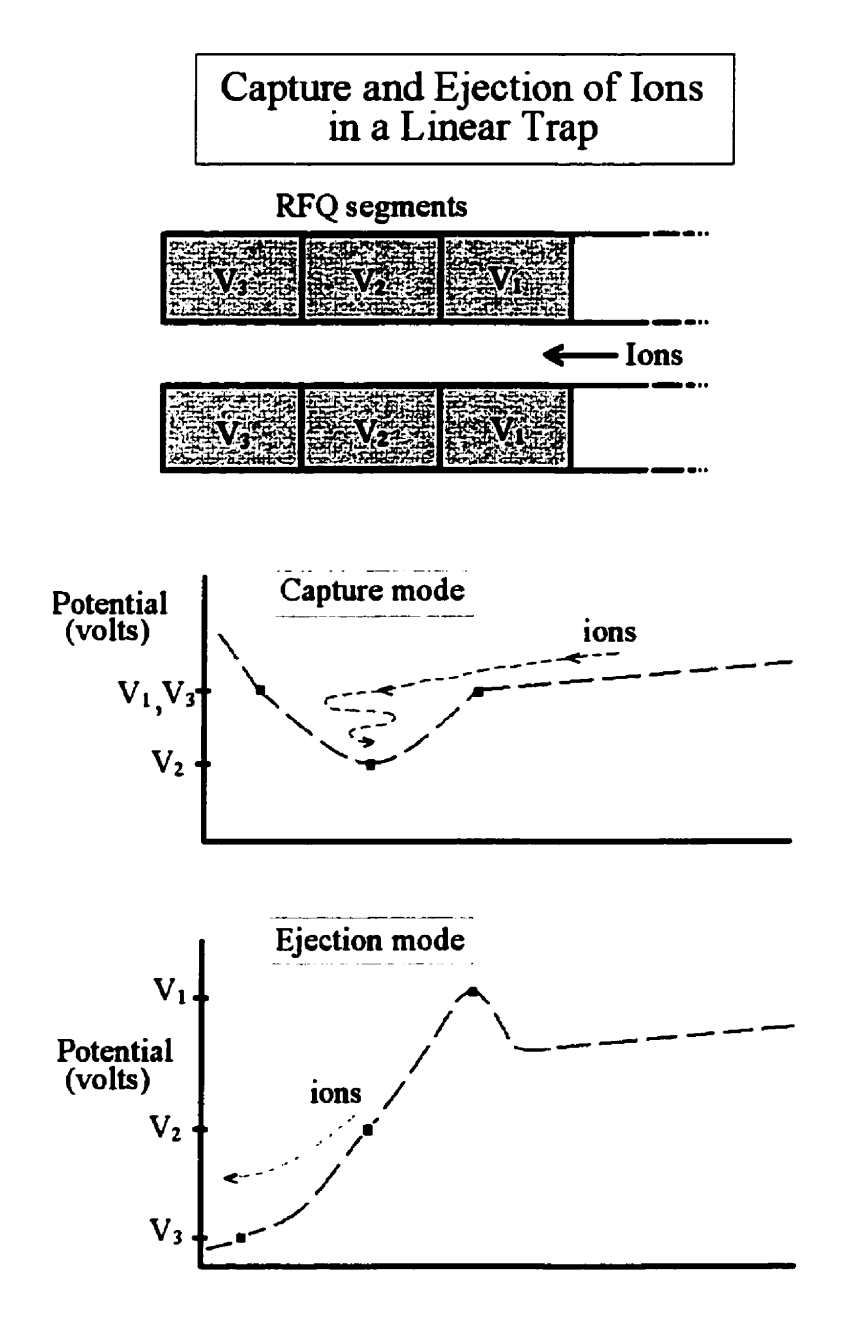


Figure 2.4: Capture and ejection potentials for linear trap. Ions are guided forward by the potential gradient, then fall into the linear trap where they are captured. A pulsed potential ejects the ions as needed.

# Chapter 3

## **Experimental Apparatus**

The work for this thesis is performed at Argonne National Laboratory (ANL) situated in Argonne, Illinois. It houses the Argonne Tandem Linac Accelerator System (ATLAS) described in section 3.1, as well as the various components of the experimental set-up needed for precise mass measurement studies. These include an Enge split-pole magnetic spectrograph, a gas cell, a gas filled RFQ mass filter system and the Canadian Penning Trap (CPT) mass spectrometer. A brief description of each of these devices is given in section 3.2. The gas filled RFQ mass filter system is described in detail in section 3.3. The detectors required for the experimental studies are described in section 3.4.

## 3.1 The ATLAS Facility

The Argonne Tandem Linac Accelerator System (ATLAS) is a superconducting linear particle accelerator. It can produce high precision beams ranging from protons beams to <sup>238</sup>U beams of energies as high as 17 MeV per nucleon, and deliver them to various experimental areas. A layout of the facility is shown in figure 3.1.

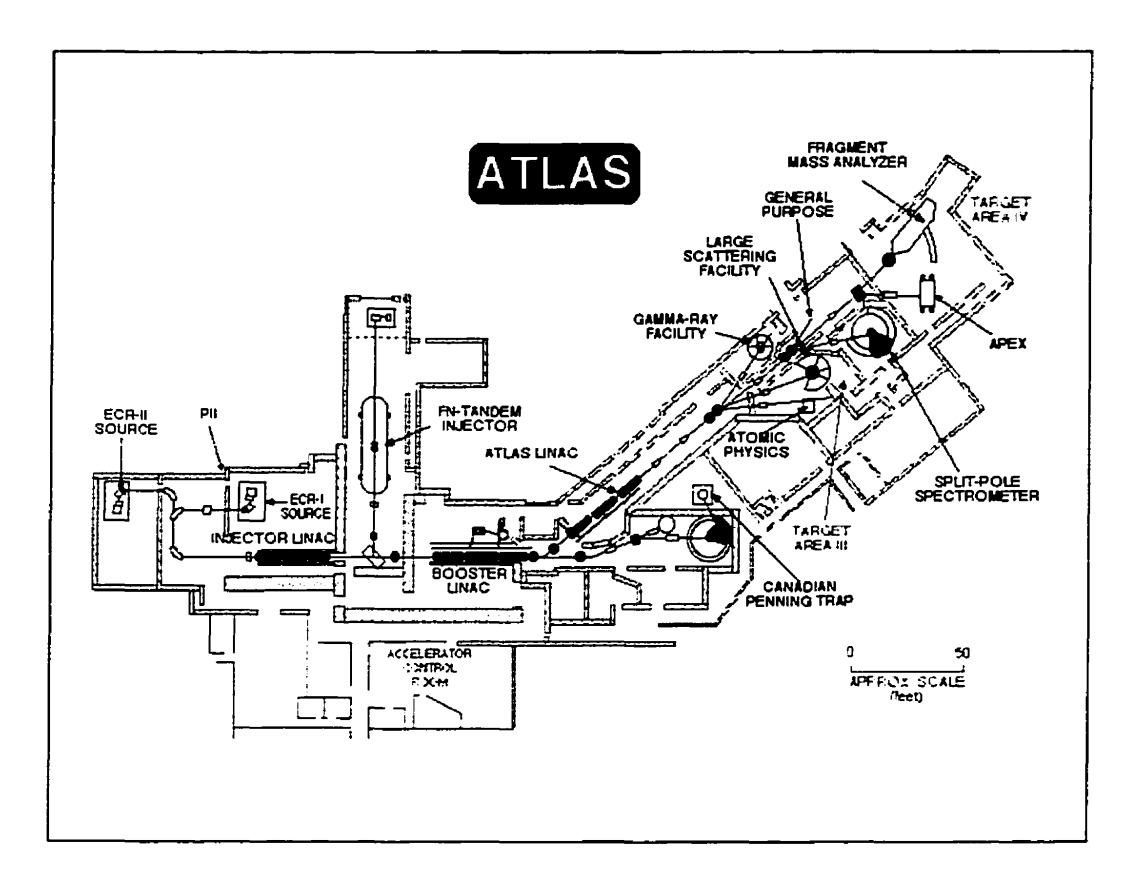


Figure 3.1: The ATLAS facility. The CPT area where mass measurements are performed is located near the bottom right corner of the layout diagram.

The FN-tandem electrostatic accelerator or the Electron Cyclotron Resonance (ECR) ion source followed by the positive ion injector (PII) can provide beams of a desired element. This ion beam is injected into the Booster Linac which accelerates the ions to the required energy before sending them to the chosen experimental area.

## 3.2 The Experimental Set-up

When carrying out on-line experiments, a beam provided by the ATLAS facility is aimed at a target in the experimental area seen more closely in figure 3.2.

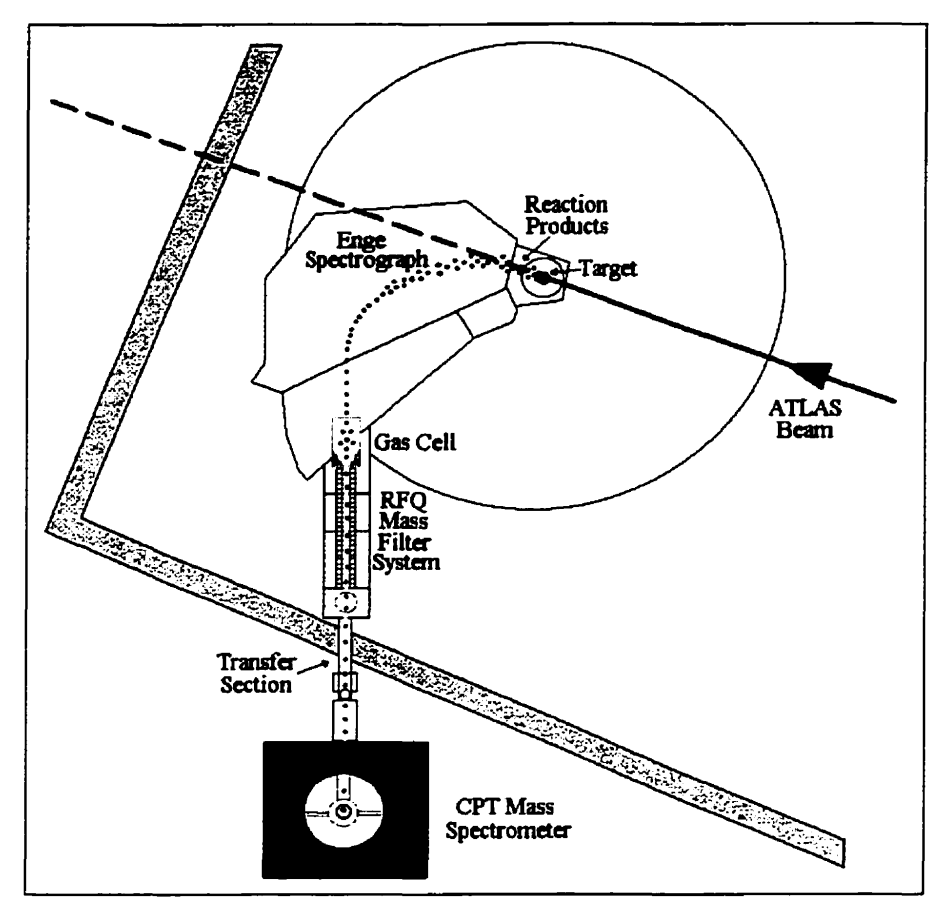


Figure 3.2: The experimental set-up used for precise mass measurement studies at ANL.

As the beam hits the target, a fusion evaporation reaction takes place and produces radioisotopes. The resulting products have wide ranges of mass, charge state, and momentum, and exit the chamber through a small slit at the entrance of the Enge split-pole magnetic spectrograph. The products are then separated by this spectrograph and focused onto the entrance window of a cell filled with 150 torr of helium gas. The gas cell thermalizes the products that are subsequently extracted into the gas filled RFQ mass filter system as singly charged ions. The RFQ mass filter system assures the efficient and selective transport of these extracted ions to the mass spectrometer while gradually getting rid of the helium gas. Once the radioisotopes are properly transported

to the CPT mass spectrometer, a precise measurement can be achieved. A brief description of each cited device follows in subsequent sections.

## 3.2.1 The Enge Split-Pole Magnetic Spectrograph

The separation of heavy ions according to their charge states and masses can be done with a gas filled Enge split-pole magnetic spectrograph such as the one at ANL schematically represented in figure 3.3.

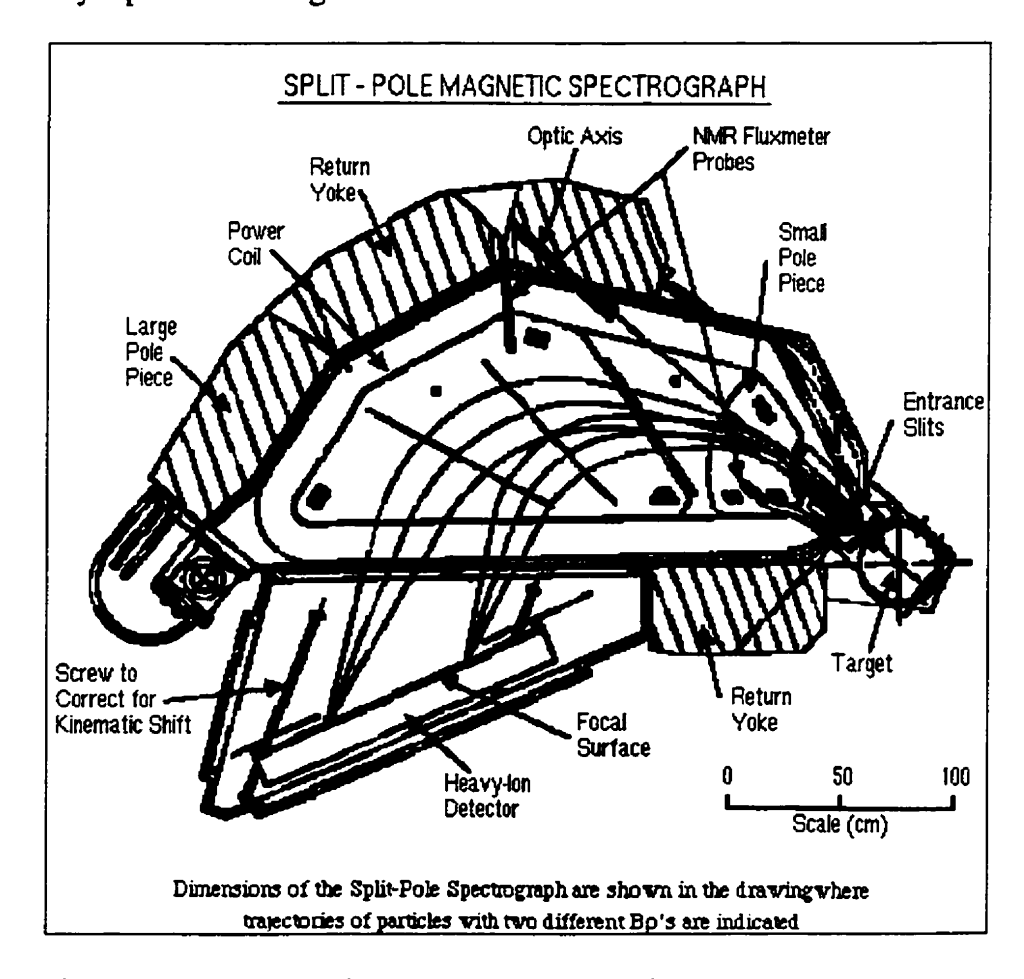


Figure 3.3: The Enge split-pole magnetic spectrograph.

Heavy ions emerging from the nuclear fusion reactions of the original ion beam on a target will have various charge states q, and therefore follow different paths in a given

magnetic field. This trajectory varies with the magnetic rigidity  $B\rho$  of the ions which is proportional to the ion's momentum divided by its electric charge. Adding gas in this region causes ion/gas collisions allowing the transfer of electrons and thus changing the charge states of the ions. It has been shown that in such a case isotopes of different momentum actually merge into a narrower region governed by the mean charge state ( $\overline{q}$ ) of the ions in the gas [Pau89]. To a first approximation, the mean charge state is dependent on the atomic number and velocity of the ion as  $\overline{q} \propto \nu Z^{\gamma}$ , with  $\gamma \sim 0.45$  [Sca91]. The magnetic rigidity is now given as  $B\rho = \frac{m\nu}{\overline{q}} \propto \frac{m}{Z^{\gamma}}$ . Consequently, ions having similar mass numbers but different atomic numbers can be effectively separated in space. The main purpose of the Enge spectrograph is to separate the reaction products from the scattered incident beam. Reaction products widely ranging in mass get focussed onto the gas cell entrance. The use of a thicker target results in greater radioisotopic yields, but also increases the products' momentum spread.

Near the exit of the Enge magnetic spectrograph is placed a movable holder to which are mounted several aluminum foils of different thickness. The foils can be put in the products' path and used as "degraders" to attenuate the energy of the reaction products before they enter the gas cell. This assures that the ions will have an energy low enough to be fully stopped in the gas cell.

#### 3.2.2 The Gas Cell

Near the focal surface of the Enge spectrograph lies a helium gas filled cell used to thermalize the reaction products. The gas cell has a 50mm inner diameter and is 220 mm

long. Normal operation pressures range from 100 to 150 torr of helium. The entrance of the gas cell is made of a 1.9 mg/cm<sup>2</sup> thick havar (metal alloy) window. Once the products enter the cell, they are thermalized and become singly charged ions due to the many collisions with the helium buffer gas. The helium gas used is 99.995% pure and further purified by a "Mono Torr" purifier and a liquid nitrogen filled "cold trap" to get rid of impurities coming from the gas lines or the gas itself. The gas cell walls consist of a complex design of electrodes. The application of DC and AC potentials to these electrodes allow a minimization of the time the ions spend in the cell by guiding them forward while keeping them away from the walls of the structure. These potentials and the strong the gas flow guide the ions through the 1.3 mm diameter exit nozzle aperture. A schematic diagram of the gas cell, along with the RFQ mass filter system that follows it, is seen in figure 3.4.

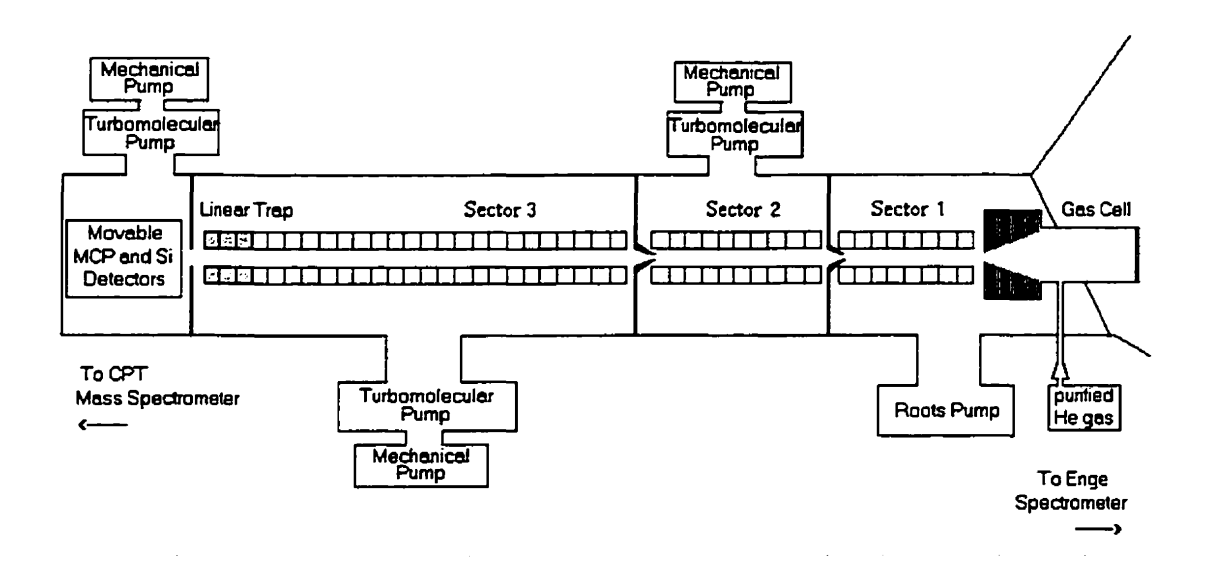


Figure 3.4: Gas cell and gas filled RFQ mass filter system. Ions thermalized in the gas cell are transferred through the 3 sectors of the RFQ mass filter system. Also shown is a representation of the differential pumping system.

# 3.2.3 The RFQ Mass Filter System

Ions from the gas cell are injected into the gas filled RFQ mass filter system along with the helium gas. The main purpose of this device is to efficiently transport the ions from the gas cell to the mass spectrometer while getting rid of the helium gas. A differential pumping system (seen in figure 3.4) is needed for the gradual pumping out of the 150 torr of helium found at the exit of the gas cell to pressures of about  $2x10^{-4}$  torr at the end of the system. These high vacuum conditions are required for the proper functioning of the CPT mass spectrometer. In the gas filled RFQ mass filter system, ions can be selectively transported according to mass to reduce contaminant ions reaching the CPT mass spectrometer. A description of this system will be discussed in more detail in section 3.4.

#### 3.2.4 The Transfer Section

Ions exiting the gas filled RFQ mass filter system are transported to the CPT mass spectrometer through a set of drift tubes and deflectors in a transfer line. A schematic diagram of this transfer section follows in figure 3.5.

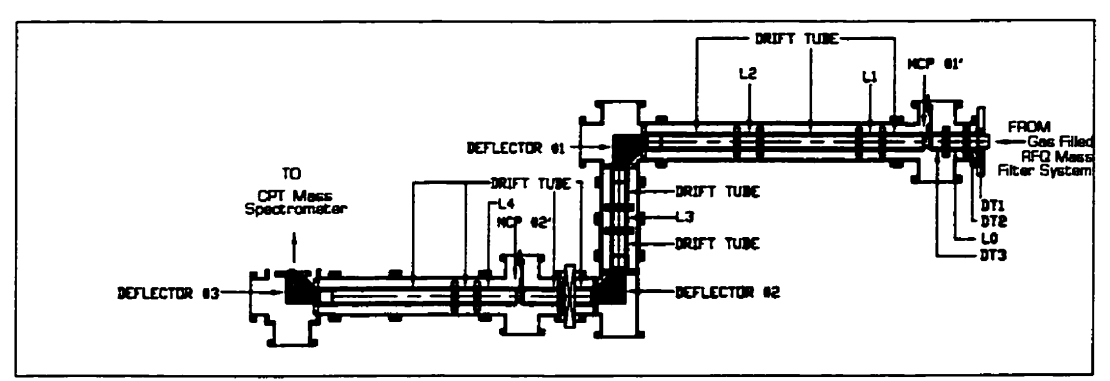


Figure 3.5: Transfer line to CPT mass spectrometer. Ions come in from the right and get transported to the mass spectrometer located above deflector #3.

Electrostatic lenses and steerers are used to focus and direct the ions through the transfer line. Two sets of ion detectors are also located along the transfer line to monitor the transfer efficiency. The drift tubes have an applied potential of -1500V thus allowing the Penning trap of the CPT mass spectrometer to operate near ground potential.

#### 3.2.5 The CPT Mass Spectrometer

Ions transported in the transfer line are delivered to the Canadian Penning Trap (CPT) mass spectrometer for precise mass measurements. Figure 3.6 schematically depicts the 4.5 m high structure.

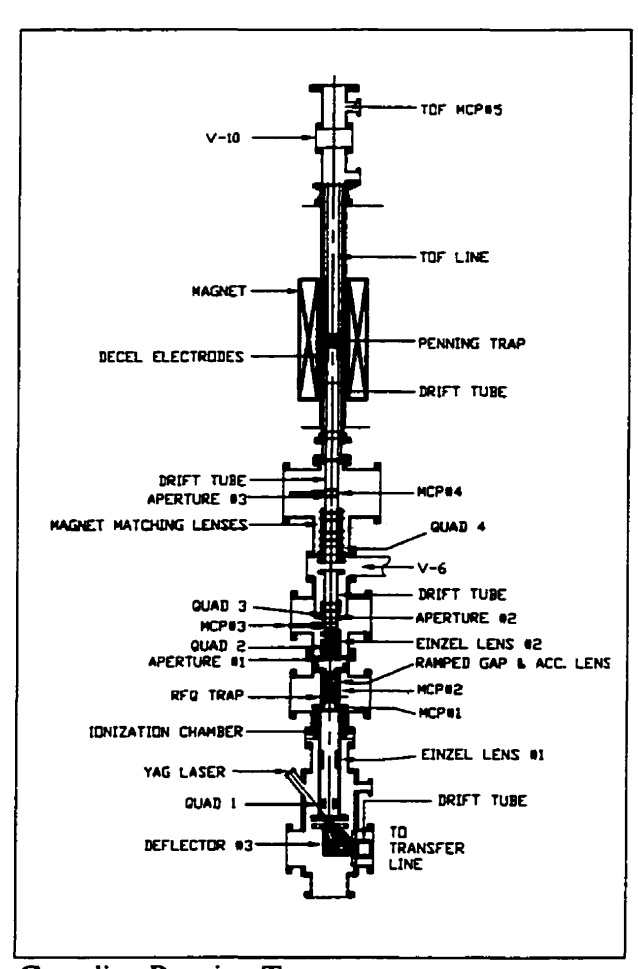


Figure 3.6: The Canadian Penning Trap mass spectrometer.

The CPT mass spectrometer consists mainly of a Paul trap (also called RFQ trap) and a Penning trap. In the Paul trap ions are selectively captured, accumulated and later transferred to the Penning Trap where the mass measurement is performed. Five microchannel plate (MCP) detectors are strategically located along the spectrometer to monitor the transfer efficiency of the system.

The Penning Trap consists of a central ring electrode with an inner radius of 11.6 mm and two end-cap electrodes separated by 20 mm, enclosed in a superconducting magnet having a 5.9 Tesla field. Ions of charge  $q_e$  and mass m in the Penning trap undergo a circular cyclotron motion with frequency  $\omega_e = q_e B/m$ , and are bound axially by the electrostatic quadrupole field due to the electric potential applied to the trap's electrodes. Ions are excited at a certain frequency in the trap and ejected into the TOF section, a 40 cm drift tube where their radial energy is efficiently converted into axial kinetic energy. At the end of this drift tube lies a MCP detector where the ions' time-of-flight (TOF) can be measured. Inside the Penning trap ions have a resonant frequency in the trap which depends on the ion's mass and charge, and the trap's magnetic field. Since ions of a certain mass will get a maximum excitation when their resonant frequency is applied, the TOF of these ions will be minimal. A mass calculation can then be achieved if one knows the charge of the ion, the magnetic field in the Penning trap, and can accurately measure the resonant frequency.

# 3.3 The Gas Filled RFQ Mass Filter System

A more detailed description of the RFQ mass filter system is presented. The following sections include the geometrical aspects of the system, the differential pumping scheme and the electrical components needed to reach an optimal transfer efficiency.

## 3.3.1 Structure and Vacuum System

As previously stated in chapter 2, common RFQ mass filters consist of a set of four rods to which potentials are applied. The simple geometry of the RFQ rods used in the gas filled RFQ mass filter system at ANL is depicted in figure 3.7.

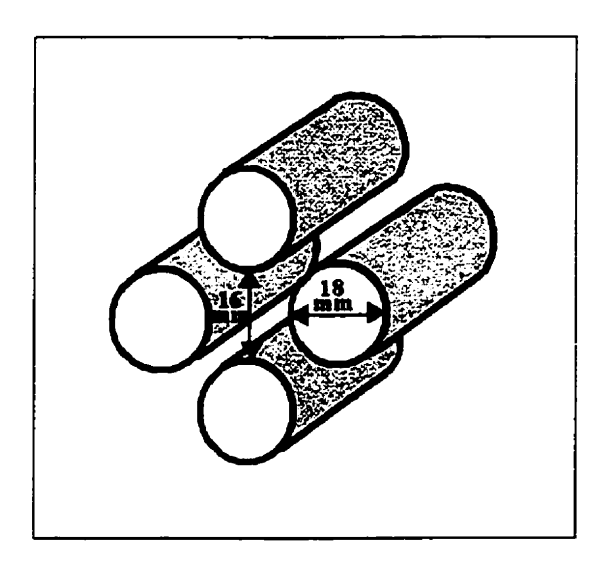


Figure 3.7: Geometrical configuration of the four rods used as RFQ mass filter systems.

The rods are 18 mm in diameter and opposite pairs of rods are separated by 16mm. Although the field and potential equations defined in the theory cite the use of rods of hyperbolic cross section, the field in the center region of four circular rods is shown to be very similar to the ideal quadrupole field and the small imperfections can be neglected [Day54, Den71]. Circular rods having a radius of  $r = 1.148r_0$  are therefore usually chosen for RFQ mass filters since they are more easily machined.

The entire RFQ rod structure is enclosed in a chamber and divided into 3 main sectors by nozzle aperture plates as previously seen in figure 3.4. Each of the sectors, referred to as sector 1, 2, and 3, are further subdivided into segments of 20 mm in length, supported by insulating Macor (machinable ceramic) strips. This isolates individual segments that are then electrically linked through a chain of resistors. Sector 1 has 8 of these segments, sector 2 has 10 segments and sector 3 has 25 rod segments. The last three segments of the third sector are used as a linear trap, to be later described.

The three nozzle plates following each sector have apertures of 2, 2, and 6 mm in diameter respectively. These aperture plates allow each sector to be operated at a desired pressure through differential pumping. A schematic representation of one of the dividing nozzle aperture plates is seen in figure 3.8. The first nozzle plate after sector 1 is a 2.5mm thick plate with a 60° open angle conical nozzle, the second plate after sector 2 is 2.5 mm thick with a 45° conical nozzle and the last plate is simply a 2.5mm thick flat plate with a 6mm diameter hole aperture.

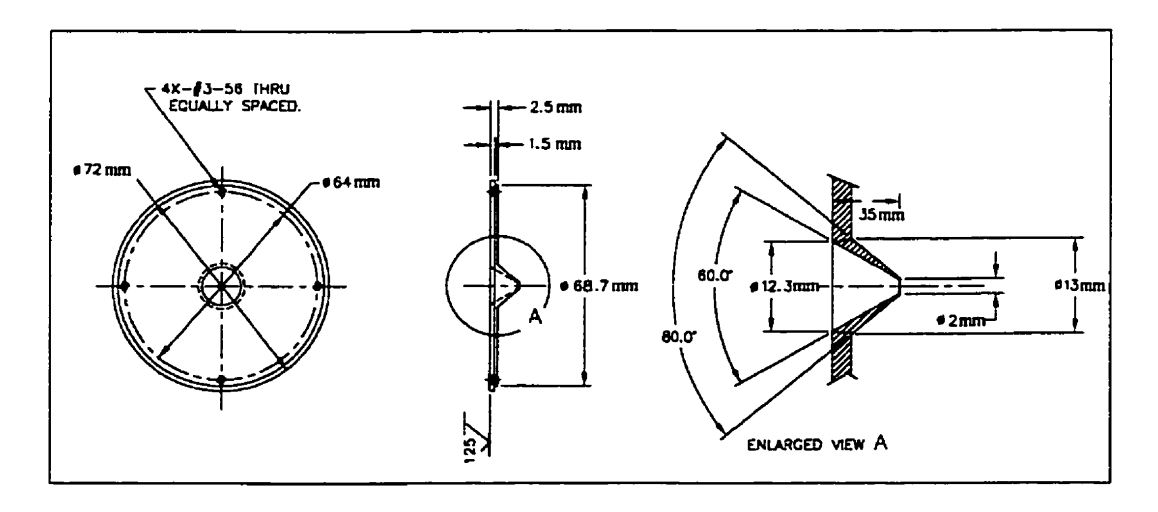


Figure 3.8: General nozzle plate schematics.

The differential pumping system consists of a 684 l/s roots pump to sector 1, a 200 l/s Alcatel turbo-molecular pump backed by a mechanical pump to sector 2 and a 360 l/s turbo-molecular pump also backed by a mechanical pump to sector 3. Another turbo-molecular/mechanical pump combination is located at the beginning of the transfer line. This pump arrangement typically results in pressures of about 400 mtorr in sector 1, 80 mtorr in sector 2, and 0.2 mtorr in sector 3 when 150 torr of helium is put in the gas cell.

# 3.3.2 Electrical Components of RFQ Mass Filter System

The rod design of the RFQ mass filter system allows the proper application of DC and RF potentials to the rod segments for the radial and axial confinement of ions. Since each of the three sectors is subdivided into individually isolated segments with linking resistors, a DC potential ( $V_{DC}$ ) between the first (DC1) and last (DC2) segment can be applied to achieve a gradient along the rod structure to guide the ions forward. On top of this DC potential is applied the RF potential essential for confining the ions radially. The initial RF signal,  $V_{RF}$ , first goes through a transformer that amplifies and splits the signal into two signals  $180^{\circ}$  out of phase,  $V_{RF+}$  and  $V_{RF-}$ . It then becomes possible to apply each RF phase signal to the pairs of opposite rods. The basic electrical coupling of the RF and DC signals and the feeding of these potentials to the rod segments is represented in figure 3.9.

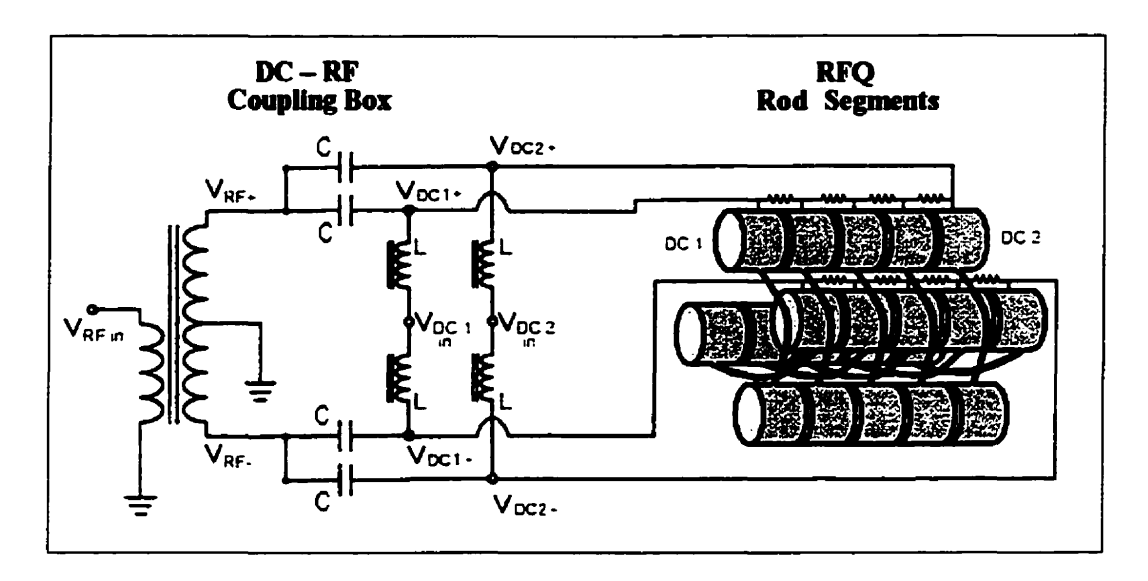


Figure 3.9: Coupling scheme of DC and RF potentials and how they are applied to the rods of RFQ mass filter system. Here the electrical components consists of C=4700 pF capacitors, L=10 mH inductors and R=330  $\Omega$  resistors. Each pair of opposite rod segments are connected by a conducting band.

For all three sectors, the DC potentials are provided by a homemade 16-channel power supply. The RF signals come from three Stanford Research Systems 30 MHz synthesized function generators amplified by ENI 50dB RF power amplifiers. A block diagram of the RFQ mass filter system's electronics is shown in figure 3.10.

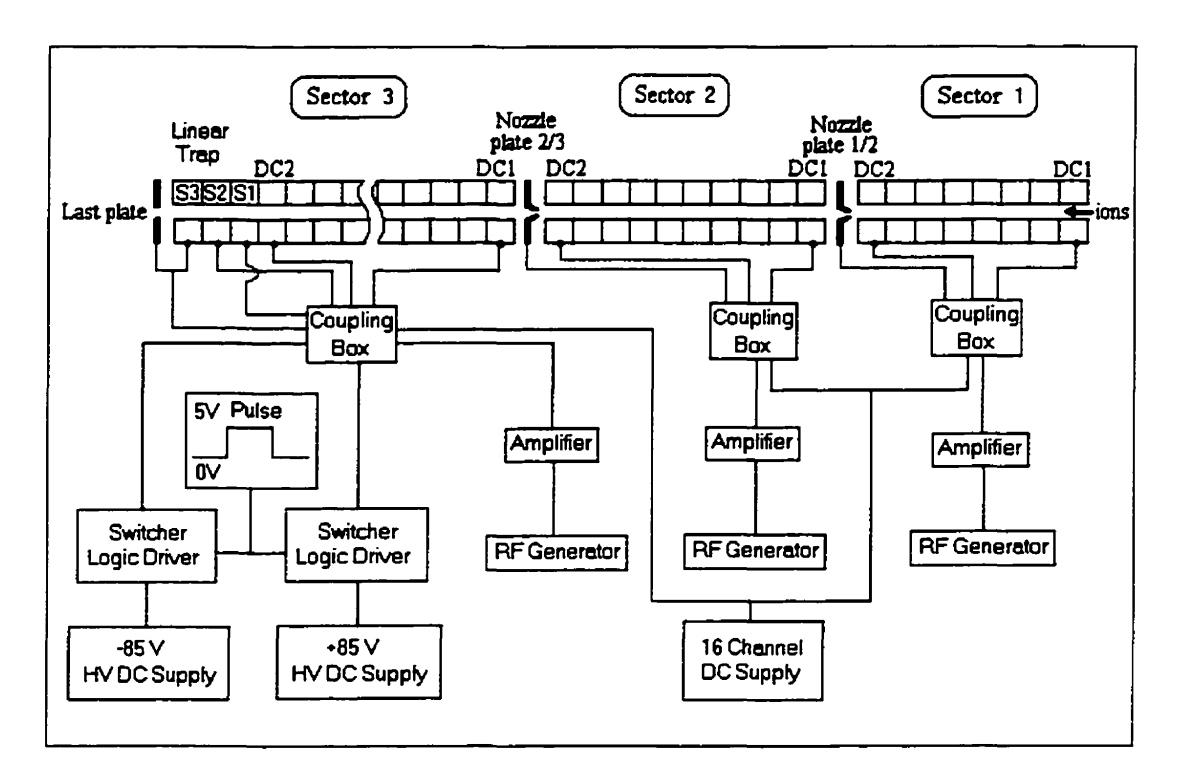


Figure 3.10: Block diagram of electronics of RFQ mass filter system. The DC and RF signals are fed in the coupling boxes before being applied to the rod segments. The linear trap at the end of sector 3 makes use of extra electronics to apply fast pulsed voltages on S1, S3 and the last plate.

Besides having the general electronic components similar to sectors 1 and 2, sector 3 requires additional electronics for the linear trap. Its purpose is to trap the ions in the z-direction by generating an axial potential well into which ions can fall, be accumulated, and cooled. The last three segments of sector 3, called S1, S2, and S3, are used as such a trap by the application of a DC potential to S2 a few volts lower than S1 and S3. A higher potential is also applied to the last aperture plate after S3 to confine the ions within sector 3. To eject these ions the last nozzle plate and S3's potentials are quickly lowered as S1's potential is raised to give an ejection "kick" to the ions. This sudden potential change is provided by two extra variable power supplies whose outputs can be pulsed at desired rates in the following manner. A pulse is obtained from a 1kHz clock that goes

through a TTL/NIM converter and a rate divider. This signal then goes through a gate delay generator to give +5V pulses of variable width and rate, typically 100 µs and 20 Hz. This pulse is sent to two high voltage switcher logic drivers that output a given variable voltage only when the pulse is high (+5V). One outputs a positive voltage (typically +85V) provided by a high voltage (HV) supply to S1, the other outputs a negative voltage (-85V) from the second HV supply to both S3 and the last aperture plate. A schematic representation of the components used for the HV switcher logic drivers is seen in figure 3.11.

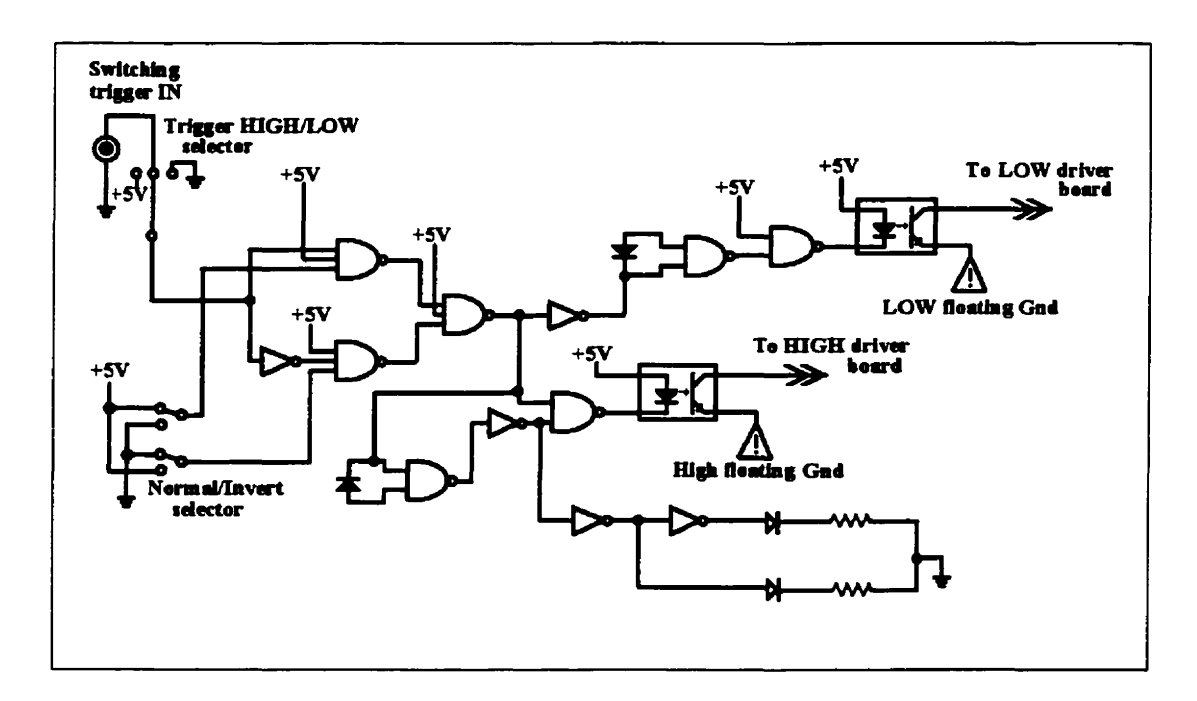


Figure 3.11: General schematic diagram of the high voltage switcher logic drivers coupled to the linear trap segments of sector 3.

Table 3.1 shows typical DC and RF potentials applied to each three sectors of the gas filled RFQ mass filter system. These parameters are optimized in order to achieve the best transfer efficiency of ions through the RFQ mass filter system.

Table 3.1: Typical voltages applied to RFQ rod segments.

RFQ Sector	DC on Rods (Volts)	RF on Rods		
Sector 1	$1^{st}$ segment : DC1 = +3	V = 300 Vp-p		
	$8^{th}$ (last) segment : DC2 = +2	f = 788  kHz		
	Nozzle plate 1/2: -2.5			
Sector 2	$1^{st}$ segment : DC1 = -5.5	V = 250  Vp-p		
	$10^{th}$ (last) segment : DC2 = -6.0	f = 550  kHz		
	Nozzle plate 2/3: -6.5			
Sector 3	1 <sup>st</sup> segment: -10.5	V = 350  Vp-p		
	22 <sup>nd</sup> (last) segment: -11	f = 650  kHz		
Linear Trap	S1 = -12.5	V = 350  Vp-p		
(Capture mode)	S2 = -14	f = 650  kHz		
	S3 = -12.5			
	Last plate: -1.5			
Linear Trap	S1 = +72.5	V = 350  Vp-p		
(Ejection mode,	S2 = -14	f = 650  kHz		
with ±85 V	S3 = -97.5			
ejection pulse)	Last plate: -86.5			

#### 3.4 The Ion Detectors

To test the performance of the gas filled RFQ mass filter system a micro-channel plate (MCP) detector is used to assess the amount and the time-of-flight (TOF) of ions transmitted through the system, and a silicon detector is used to determine the radioactive decays of these ions. Both detectors are mounted on the same holder located at the end of the RFQ mass filter system as previously seen in figure 3.4. This holder is attached to a feed-through that can be moved up or down according to the type of detector one wishes to use. A schematic drawing of this holder is seen in figure 3.12.

# MCP / Silicon Holder Measures are in inches

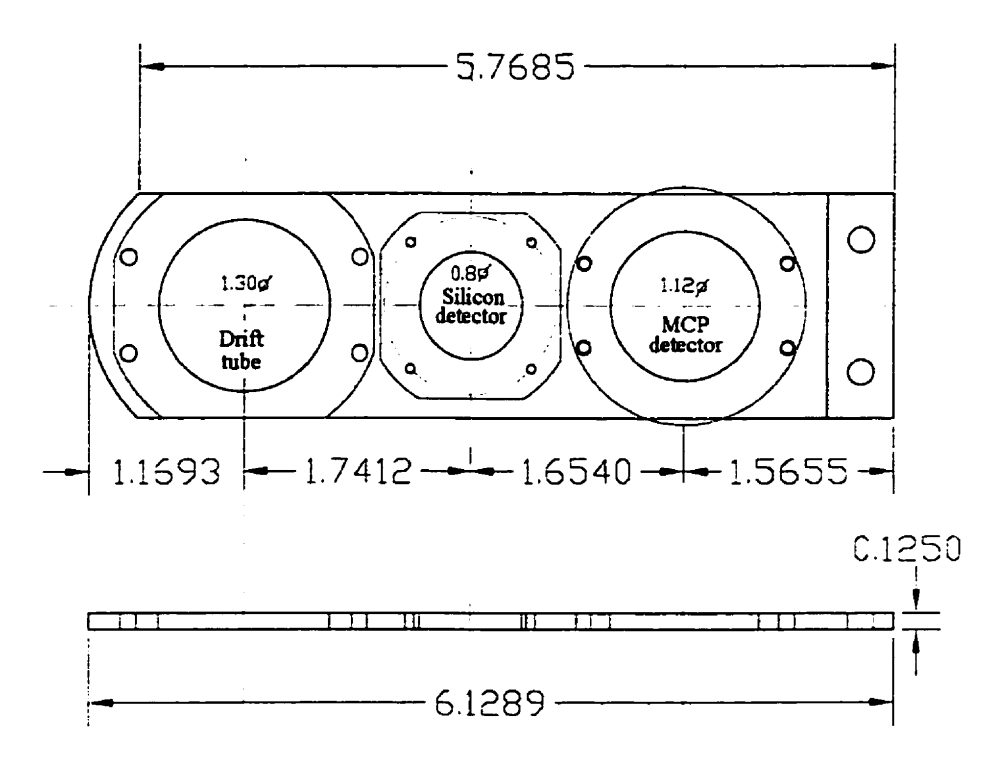


Figure 3.12: Schematic diagram of the detector holder. This holder can be moved up or down in the ion beam line so that either the silicon or MCP detector can be used. Otherwise, the holder is moved to put the drift tube in the middle of the beam line to let the ions pass through unaffected.

A similar holder is located after the second deflector in the middle of the transfer line to enable a measurement of the efficiency of transmission in the transfer line. Five additional MCP detectors are located at strategic points along the CPT mass spectrometer.

#### 3.4.1 Silicon Detectors

Silicon detectors are a type of semiconductor detectors. Ionizing radiation from a  $\beta$ -decay creates electron-hole pairs in the silicon while passing through the detector. The

resulting charge is gathered by applying a biased potential [Leo94]. A bias voltage of +50 V is applied on the silicon detector placed at the end of the linear trap of the gas filled RFQ mass filter system. The front faces of the silicon detectors are covered by aluminum foils set at a voltage of -1500 V to collect the ions. The captured ions subsequently decay and the detector registers those events. The resulting signal goes through a preamplifier and a shaping amplifier. A threshold on the pulse height is set so that only pulses larger than a certain amplitude will get counted as actual decay events. As a result, low amplitude noise often coming from RF signals applied to the nearby RFQ rods can be filtered out.

#### 3.4.2 MCP Detectors

Micro-channel plate (MCP) detectors are leaded-glass discs having thousands of small lead oxide pores called channels. Ions hitting the wall of a channel free electrons through secondary electron emission and these are guided down the channels by the application of an accelerating voltage, typically –1700 V to –1900 V. Subsequent wall collisions create a cascade of electrons resulting in a detectable signal. MCP detectors therefore allow single ions to be detected and counted. Alternatively, ions can be accumulated in the linear trap and the time-of-flight (TOF) spectrum of the group of ions arriving at the MCP detector after ejection from the trap can be obtained. From this spectrum, it becomes possible to extract information on the mass of the detected ions.

# **Chapter 4**

# **RFQ System Simulations with SIMION**

Simulations of the ions' trajectories in the system are obtained with the use of a computational program called SIMION, versions 6.0 and 7.0, by David A. Dahl of the Idaho National Engineering Laboratory. SIMION is designed to model ion optic problems in two or three-dimensional electrostatic or magnetic potential arrays by solving Laplace's equation with the finite difference method [Dah95]. For a given geometry of electrodes, the program will determine the electrostatic fields created at any point inside these electrode structures so that one can view the resulting behavior of ions within the fields. In addition, SIMION allows the incorporation of program files which enables the modeling of more complex systems such as ones that include varying potentials, viscous drag and collisions due to the addition of gas in the system.

Programs such as SIMION can be powerful tools in the understanding of the behavior of ions under various conditions. Here the ultimate goal is to adequately model the gas filled RFQ mass filter system in use at Argonne National Laboratory in order to

recognize the factors which restrict the choice of parameters to achieve optimal performance.

The simulation of the complete gas filled RFQ mass filter system is applied independently to the three sectors, but the exiting conditions of the ions from one sector are kept in mind when simulating the injection conditions into the subsequent sector. The main electrode configuration in each sector consists of sets of four segmented rods of circular cross section to which an RF potential is applied, coupled with a DC potential. Entrance and exit aperture plates are also included in each modeled sector.

Furthermore, close attention is paid to simulating the motion of ions in helium gas inside the rod electrode structures. Here there are a few factors to take into account, namely the flow of the gas between neighboring sectors of our model caused by the differential pressures, the diffusion of the gas due to its thermal energy, and the collisions of the ions with the buffer gas. Within the nozzles dividing each sector, the radial and axial flow velocity of the ions is dependent on its position coordinates and the initial entry velocity. Once the ion exits the nozzle, the radial flow velocity component is neglected and only its axial component is kept through the remainder of the sector. The pressure at a given point within the nozzle depends on the initial pressure in the previous sector, the entry velocity and the nozzle aperture area as well as the cross sectional area and flow velocity at that point, as stated in equation (2.4.27). The probability of collision is based on a potential scattering model involving a positive cesium ion onto a neutral helium atom. This allows the determination of the scattering angle of the ion, dependent on the impact parameter and relative energy of the collision. With the information gained from the above calculations, the trajectories of the ions can be successfully determined.

The following sections present detailed descriptions of the simulation methods and results for the three sectors of the gas filled RFQ mass filter system used at Argonne National Laboratory.

# 4.1 Sector 1 of the Gas Filled RFQ Mass Filter System

A representation of the first sector of the RFQ system is seen in figure 4.1, followed by figure 4.2, a schematic diagram defining the important parameters. All ions are injected into this sector from the exit nozzle plate of the gas cell, a grounded plate with a 1.3mm diameter aperture. Both RF and DC voltages are applied to the rod segments. A simulation of the flow of helium gas from the gas cell into sector 1 is particularly important since this factor has a significant effect on the entry of the ions into the RFQ mass filter system. One of the main characteristics of this sector is its relatively high gas pressure, typically 0.25 to 1 torr.

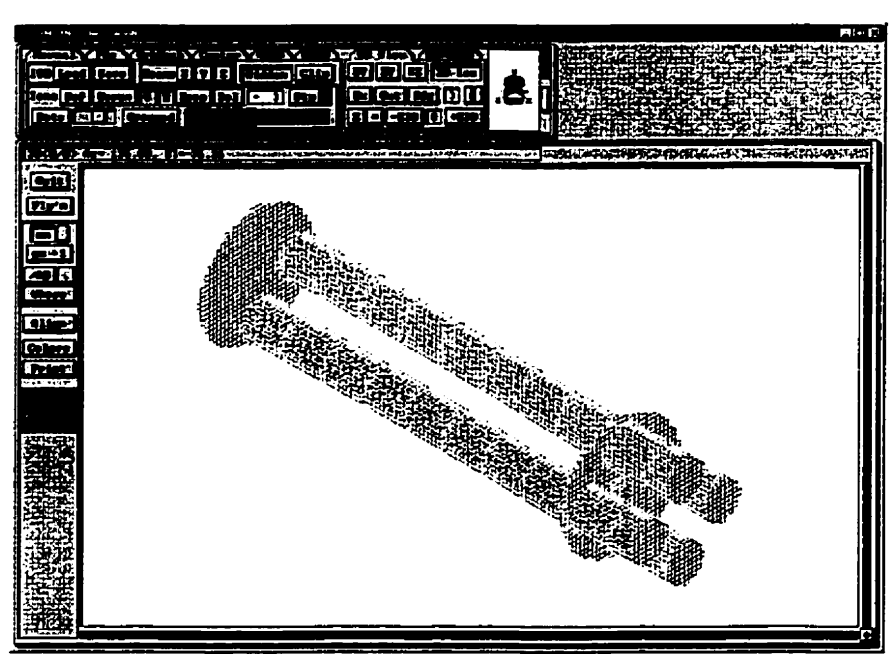


Figure 4.1: Model of sector 1; 4 rods of circular diameter segmented into 8 electrodes preceded by the gas cell nozzle plate (upper left corner) and followed by the nozzle plate between sectors 1 and 2, and 2 segment electrodes from sector 2.

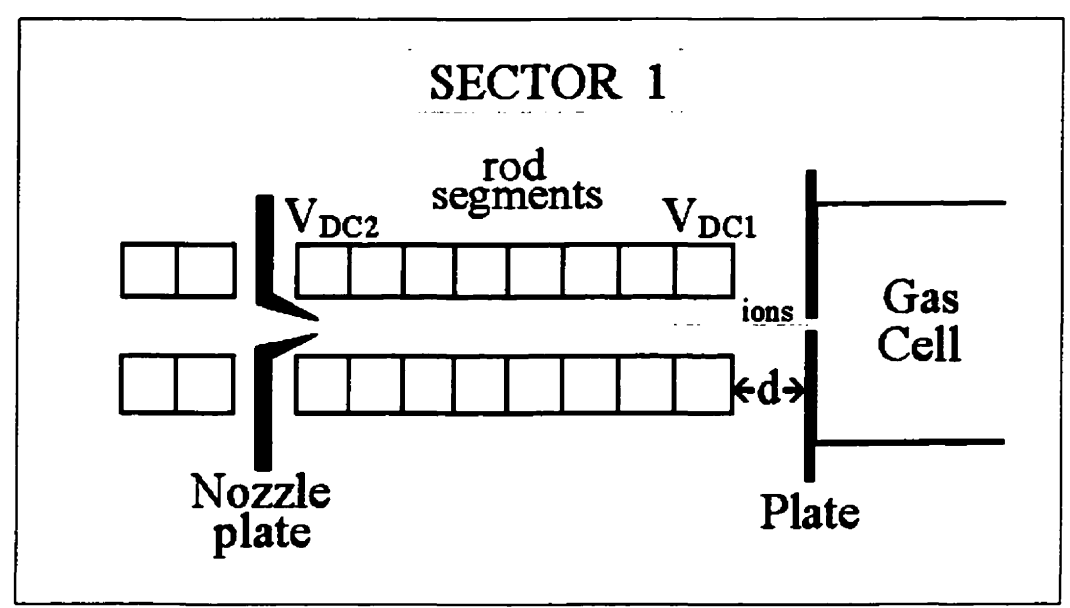


Figure 4.2: Schematics of sector 1. The ions are sent from the exit of the gas cell plate and enter the rod structure located at a distance d away from the plate. The gas cell is not included in the simulation but exiting velocities of ions from the gas cell are calculated and added to the simulation as an initial condition. The DC potential gradient along the rods is simply the difference between  $V_{DC1}$  and  $V_{DC2}$  over the length of the sector.

Electric potentials are applied to the rods such as to create a quadrupole field within the structure. The resulting equipotential field lines can be seen in figure 4.3, a cross-sectional view of the four rod electrodes of the RFQ mass filter system.

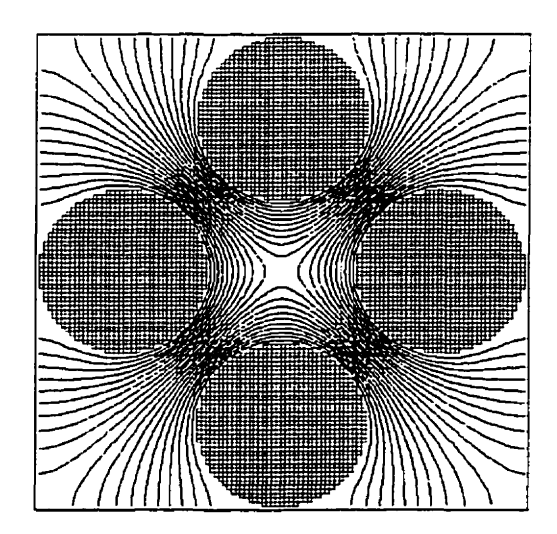


Figure 4.3: Cross section of the 4 rod structures with equipotentials created when potentials 180° out of phase are applied to each opposite pair of rods.

When an adequate RF potential is applied to the rods (about 280 Vp-p with a frequency of 788 kHz), ions are radially confined once they enter the rod structure. At a pressure of 0.4 torr, the mean free path of the ions is 0.2 mm and many collisions occur within the 160 mm long structure as the ions move along the axial, or z-direction. The radial trajectory of the ions gets sufficiently damped at this pressure and they can successfully enter the 2 mm diameter nozzle aperture at the end of the sector. Studies of the effects of varying certain parameters such as the distance of the rods from the gas cell plate, the ion's entrance velocity, the gas pressure in the sector, the RF potential amplitude, and the DC gradient along the rods are presented in the sections that follow.

# 4.1.1 Ion's Initial Velocity, Pressure in Sector 1, and Distance between Gas Cell Plate and Rods

In the region between the gas cell plate and the first rod segment of sector 1, the ions experience a repulsive force due to the fringing fields at the beginning of the rods. This force must be counterbalanced in order to get the ions transferred. In the following simulation, the RF voltage applied to the rods is 280 Vp-p at a frequency of 788 kHz, and there is a DC potential gradient of 0.5 V over the 160 mm long rod structure (3.125 V/m). The pressure in the sector is set to an initial value at the exit of the gas cell plate aperture and gradually decreases to 250 mtorr by the end of sector 1. This pressure gradient is based on a function that is inversely proportional to the square of both the radial and axial position coordinates of the ion. This approximation is assumed to be a good representation of the actual gas distribution in sector 1 of the gas filled RFQ mass filter system at ANL. The initial gas pressure or the initial forward velocity of the ions can

then be varied and the effects on transfer efficiency observed. Figure 4.4 shows a diagram of the ions injected from the gas cell plate aperture into sector 1 for various initial ion velocities and pressures while keeping the rods of sector 1 20 mm away from the gas cell plate.

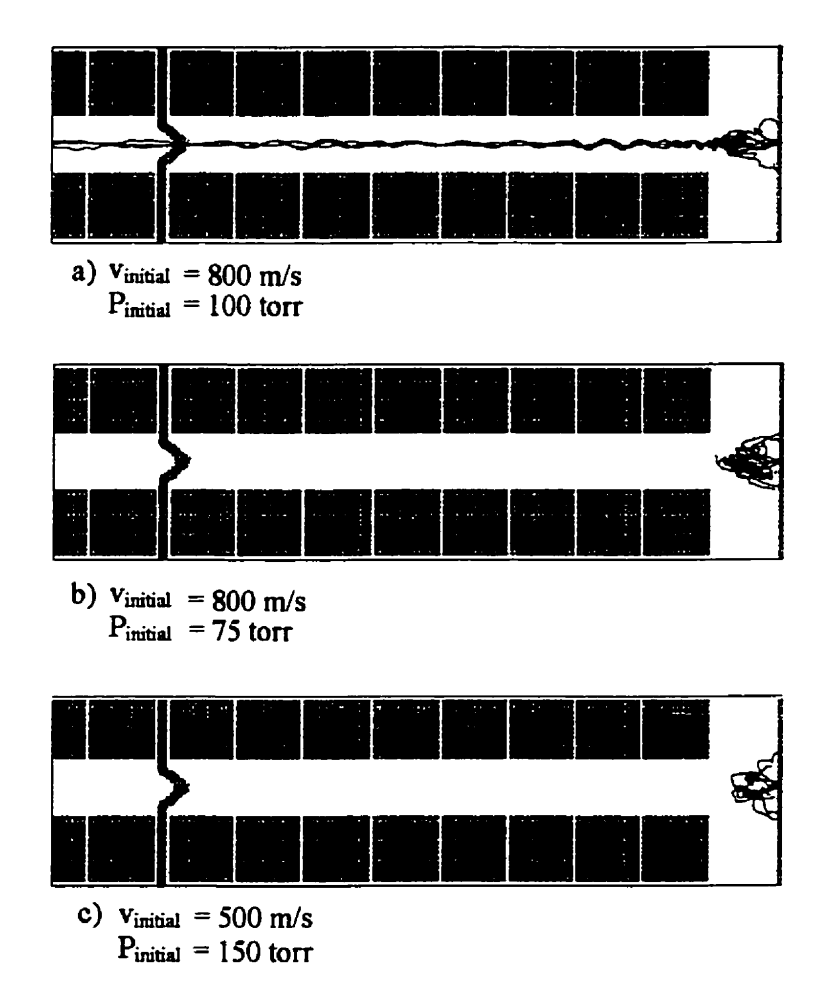


Figure 4.4: The ions' trajectories through sector 1 for different initial ion velocities and initial pressures at the exit aperture of the gas cell plate (to the right); a) the initial velocity is 800 m/s and pressure is 100 torr, b) the pressure is reduced to 75 torr, c) the initial velocity is reduced to 500 m/s and pressure increased to 150 torr.

The above diagram shows that ions having an initial velocity of 800 m/s get transferred if the initial pressure is 100 torr, but do not get transferred if the initial pressure is 75 torr. Instead, the ions are repelled back from the rods and end up hitting the gas cell exit plate. One also sees that an initial velocity of 500 m/s is insufficient to

transmit the ions even if the gas pressure is increased to 150 torr. This test demonstrates the importance of these parameters.

To minimize this repulsion effect, the distance between the gas cell plate and sector 1 is reduced. Figure 4.5 shows the equipotential field lines inside sector 1 and the resulting transmission of ions when d is varied from 10 mm to 20 mm.

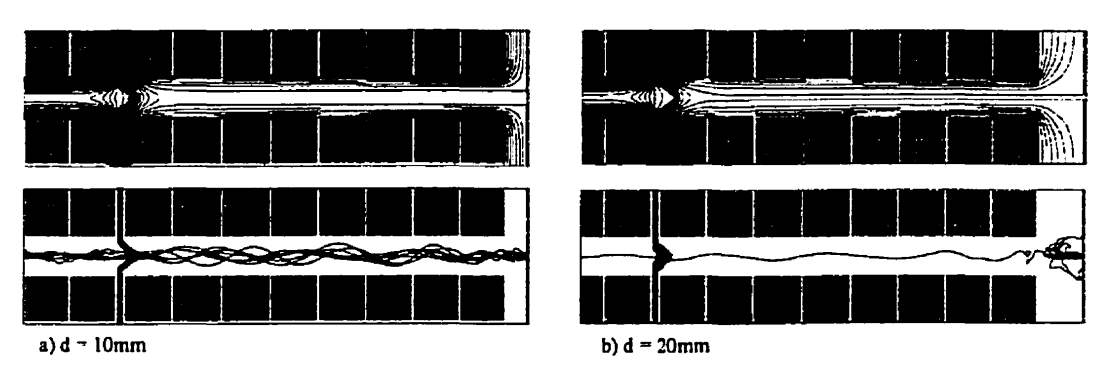


Figure 4.5: Representation of equipotential field lines along the axial (z) direction (top picture) and trajectory of ions (bottom picture) for a) distance between the gas cell and sector 1 of 10 mm and b) distance between the gas cell and sector 1 of 20 mm. The RF potential is 100 Vp-p at a frequency of 788 kHz and the DC potential gradient along sector 1 rods is 0.5 V over 160 mm (3.125V/m) in both cases.

The above diagram clearly indicates that ions are more effectively transmitted through the sector if the rods of sector 1 are closer to the exit plate of the gas cell.

# 4.1.2 RF Potential Amplitude of Sector 1

The effect of varying the RF potential amplitude applied to the rods on the transfer of ions is studied. In this simulation 100 ions of mass 105 a.m.u. and 145 a.m.u. are injected into sector 1. The initial pressure, ion velocity, DC potential gradient on the rods and RF frequency are kept constant and similar to experimental conditions. The resulting transmission through the sector is plotted in figure 4.6.

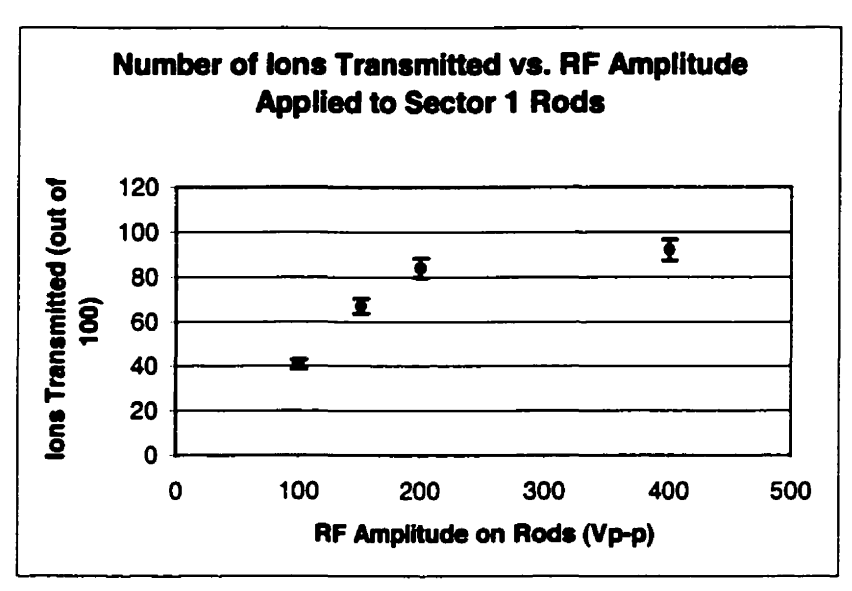


Figure 4.6: Plot of the number of ions transmitted through sector 1 as a function of the RF amplitude applied to sector 1 rods.

Not only does the RF amplitude affect the stability of ions within the rod structure, but it also influences the entry of the ions into the structure. At a fixed RF frequency of 788 kHz, the number of ions successfully entering the rod structures increases for greater RF amplitude and seems to plateau at about 400 Vp-p. Upon entry of the ions, greater amplitudes exert a stronger radially confining force which is especially important in this region.

#### 4.1.3 Effect of the DC Gradient on Transfer

Finally, the DC potential gradient applied along the rod electrodes ( $V_{DC2} - V_{DC1}$ ) is studied. Gradients ranging from 10 V to -1 V over 160 mm (62.5 V/m to -6.25 V/m respectively) are applied and found not to significantly affect the number of ions transmitted. One can conclude that the potential gradient is far less crucial than the gas flow in guiding the ions forward in this sector. A lack of sensitivity is also seen when varying the DC potential difference between the gas cell aperture plate and the first

segment of sector 1. For example, when an RF amplitude of 280 Vp-p is applied to the rods and the potential gradient is 1 V over the whole sector (6.25 V/m), about 80% of the injected ions are adequately transferred even when the gas cell plate is at 0V and the first segment is at 3V (creating a 3V potential "hill" that the ions have to climb). The potential applied to the first segment has to be raised to 10 V in order to stop the transfer of ions. This once again indicates that the gas flow in this region is the overwhelming contributor to ion transport.

### 4.1.4 Summary of Sector 1 Tests

The simulation indicates that parameters such as the distance of the rods from the gas cell plate, the initial velocity of the ions from the gas cell, the helium gas pressure in this region, and the RF amplitude applied to the rods all play important roles in the entry and capture of ions into this sector. Once the ions are confined inside the rods, the RF potential and DC gradient along the structure are less crucial as long as kept within a reasonable range of values. Table 4.1 summarizes the approximate ranges of operation for the variable parameters mentioned above. Here one must keep in mind that even if values that are out of a parameter's ideal range of operation are used, other parameters can be modified to compensate and a good transmission efficiency can still be achieved.

Table 4.1: Summary of the range of operation for sector 1 parameters.

Parameter	Range of operation		
Distance of rods to gas cell plate, d	Less than 20 mm		
Initial ion velocity	Over 600 m/s		
Initial pressure	Over 100 torr		
RF potential amplitude	Over 280 Vp-p		
$\Delta V$ between gas cell plate and 1 <sup>st</sup> segment of sector 1	Less than 10 V		
DC gradient along rods	-1 V to 10 V over 160 mm (-6.25 to 62.5 V/m)		

# 4.2 Sector 2 of the Gas Filled RFQ Mass Filter System

The geometry of electrodes used for the simulation of sector 2 is seen in figure 4.7 and a schematic diagram follows in figure 4.8. This reproduction includes the 10 rod segments of sector 2, the nozzle plates which precede and follow it, and 2 rod segments from sector 1 and sector 3 on either side. Applied DC and RF potentials and gas pressures are chosen to mimic the experimental operating conditions. The flow and pressure of the gas between the sectors within the dividing nozzles is determined by an extra subroutine to the simulation program. This treatment is previously described at the beginning of chapter 4. In the region between the two nozzle plates, the velocity of the ions due to gas flow and the pressure are kept constant.

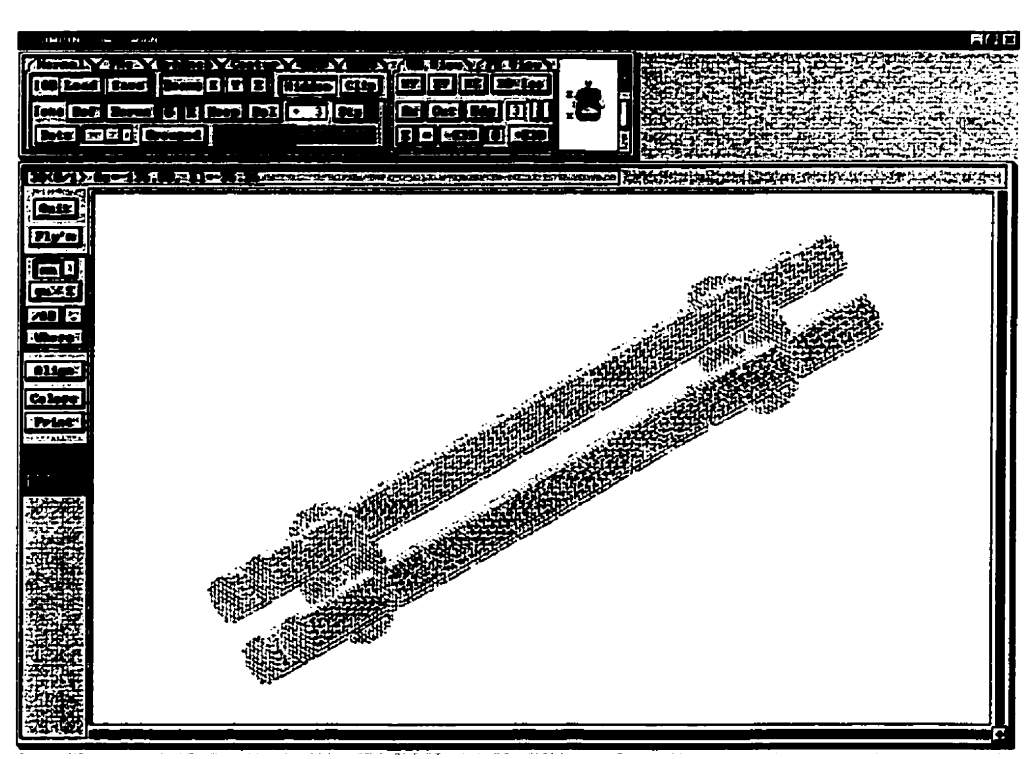


Figure 4.7: Model of Sector 2. The ions enter the 10 segments of sector 2 rods through the nozzle plate between sectors 1 and 2 (lower left corner).

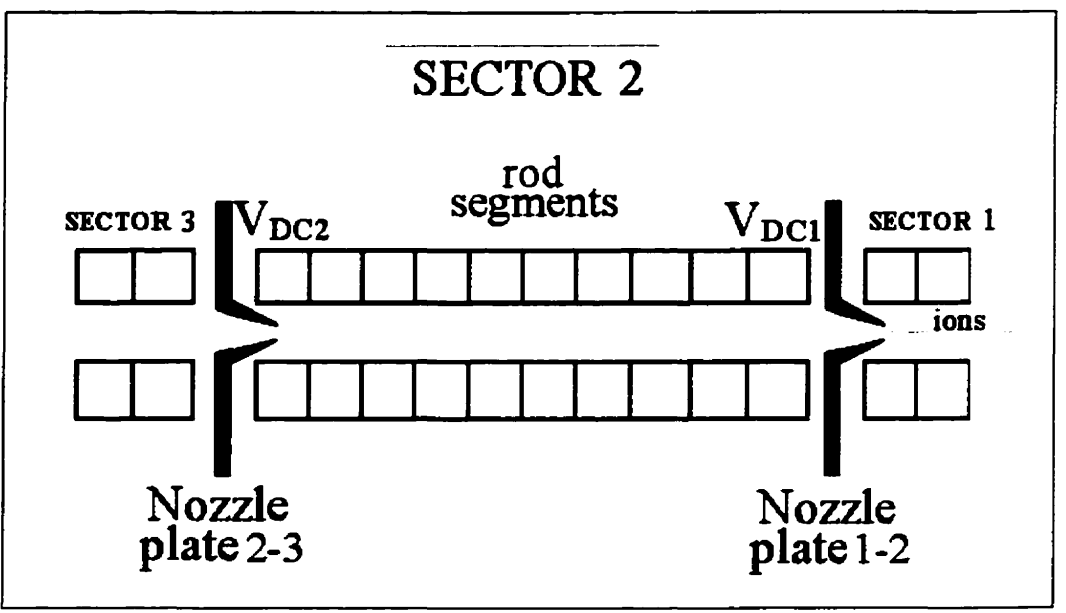


Figure 4.8: Schematic diagram of sector 2 simulation. Ions are injected from the last few segments of sector 1.

The main functions of sector 2 are: 1) to damp the trajectory of the ions radially with the buffer gas so that they can enter sector 3 close to the axial origin, and 2) to select certain ions according to their mass and filter out unwanted species. The variable parameters used to optimize the two functions are investigated in the following sections.

#### 4.2.1 Effect of the DC Gradient and Gas Pressure in Sector 2

Several tests are conducted to examine the effects of the DC potential gradient along the structure and the operation pressure. First the DC gradient along the rods is varied and ions are injected into sector 2 for four different gas pressures. The number of ions transmitted through the nozzle at the end of sector 2 is counted and results are summarized in figure 4.9.

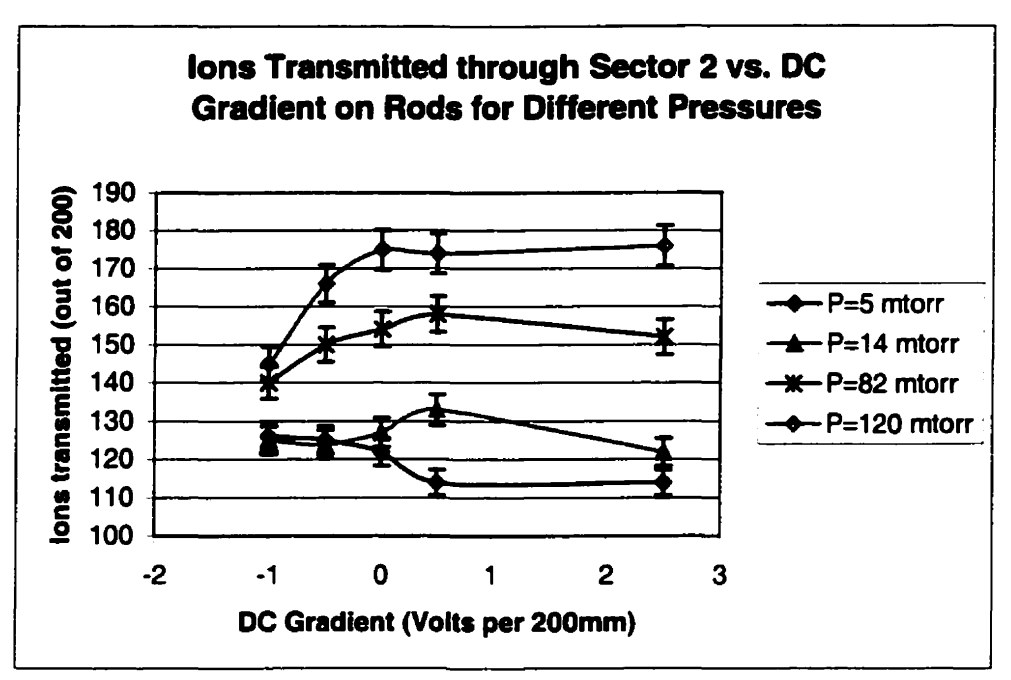


Figure 4.9: Ion transmission for different pressures and DC gradients along the rods of sector 2.

The key to proper transfer lies in damping the radial motion of the ions within the 200mm long structure before they reach the second nozzle aperture of only 2mm in diameter at the end of the sector. One can conclude from this simulation that higher pressures lead to better transmission efficiencies since the mean free path of ions is reduced and greater damping occurs. The mean free paths in 5 mtorr, 14 mtorr, 82 mtorr and 120 mtorr of helium gas are 16 mm, 6 mm, 1 mm, and 0.7 mm respectively. The DC gradient along the rods is also seen to affect the transmission. At lower pressures a large gradient increases the ion's axial kinetic energy and does not allow for proper damping of the ion's motion before it gets to the nozzle aperture. On the other hand a negative DC gradient tends to trap the ions in the sector, especially at higher pressures such as 120 mtorr. The motion of ions with mass of 145 a.m.u. in the xz plane for different pressures

is depicted in figure 4.10. Here the DC gradient along the rods is 0.5 V over 200 mm (2.5 V/m), U = 0V and V = 225 Vp-p with f = 550 kHz.

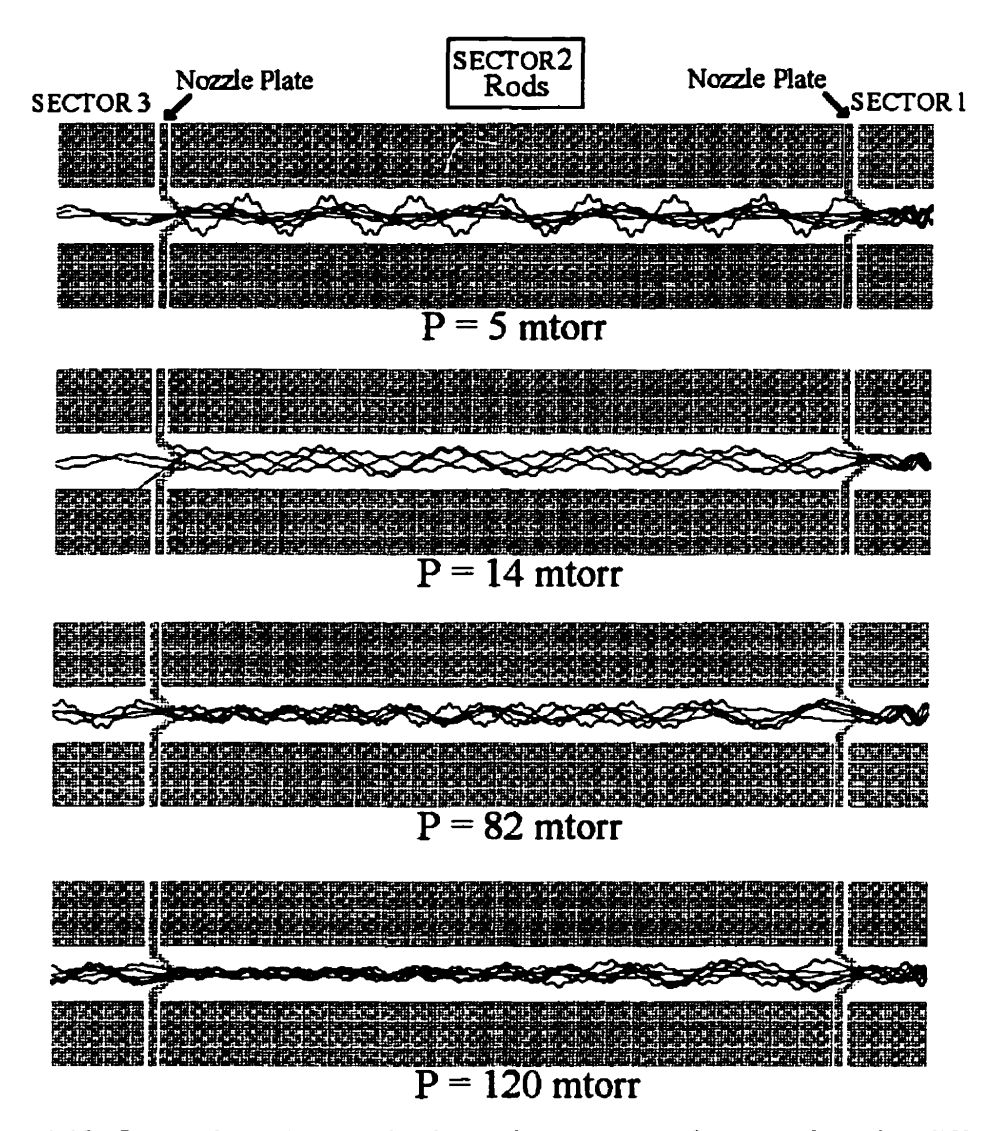


Figure 4.10: Ion trajectories inside the rod structures of sector 2 under different pressures as seen from xz plane. At lower pressures, fewer ions get transferred since they hit the nozzle plate between sectors 2 and 3.

One clearly sees the ion trajectories being more significantly damped as the pressure in the rod sector is increased, explaining the better transfer efficiency. Figure 4.11 shows the trajectory ions in sector 2 for different DC gradients. Gradients of +2.5V and -1 V

over 200 mm (12.5 V/m and -5V/m respectively) are compared for pressures of 14 mtorr and 120 mtorr.

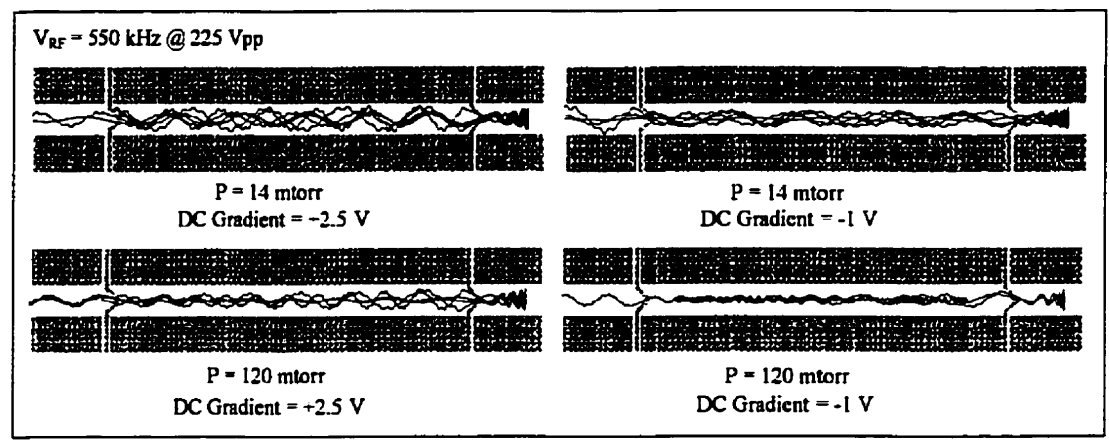


Figure 4.11: Ion trajectories under different DC gradients seen from xz-plane. The RF potential applied to the roes is 225 Vp-p at 550 kHz, and U = 0V.

The above diagram shows the close interrelation between the DC gradient and pressure of sector 2. A reasonable transfer efficiency can be conserved even at lower pressures if the DC gradient is also adequately reduced. Special notice should be given to the -1V DC gradient, 120 mtorr model (bottom right) where ions are seen getting trapped inside sector 2. At this pressure, many collisions occur and the initial kinetic energy of the ions and the gas flow are not sufficient to guide the ions forward against the repulsing potential gradient.

# 4.2.2 Sector 2 Mass Filtering

A DC potential U can be applied between pairs of opposite rods in order to change the mass acceptance of the system and use sector 2 as a mass filter of transmitted ions (see section 2.1.1). Ions of a given mass become unstable in the x-direction if the applied frequency is too high and in the y-direction if the frequency is too low. This effect is seen in figure 4.12. Here a DC offset of U = 20 V is put between pairs of opposite rods

and the RF amplitude is V = 225 Vp-p. The frequency used in the first graph is 545kHz and 365kHz in the one below. Both show the trajectories of ions with a mass of 145 a.m.u., and the pressure in the sector is 82 mtorr.

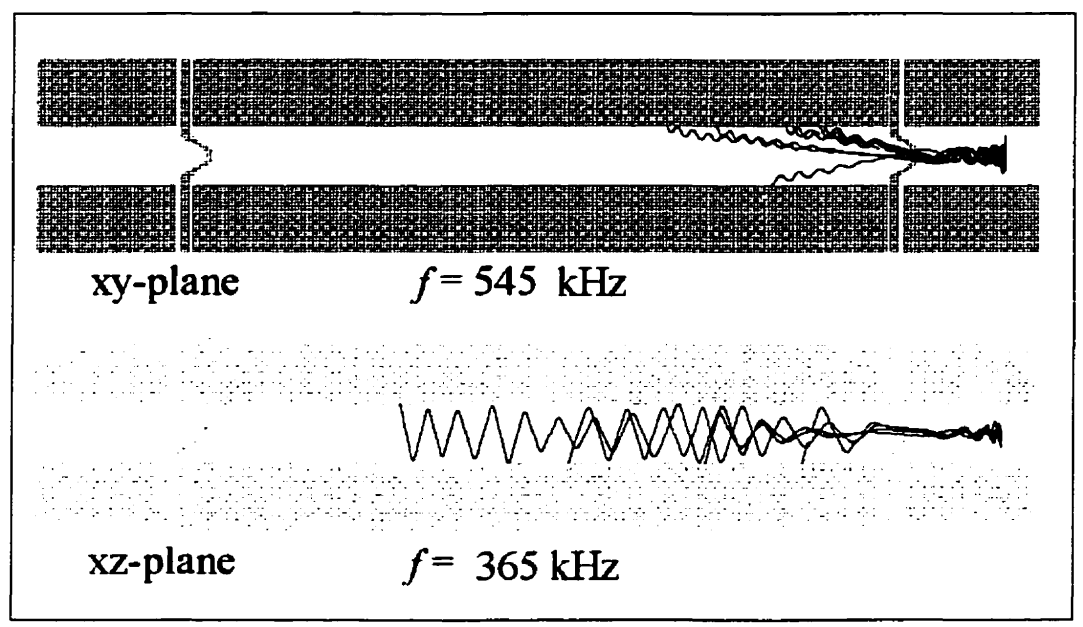


Figure 4.12: Ion trajectories in xz and yz planes. At higher frequencies, ions are unstable in the x-direction and at lower frequencies they are unstable in the y-direction.

To find the stability region for ions in the device, the following mass filter simulation can be performed. Ions of mass 149 a.m.u. are injected into sector 2. For a given U value applied to the rods the maximum and minimum frequencies at which half of the ions are successfully transferred to the end of the sector are noted. These frequencies are taken as cut-off frequencies for the ion's stability. These values are then used to calculate the a and q parameters defined in equations (2.4.10) and (2.4.11). Plotting a versus q will give the stability region of ions under such conditions. Figure 4.13 shows the stability region obtained with the simulation for ions of mass 149 a.m.u. when an RF potential amplitude of 225 Vp-p is applied to the rod segments of sector 2.

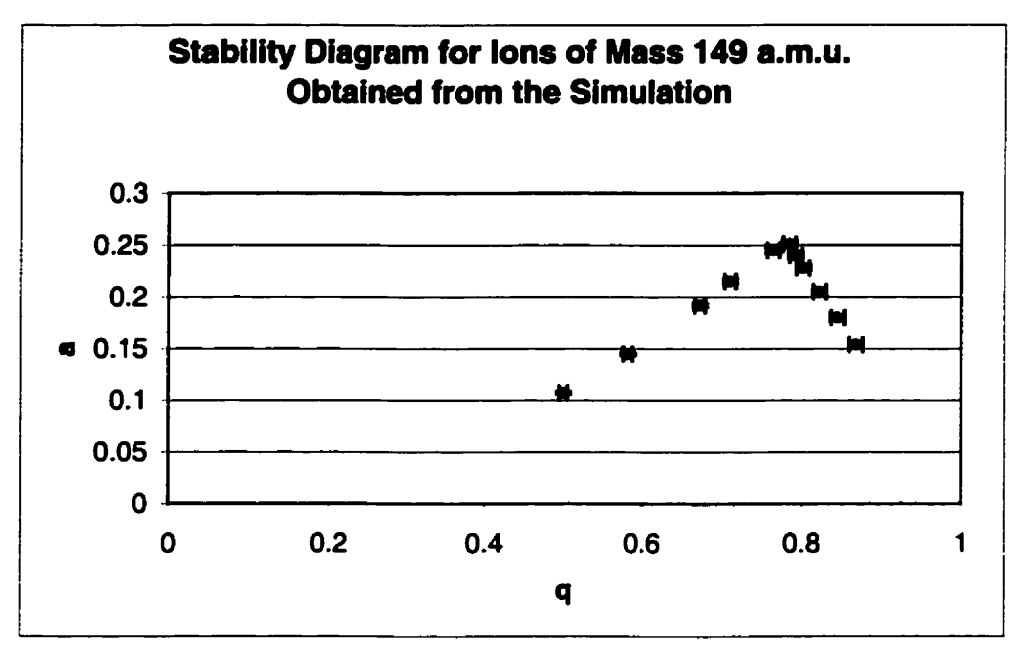


Figure 4.13: Stability diagram for sector 2 mass filter. The region under the triangular curve is where the ions are considered to have stable trajectories in both the x and y-directions.

The curve obtained with the simulation is similar to the one dictated by the Mathieu equation although the peak q value seems slightly shifted towards the right of the diagram. The peak q value of  $0.78 \pm 0.01$  from the simulation differs by 10% from the theoretical value of 0.706 (see section 2.1). This can be due to the addition of gas in the system, a parameter not considered in the theoretical stability diagram.

# 4.2.3 Nozzle Geometry

The geometry of the nozzles mounted on the plates dividing each RFQ system sector plays an important role in the transfer efficiency. However, the flow of gas and ions through a nozzle aperture involves many complex properties of ion and flow dynamics. A perfect simulation is therefore difficult, but a general treatment of the gas flow and pressure such as the one described at the beginning of chapter 4 is assumed to give a fairly accurate representation of the behavior of ions through the nozzles. The transfer

efficiency of ions going through the nozzle aperture plate dividing two sectors of the gas filled RFQ mass filter system is explored for various geometry of nozzles. In this simulation, ions are injected from the last few segments of sector 1, into the nozzle. The pressure difference between the two sectors is 0.17 torr (0.25 torr in sector 1 and 0.08 torr in sector 2). Both the opening angles and lengths of the nozzles are varied, but the entrance aperture remains at 2 mm in diameter. The transfer efficiency through the nozzle is observed and results are given in figure 4.14.

Nozzle Geometry	O I		SHAME AND STATE			
Outer Opening Angle,O	80°	80°	180°	80°	90°	102°
Inner Opening Angle,I	60°	34°	60°	30°	60°	60°
Nozzle Length, L	36 mm	36 mm	10 mm	22 mm	28 mm	18 mm
Transmission Efficiency	93 %	55 %	69%	76%	93 %	70 %

Figure 4.14: Transmission efficiency of ions injected into various nozzle geometries. In the above diagrams, the ions enter the nozzle from the right side.

One notices from the above figure that generally, longer nozzles have a better transfer efficiency. The same can be said for nozzles with a larger inner opening angle. But this parameter also has an effect on how the ions exit the nozzle and move into the following sector. For example, ions ejected from a nozzle with a larger exit angle will have a greater radial position distribution, and their trajectories might not undergo

enough damping for the ions to enter the subsequent sector's nozzle aperture. Of course this effect is mostly important when the sector is at a low pressure and the mean free path is large. Other factors such as the DC potential applied to the nozzle relative to the rod segments and the entrance aperture size are also involved in the transfer efficiency. Since all of the above parameters are in some way related, further tests are needed to evaluate the importance of each one of them. For this thesis, the interest mainly lies in confirming that the nozzles that are currently used in the gas filled RFQ mass filter system at ANL are of adequate geometry. This is seems to be the case since the nozzle that is used (35 mm long with 60° inner opening angle) gives a transfer efficiency of 93% in the simulation results.

#### 4.2.4 Summary of Sector 2 Tests

In sector 2, the pressure and the DC gradient along the rods are closely related since both affect the amount of damping the ions will get inside the structure. The RF amplitude and frequency depend on the stability requirements of a particular ion, which varies with the ion's mass and charge. For singly charged ions of mass above 60 a.m.u. an RF amplitude of around 250 Vp-p with a frequency of 550 kHz is adequate for stability when the sector is used without its mass filtering capabilities (U = 0). A non-zero U can also be applied if one wishes to use the sector as a mass selective filter of variable resolution. The mass filter's highest resolution is found at a q value of 0.78±0.01. The nozzle geometry is important in both the entry and exit of the ions into neighboring sectors. An overview of the parameters' ranges of operation is given in table 4.2.

Table 4.2: Summary of ranges of operation for sector 2's parameters.

Parameter	Range of operation		
Helium gas pressure	over 80 mtorr		
DC gradient	-0.5 V to 2.5 V over 200 mm (-2.5 V/m to +12.5 V/m)		
RF amplitude and frequency (ions with mass above 60 a.m.u.)	250 Vp-p at frequency of 550 kHz		
Nozzle opening angle	60 degrees		
Nozzle length	20mm to 40 mm		

# 4.3 Sector 3 of the Gas Filled RFQ Mass Filter System

The electrode structure of sector 3 is seen in figure 4.15 and a schematic diagram follows in figure 4.16. The model also includes simulations of the gas flow and pressure within the system. Two segment electrodes from the previous sector and the nozzle plate that divides them are included to make the injection of the ions into sector 3 more realistic.

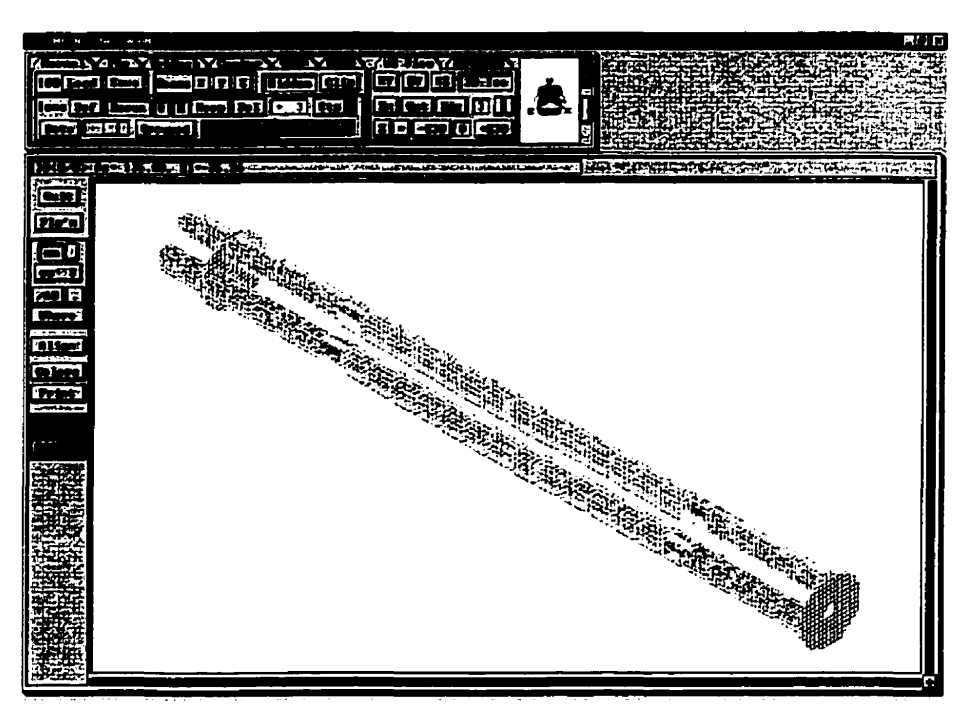


Figure 4.15: Model of sector 3. Ions enter the 25-segment rod structure through the nozzle plate between sections 2 and 3 (upper left corner). They exit the sector through a flat plate with a 6 mm aperture.

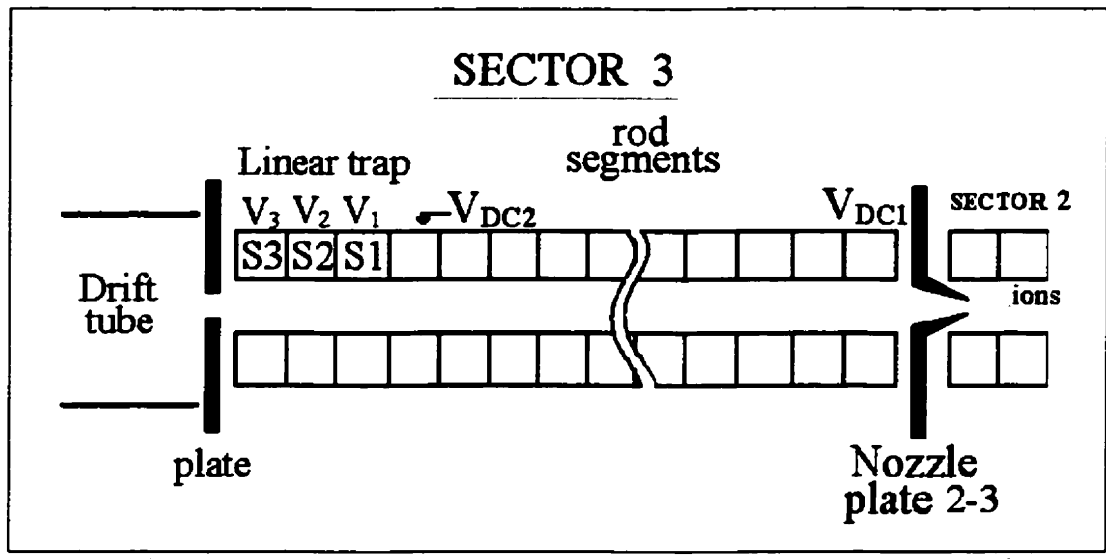


Figure 4.16: Schematic diagram for the simulated sector 3. Ions are injected from the last few segments of sector 2. The DC gradient along the segments is simply the potential difference between  $V_{DC1}$  and  $V_{DC2}$  over the length or the sector. The last 3 segments are used as a linear trap, with applied voltages  $V_1$ ,  $V_2$ , and  $V_3$  on electrodes named S1, S2, and S3 respectively. The last plate before the drift tube is also part of the linear trap, with the same pulsed voltage as the one applied to the last rod segment.

As previously described in section 3.3.2, the last 3 rod segments of sector 3 are used as a linear trap by applying a lower DC potential to the middle segment and setting the potential on the last plate at a higher value, typically 10 to 15 volts above the last segment. This creates a potential well where ions can be accumulated. Ions entering sector 3 go back and forth throughout the structure until they lose enough energy through helium gas collisions to fall into the potential well where they are further cooled and trapped. To eject ions from the trap a positive ejection pulse is applied to S1 and a negative pulse of the same amplitude and width is applied to S3 and the last plate. This quickly sends the bunched ions through the last plate's aperture into a 30 cm drift tube set at -1500 V. It is then possible to extract time-of-flight (TOF) and energy distribution information at the end of the drift tube for the bunched ions under different experimental circumstances.

A number of conditions affecting the transfer efficiency in sector 3 are examined and discussed in the following section. Namely, tests are executed to study the effect of the DC potential gradient applied to the rod electrodes, the cooling time of ions in the linear trap at different pressures, the depth of the potential well of the linear trap, and the ejection pulse width, amplitude and rate of application.

#### 4.3.1 The Effect of the DC Gradient on Transfer

By varying the DC potential gradient along the rods of sector 3, one changes the axial kinetic energy the ions acquire as they travel along the sector. The effect of changing this parameter is explored and the trapping and transmission of ions is found to remain more or less constant until the DC gradient is excessively high. Ions then gain too much axial kinetic energy and hit the last plate before they can get captured. This is seen with a 10 V gradient across the 440 mm rods (22.7 V/m) with  $2x10^{-4}$  torr of helium inside sector 3. A general conclusion is that the DC gradient along the segmented rods used to guide the ions forward is best kept reasonably small especially when the pressure is low.

# 4.3.2 Cooling Time of Ions in Linear Trap

Once the ions enter sector 3 and fall into the linear trap, they undergo collisions with the helium gas and lose energy. This "cooling" time is dependent on the mean free path of the ions related to the helium gas pressure in the sector. Higher gas pressures lead to more ion collisions and effective cooling. The mean free path of ions can be calculated from equation (2.4.20). For example, ions in 10<sup>-4</sup> torr of helium have a mean free path of 78 cm and as a result have to travel back and forth many times inside the trap before

experiencing a collision. On the other hand, the mean free path is 7.8 cm at a pressure of  $10^{-3}$  torr and such a condition makes it possible for the ions to get cooled more rapidly. The simulation of sector 3 is used to find this cooling time by performing the following test. Ions are injected into sector 3's linear trap for various pressures while keeping the trap depth at 2 V, and the RF potential on the segments at 350 Vp-p with a frequency of 650 kHz. The time taken by the ions to be cooled to a given energy is noted. Results are shown in figure 4.17.

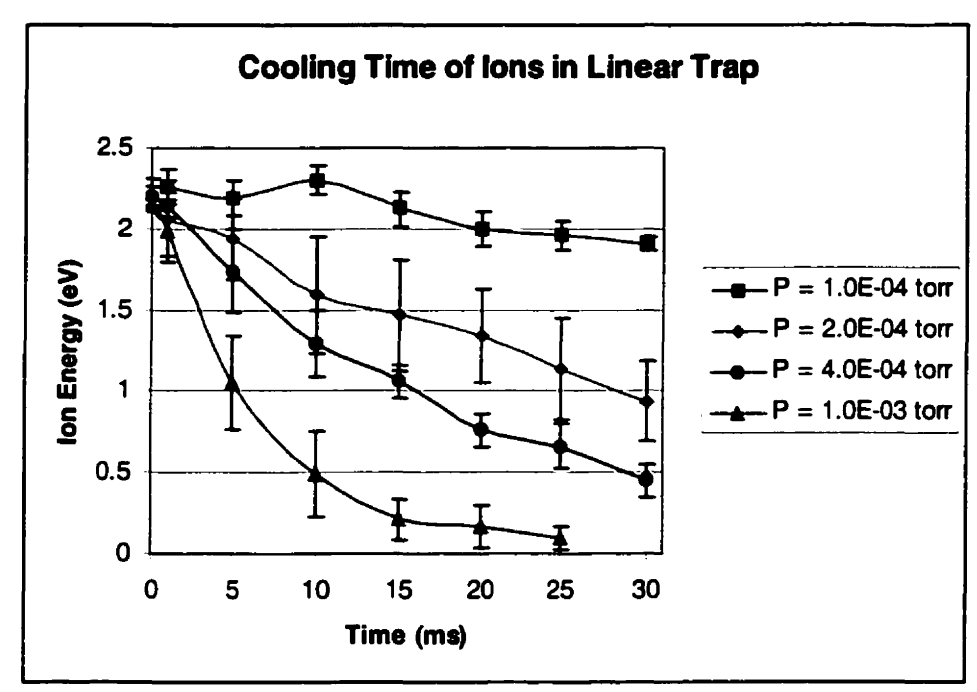


Figure 4.17: Time taken for ions in sector 3's linear trap to get cooled to a given energy.

One can see from the above plot that the cooling time is inversely related to the pressure in the system. Such a factor needs to be taken into consideration while setting an ejection rate for the linear trap. Most ions should remain inside the trap long enough to be cooled before being ejected.

#### 4.3.3 Capture and Ejection in the Linear Trap

When the ions reach the trap and fall into the potential well, they oscillate back and forth in the z-direction (axial direction). They also undergo the radial oscillations governed by the RFQ mass filter system's applied RF potentials. Therefore, when the ejection pulse is applied, ions may not necessarily be in the middle of the trap, but will rather have a distribution in position and energy within the trap. This "cloud" of ions is sent into the drift tube with an energy distribution that should remain constant after ejection, and that depends on the applied electrode and pulse voltages. On the other hand, the time-offlight (TOF) distribution will also depend on the distance the ions travel before the measurement is taken. The effects of the ejection pulse's width, amplitude, and rate, as well as the depth of the linear trap on the transmission yield and the TOF and energy spreads of the ion bunches in the drift tube are studied. Since the TOF and energy spreads have an effect on the ion capture efficiency of the CPT mass spectrometer's Paul trap, which follows the linear trap in the experimental set-up at ANL (see section 3.2.5), it is important to study the linear trap's capture and ejection conditions [Mar98, Fuk00]. The goal is to understand how to manipulate the extraction parameters in order to minimize the TOF and energy spreads while retaining an optimal transfer efficiency.

It should be noted that ion-ion interactions inside the linear trap are considered negligible and therefore omitted from the simulation.

First, the effect of varying the linear trap's potential well depth while keeping all other parameters constant is considered. Since the test results will depend on the location at which the ions are detected, all measurements are taken at the end of the 30 cm drift tube after the linear trap. Ions of mass 145 a.m.u. are injected into sector 3 which is kept

at a pressure of  $2x10^4$  torr. The ejection pulse is applied at a rate of 100 Hz. A short summary of the results of this test along with the subsequently described linear trap tests is given in table 4.3. It is found that the TOF spread of the bunched ions can be initially reduced by increasing the depth of the trap. The energy spread of the ions at the end of the drift tube is also seen to go down as the trap depth is increased. However, it is observed that for larger trap depth, the radial stability of the ions starts to get affected. This could be due to the fact that the field lines are not parallel to the axial direction in the trap area and ions may acquire a greater radial velocity once they enter the trap if the potential difference between the segments is increased. Consequently, ions can hit the electrodes and be lost. Indeed, the transfer efficiency is reduced by a few percent when the trap depth is 20 V and to 48±1 % when the trap depth potential is 40 V.

Next, the amplitude of the ejection pulse is varied to find the resulting effects. It is found that pulses of greater amplitude do not affect the transfer efficiency but increase the energy spread and reduce the TOF spread of the ejected ions. For example, the energy spread after ejection approximately quadruples when the pulse amplitude is increased from 85 V to 350 V with other parameters constant, while the TOF spread is reduced from 0.70 to  $0.100~\mu s$ . Other examples are seen in table 4.3.

It is important for the pulse to be applied for a sufficiently long time for all the ions inside the trap to be ejected. The effect of varying the pulse width is tested, and pulses shorter than 7  $\mu$ s in width are found to be insufficient for proper transfer. The energy and TOF spreads are otherwise comparable for pulse widths in the 7  $\mu$ s to 100  $\mu$ s range. These results are also summarized in table 4.3.

Table 4.3: Transfer efficiency, time-of-flight (TOF) spread and energy spread of ions captured and ejected from linear trap for different trap depths, pulse widths, and pulse amplitudes.

Trap Depth	Trap Depth Pulse Width		TOF Spread	Energy	Transfer	
(V)	(μs)	Amplitude	(μs)	Spread (eV)	Efficiency	
		(V)			(%)	
2.0	100	± 85.0	0.70±0.05	28±1	88±1	
2.0	100	± 350.0	0.100±0.003	111±3	91±1	
2.0	7.0	± 350.0	0.100±0.003	123±3	92±1	
2.0	7.0	± 85.0	0.40±0.02	22.4±0.6	88±1	
8.0	100	± 350.0	0.100±0.003	46±2	88±1	
8.0	100	± 85.0	0.60±0.1	16.3±0.5	92±1	
20.0	100	± 85.0	0.30±0.01	9.8±0.3	84±1	
20.0	100	± 350.0	0.100±0.002	37±1	83±1	
40.0	100	± 85.0	0.20±0.01	9.0±0.6	48±1	

The repetition rate at which the pulses are applied determines how long the ions remain in the trap and therefore how much cooling they undergo before ejection. In the following test, the ejection rate of the linear trap is varied and resulting transmission is observed. Results are plotted in figure 4.18. In all cases the pulse width is  $100 \mu s$ , the pulse amplitude is  $\pm 85 V$ , and the trap depth is 2 V.

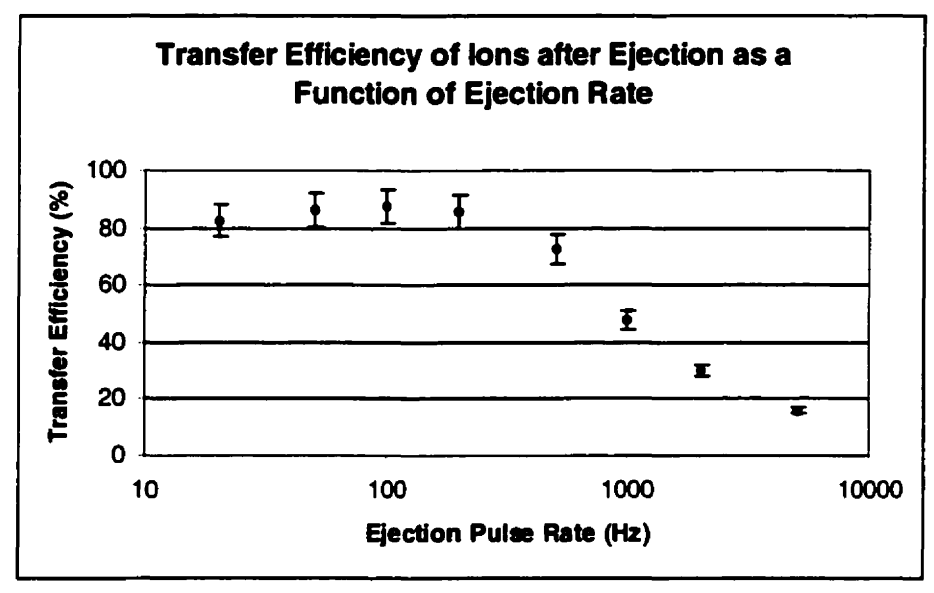


Figure 4.18: Study of the number of ions transferred into the drift tube for different ejection pulse rates.

An inverse relationship between the efficiency of ion transfer and the rate of ejection is seen in the figure above. With higher ejection rates, the ions do not get a chance to be fully cooled in the trap before ejection. Also, in this case S1 is found in the +85 V "ejection" mode more frequently and some of the ions never enter the trap. They are instead sent back to hit the nozzle plate at the entrance of sector 3.

#### 4.3.4 Summary of Sector 3 Tests

For this sector of the gas filled RFQ mass filter system, one needs parameters that enable ions to get properly transferred to the linear trap which can capture, cool, an bunch the ions before being ejected into the subsequent mass spectrometer system. The two main factors controlling the transport and capture of ions into the linear trap are the pressure in the sector and the DC gradient along the rods. Because of the requirements of the mass spectrometer system, the pressure must remain low so the DC gradient must also be kept small. Stability conditions involving the RF potential amplitude and frequency are important but less crucial since the ions entering the sector are already close to the axial origin. An increase in trap depth reduces both the TOF and energy spreads of the ions but larger trap depths of 20 V and 40 V reduce transfer efficiency. Once the ions are trapped, ejection parameters like pulse width and pulsing rate have a considerable effect on the transmission efficiency. The pulse needs to be wide enough so that all ions inside the trap get ejected, and it has to be applied at a slow enough rate for the ions to get sufficiently cooled before ejection. The pulse amplitude does not seem to affect the overall transfer efficiency, but does influence the TOF and energy spread of the ejected ions. Greater pulse amplitudes result in larger energy spreads and smaller TOF spreads.

A table summarizing the range of operation for the parameters of sector 3 and its linear trap follows in table 4.4.

Table 4.4: Summary of ranges of operation for sector 3's parameters.

Parameter	Range of operation				
Helium pressure	over 2x10 <sup>-4</sup> torr				
DC gradient	0 V to 5 V over 440 mm (0 V/m to 11 V/m)				
Linear trap depth	2 V to 8 V				
Linear trap pulse amplitude	85 V to 350 V				
Linear trap pulse width	over 7 µs				
Linear trap ejection rate	10 to 100 Hz				

## Chapter 5

# Off-Line Testing of the Gas Filled RFQ Mass Filter System

To test the gas filled RFQ mass filter system, experiments are conducted with the use of a  $^{252}$ Cf fission source placed immediately before the entrance window of the gas cell. The most abundant fission fragments from this decaying source that have half-lives of under 3 minutes are listed in table 5.1.

Table 5.1: Most abundant fission products from a <sup>252</sup>Cf source.

Mass (amu)	Z	T <sub>1/2</sub> (s)	Cumulative Yield (%)	Z	T <sub>1/2</sub> (s)	Cumulative Yield (%)
94	Sr	85	0.547			
95	Sr	25.1	0.767			
96	Sr	1.06	0.888	Y	6.2	0.0545
98	Y	0.59	0.643	Zr	30.7	0.587
99	Zr	2.2	1.25	Y	1.47	1.15
100	Zr	7.1	2.06	Nb	1.5	0.285
101	Zr	2.1	2.2	Nb	7.1	1.3
102	Nb	1.3	2.04	Zr	2.9	1.45
103	Nb	1.5	3.06	Tc	54	0.057
104	Mo	60	2.83	Nb	4.8	2.15
105	Mo	36	3.02	Nb	3	0.999
106	Mo	8.4	3.47	Tc	36	2.19
107	Тс	21.2	3.63	Mo	3.5	2.01
108	Тс	5.1	3.33	Rh	17	0.0573
109	Ru	34.5	2.99	Tc	1.4	1.89
110	Ru	15	3.62	Rh	3.1	0.672

111	Rh	11	2.46	Ru	1.5	2.26
112	Rh	4	2.39	Ru	4.5	0.939
113	Rh	0.9	1.95			
114	Ag	4.6	0.913			
115	Pd	47	1.7			
116	Ag	160.8	0.65			
118	In	5	0.00264			
133	Sb	180	1.06			
137	I	24.5	1.57			
138	I	6.5	1			
139	Xe	39.7	3.5			
140	Xe	13.6	2.55			
141	Cs	24.9	3.79	Xe	1.72	1
142	Cs	1.8	2.53			
143	Ba	14.3	4.4			
144	Ba	11.4	3.37	La_	40.7	1.86
145	La	24	2.51	Ba	4	2.06
146	La	6.3	2.39	Ba	2.20	0.981
147	La	4.02	1.94	Ce	56	1.91
148	Ce	56	2.35	La	1.1	0.986
149	Ce	5.2	1.5	Pr	138	0.929
150	Pr	6.2	1.3	Ce	4.4	0.941
151	Pr	22.4	1.07			
153	Nd	28.9	0.799			

A gold foil is put right after the source to attenuate the energies of the fission fragments before they enter the helium filled gas cell. This allows the fragments to be adequately stopped inside the cell. Once the fragments are thermalized, the gas flow from the cell transports them into the RFQ mass filter system. They then pass through each of the three sectors of the system and are accumulated in the linear trap at the end of the third sector. The trapped fragments are subsequently ejected, and detectors placed after the linear trap can monitor the transfer efficiency. As previously described in section 3.4, two different detection methods are used to test the system. In one case, a micro-channel plate (MCP) detector is used to obtain the time-of-flight (TOF) spectrum of the ions ejected from the linear trap. Alternatively, a silicon detector can be used to

monitor the radioactivity of the transmitted ions. The total RFQ mass filter system transfer efficiency can be assessed by comparing the yields of this silicon detector to the yields obtained from an additional silicon detector that can be temporarily put right at the exit of the gas cell.

The operating parameters of the gas filled RFQ mass filter system are experimentally studied by using the <sup>252</sup>Cf fission fragments as a source of ions. Each of the three sectors is tested individually and the following sections describe the performed studies and their results.

#### 5.1 Sector 1 of the Gas Filled RFQ Mass Filter System

As discussed in section 4.1, the main purpose of this sector is to successfully capture and transport the fission fragments that exit the gas cell while getting rid of the gas. The particular features affecting transfer include a strong gas flow from the cell, calculated to be around 700 m/s, and a relatively high gas pressure of roughly 0.5 torr. Here numerous ion collisions with the gas occur resulting in a mean free path of about 0.15 mm. Because of this feature, sector 1 does not need to be of great length since the radial trajectory of the ionized fragments is quickly damped.

Other parameters like several DC potential differences along the rods of sector 1 and the RF potential applied to the rods can be additionally helpful in guiding the ions into and through this sector. In the sections that follow, the effects of varying these parameters are studied to ultimately achieve the best possible transfer efficiency.

#### 5.1.1 The DC Potentials

Three DC potential parameters can be varied: the potential difference between the gas cell and the first segment of sector 1, the potential difference between the first and last segment (also called DC potential gradient), and the potential difference between the last segment and the nozzle plate at the end of the sector.

First, a test of the effect of the potential difference between the gas cell and the first segment of sector 1 is executed by varying this value and looking at the silicon detector at the end of the gas filled RFQ mass filter system to compare transfer yields. All the other variable parameters of the system are set to values close to the ones found to be optimal from the simulation. The results from this test are plotted in figure 5.1.

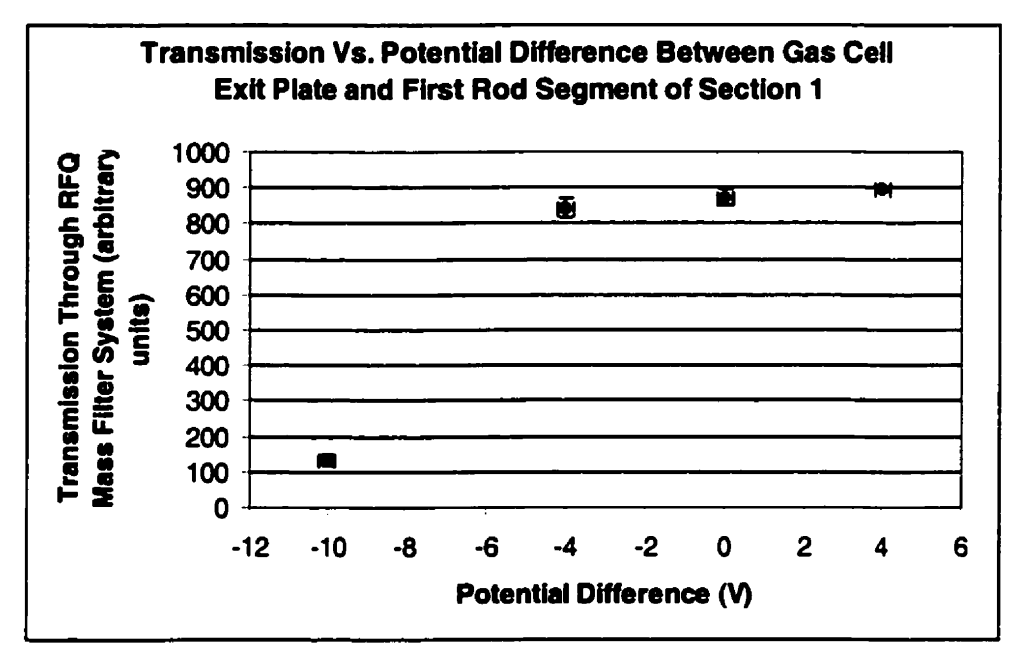


Figure 5.1: Transmission of ions through the gas filled RFQ mass filter system for various DC potential differences between the exit plate of the gas cell and the first segment of the rods of sector 1. Here the potential difference is defined as the voltage on the gas cell exit plate minus the voltage on the 1<sup>st</sup> rod segment.

As seen in the above figure, the transfer efficiency decreases by over 80% when the potential difference between sector 1 and the gas cell exit plate is changed from 0 V to - 10 V while keeping the DC gradient along sector 1 constant. The positive ions are clearly repulsed by this negative potential difference. But most ions are still transferred even with a potential difference of -4 V, indicating that the gas flow has a significant influence on transfer in this region. This effect is also seen with the simulation.

Next the effect of the DC potential difference between the first and last segment of the sector (potential gradient) is explored. Only this parameter is varied while keeping others constant, as previously explained. Results are shown in figure 5.2.

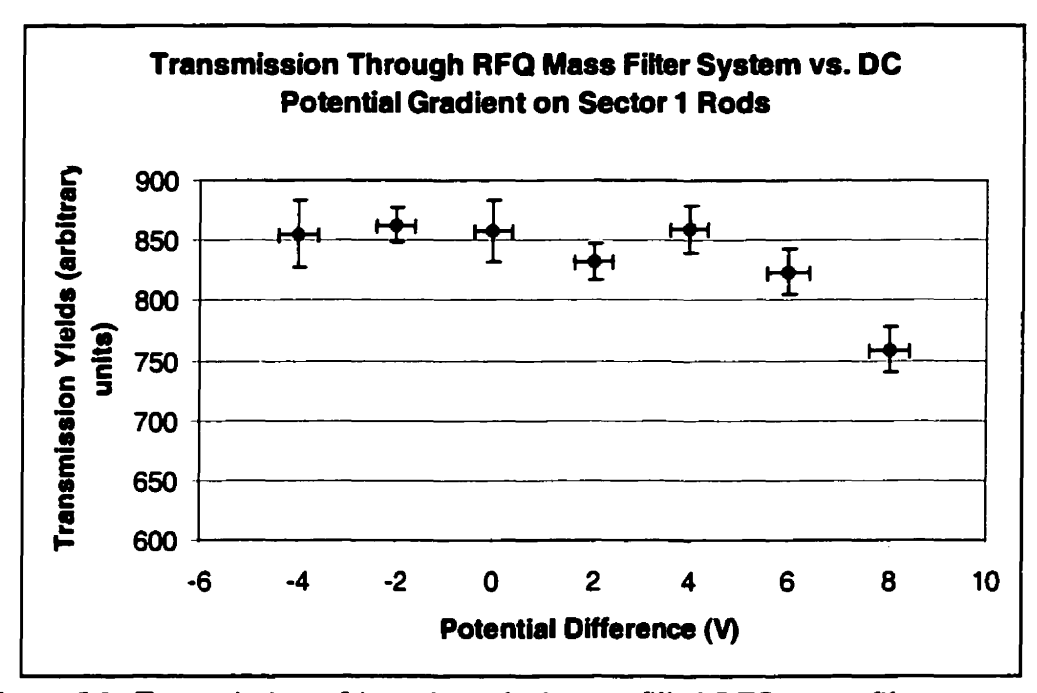


Figure 5.2: Transmission of ions through the gas filled RFQ mass filter system for various DC potential differences between the first and last segments of sector 1's rods (potential gradient).

Results agree with the simulation showing that the DC potential gradient is not of crucial importance as long as values are kept within a reasonable range. More precisely,

DC gradients of -4 V to 6 V over the 160mm rods (-25V/m to 37.5V/m respectively) are shown to have no significant effect on the transfer efficiency in this sector. The transmission yield starts to decrease at a potential difference of 8 V (50V/m). In this test, the potential difference between the gas cell exit plate and the first segment of sector 1 is kept at a constant 0 volts.

Another relevant DC potential difference is the one between the last segment of sector 1 and the nozzle plate at the end of the sector. This parameter is varied, and results are plotted in figure 5.3.

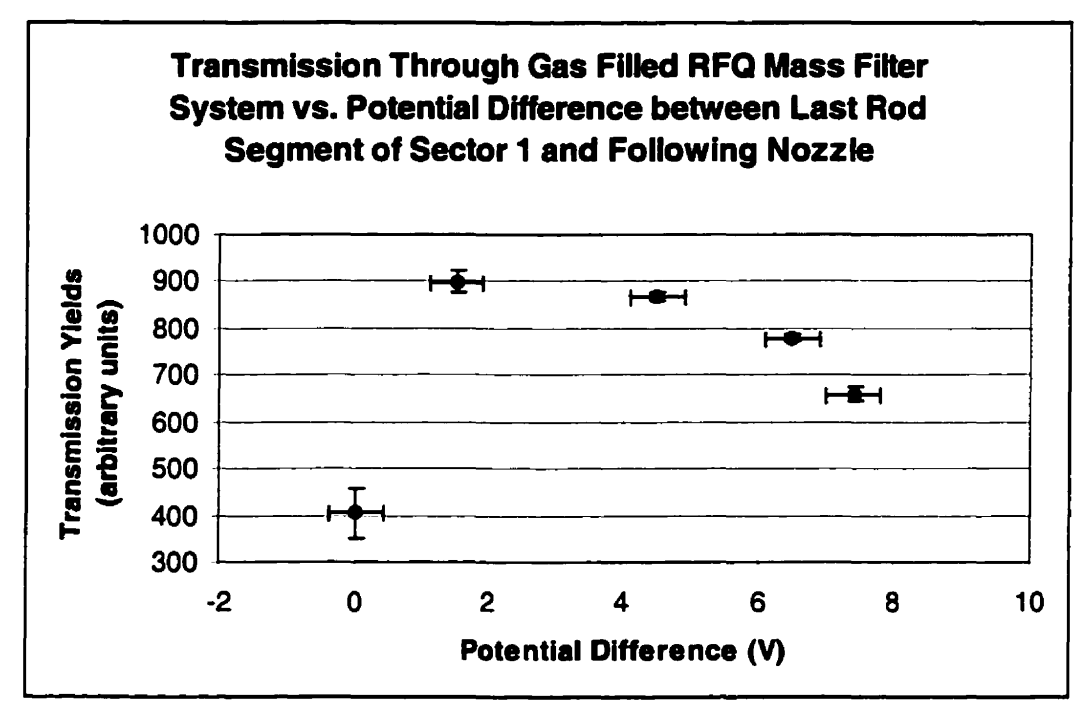


Figure 5.3: Transmission of ions through the gas filled RFQ mass filter system for various DC potential differences between the last segment of sector 1's rods and the nozzle plate which follows it.

The above curve shows that there is maximum transmission in the 1.5 V to 4.5 V range. Higher or lower potential differences are detrimental to transfer, indicating that in these cases the ions cannot get transferred through the nozzle.

#### 5.1.2 The RF Potential Amplitude

The importance of the amplitude of the RF potential applied to the rods of sector 1 is investigated. Just like the tests previously described, all of the RFQ mass filter system's parameters are set to what the simulation indicates is adequate, and only the RF potential amplitude is varied. Due to restrictions imposed by the electronics used, the RF potential frequency must be kept at 788 kHz. Once again, the silicon detector at the end of the RFQ mass filter system is used to compare the yields for the various RF amplitudes, and results are shown in figure 5.4.

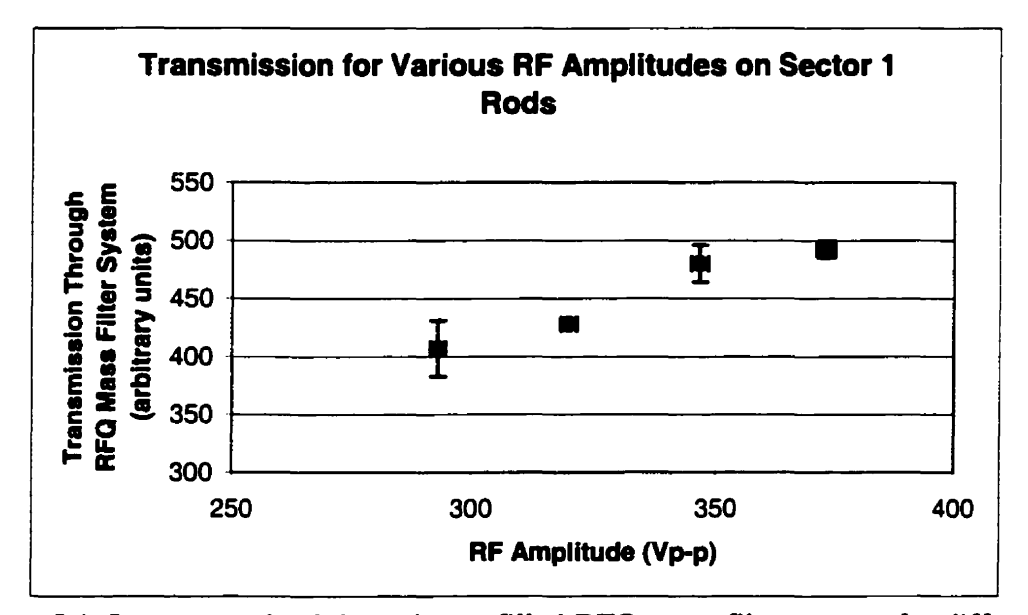


Figure 5.4: Ions transmitted through gas filled RFQ mass filter system for different RF amplitudes applied to the rods of sector 1.

From this test, we can clearly see that the transmission efficiency is improved for higher RF amplitudes. From this experiment it is difficult to know if this behavior originates from the effect the RF amplitude has on the entry of the ions into the rod structures or on the greater stability of ions within the rods once they are radially trapped, but the simulation indicates that the first case applies. The transmission curve of figure

5.1 seems to plateau close to, or after 400 Vp-p, but higher RF amplitudes are unfortunately impossible to apply since they cause electrical discharges inside the system [Mee53]. Near the end of the curve, an increase in 50 Vp-p in RF amplitude results in a 13% transmission increase. According to the simulation, decreasing the distance between the gas cell and the beginning of the sector 1 rods would allow comparable transmission efficiencies to be obtained for lower RF amplitudes. This is experimentally tested and the resulting transmission of ions at different RF amplitude with the rods moved closer to the exit of the gas cell by about 1 cm is shown in figure 5.5.

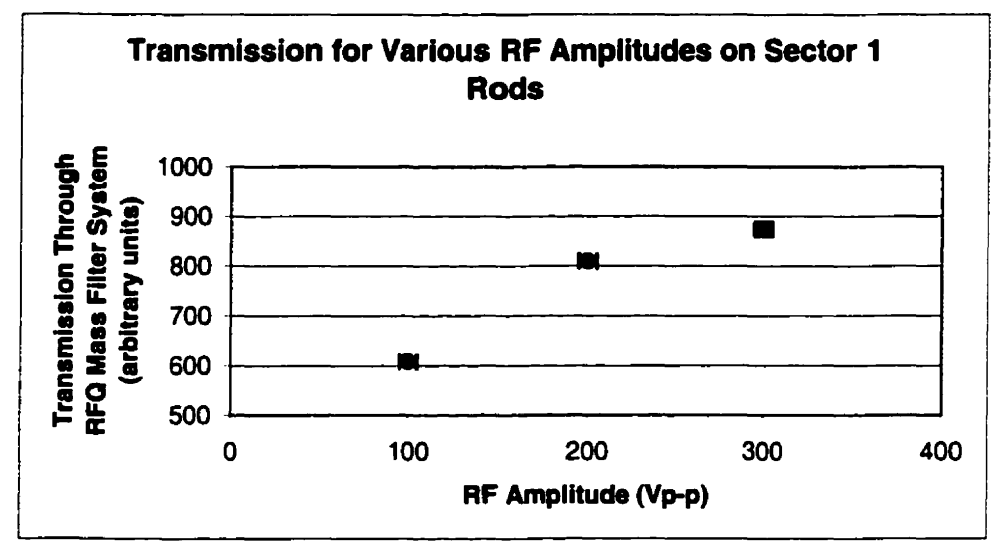


Figure 5.5: Ions transmitted through the RFQ mass filter system for different RF amplitudes applied to the rods of sector 1. In this test the rods of sector 1 are moved 1 cm closer to the exit plate of the gas cell.

Once again, electrical discharges occur at an RF amplitude of 400 Vp-p and impose a limit to the applied amplitude. From this graph, a 50 Vp-p increase in RF amplitude near the end of the curve results in a transmission increase of 2%. From this crude analysis, one can deduce that in this case, 300 Vp-p is much closer to the curve's plateau than the 375 Vp-p in the previous curve of figure 5.2. This seems to indicate that the RF

amplitude can indeed be reduced while keeping a good transfer efficiency if the rods are moved closer to the gas cell's exit plate.

#### 5.1.3 Summary of Sector 1 Tests

The performed tests show that the fragments get transferred through sector 1 by setting the operation parameters at values close to the ones used for the simulation. The DC potential differences along the rods are not crucial which indicates that the gas flow and pressure play a more significant role in the transfer of ions through this sector. The DC potential difference between the gas cell plate and the first rod segment of sector 1 only needs to remain above -4 V. The DC potential gradient along the rods can range between -4 V and 6 V over the 160 mm long rods (-25 V/m to 37.5 V/m). The DC potential difference between the last segment of sector 1 and the following nozzle is best kept around 1.5 to 4.5 V. Higher RF amplitudes applied to the rods improves the entry efficiency of the ions into the sector but discharges limit the RF amplitude to under 400 Vp-p. By moving the rods closer, it becomes possible to use lower RF amplitudes to obtain comparable transfer yields.

#### 5.2 Sector 2 of the Gas Filled RFQ Mass Filter System

The general characteristics of sector 2 are described in section 4.2. This 20cm long sector has a much lower pressure than the previous sector, namely around 80 mtorr of helium. This corresponds to an ion mean free path of about 1 mm. Sector 2 can be used as a mass filtering device by the application of a potential difference (U) between the pairs of opposite rods allowing the selective transfer of ions of chosen mass. The

operation parameters needed for the efficient transfer of ions through this sector are examined. First, the effects of varying the pressure and the DC gradient along the rod segments are studied. Then, the conditions needed to use sector 2 as a mass selective filter are determined by making a calibration of the device which can be used to find the mass distribution of the fission fragments from the <sup>252</sup>Cf source.

#### 5.2.1 Effects of the DC Gradient and Pressure

As seen with the SIMION simulations in section 4.2.1, certain conditions are needed for the efficient transfer of ions through sector 2 of the gas filled RFQ mass filter system. Particularly, a relationship between the DC potential gradient along the rods (defined as the potential difference between the first and last of the 10 rod segments) and the pressure in sector 2 is evident. To test this experimentally, the following study is performed. For two different gas pressures in sector 2, fission fragments from the gas cell are injected into the gas filled RFQ mass filter system. The operation parameters of sector 1 and sector 3 are kept constant and only the potential gradient along the rods of sector 2 is varied. The transfer yields are compared with the use of the silicon detector at the end of the RFQ mass filter system. The results of this study are plotted in figure 5.6.

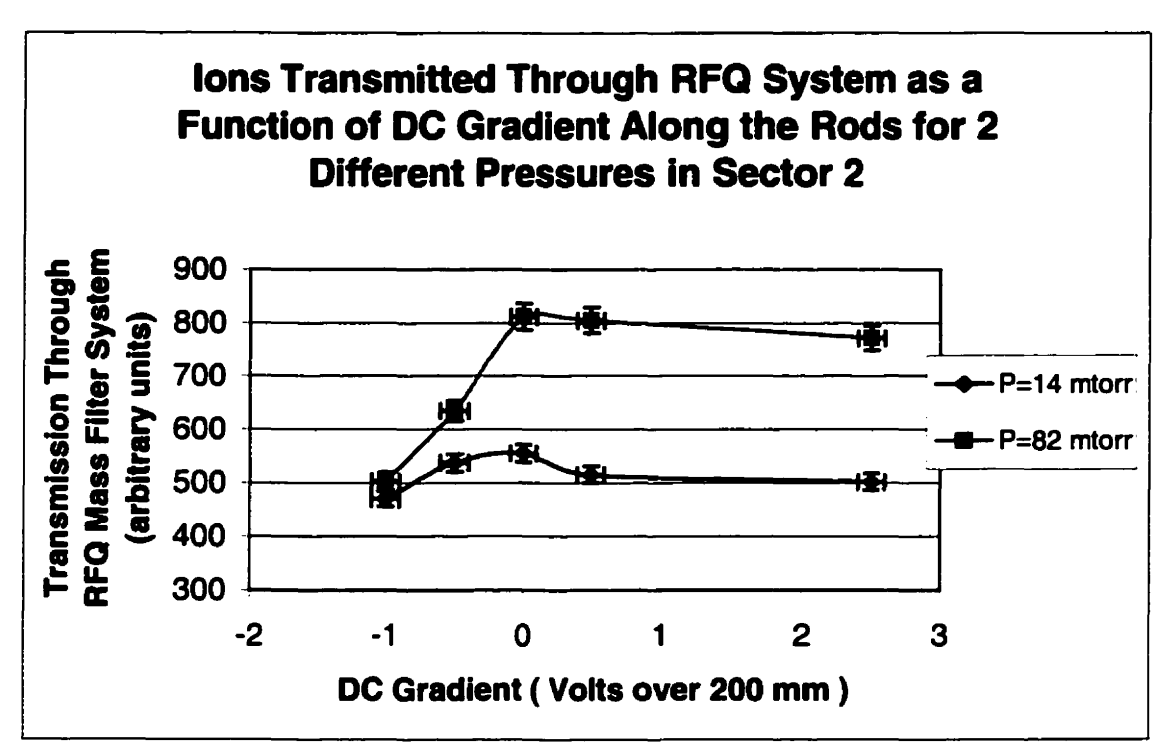


Figure 5.6: Ions transmitted for different DC gradients and pressures in sector 2.

From the results, one can conclude that the higher pressure is best for the transfer of ions. Indeed, the radially oscillating motion of the ions within sector 2 needs to be damped sufficiently so they can enter the 2 mm nozzle aperture at the end of this sector. Higher pressures are consequently preferable since they reduce the mean free path. In addition, it is seen that the DC potential gradient along the rods affects the transfer of ions. At both pressures the maximum transfer efficiency is found with a DC gradient near zero volts. A negative DC gradient merely attracts the ions in the wrong direction and few will have the initial kinetic energy required to overcome this force. On the other hand, putting a positive DC gradient of a few volts along the rods slightly reduces transfer yields at the lower pressure value of 14 mtorr. With greater DC gradient, the axial velocity of the ions increases and less time is therefore spent in the sector. Ions can gain too much momentum and hit the exit plate before their radial oscillations get

adequately damped to enter the small nozzle aperture. Similar behavior is seen with the simulation (see section 4.2.1). The simulation also indicates that an even higher pressure would be desirable here but this would demand modifications to the set-up's differential pumping system.

Another factor worth investigating is the effect of varying the potential applied to the exit nozzle plate. This will change the potential difference from the last segment of sector 2 to the nozzle, affecting the ion's entry conditions. To test the effects of varying this parameter, the DC potential gradient along the rods is kept at 0.5 V over 200 mm (2.5 V/m), the pressure in sector 2 is 80 mtorr, and only the potential difference between the last segment and the exit nozzle plate is modified. Results are plotted in figure 5.7.

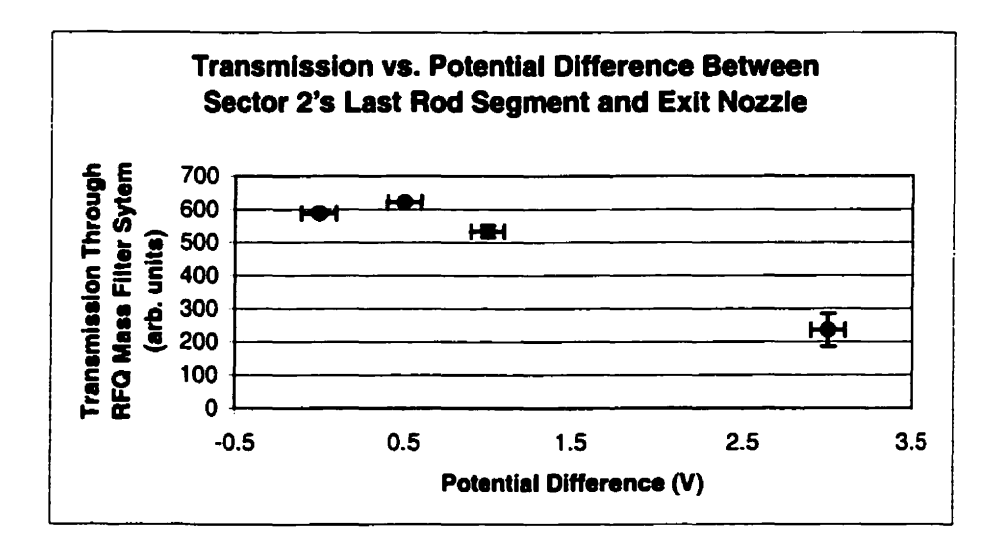


Figure 5.7: Ions transmitted through the gas filled RFQ mass filter system for various DC potential differences from the last segment of sector 2's rods to the exit nozzle plate of sector 2.

Once again small potential differences are preferable for efficient transfer. One can safely assume that a too large potential difference between the last segment and the exit nozzle plate has an effect similar to increasing the DC potential difference across the

rods of sector 2. The ions gain too much momentum and hit the plate before they can enter the nozzle aperture.

#### 5.2.2 Mass Filter Calibration

Since each pair of opposite rods in sector 2 is electrically isolated, it is possible to apply a DC offset, U, between the pairs and use the device as a mass selective filter. As described in section 2.2.1, with a non-zero U only ions of a certain range of masses are stable in the filter. Varying U has the effect of moving the mass scan line up or down the Mathieu stability diagram, changing the filter's resolution. By calibrating the mass filter, the stability region for ions can be experimentally determined. The following study describes the method used to find the Mathieu parameters a and q which delimit the stability region. Figure 5.8 shows a time-of-flight (TOF) spectrum of ions detected by the micro-channel plate (MCP) detector placed at the end of the gas filled RFQ mass filter system, used with U = 0.

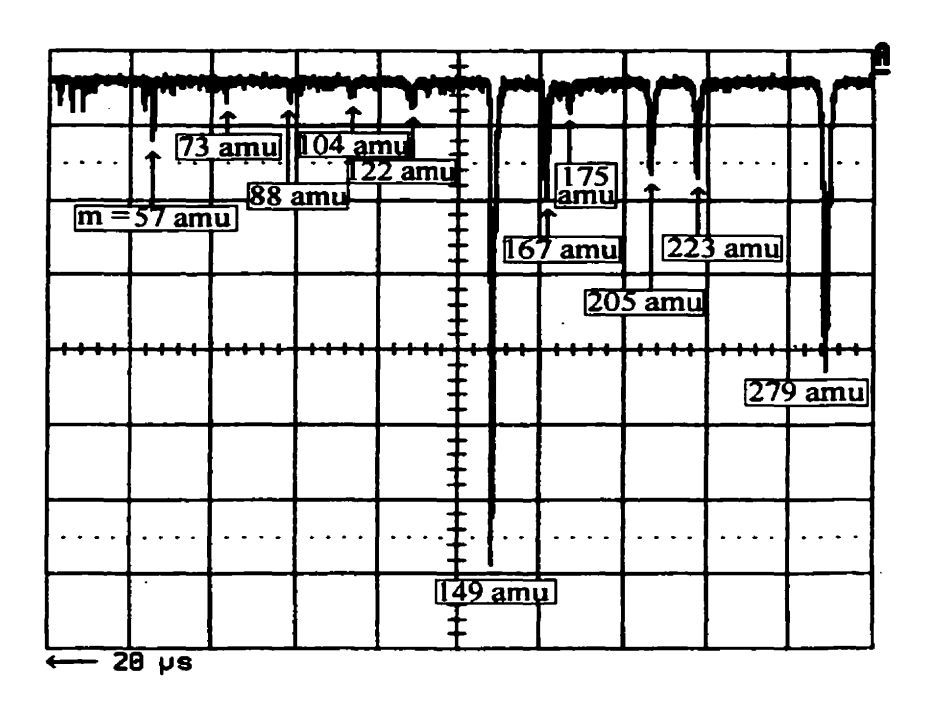


Figure 5.8: TOF spectrum of ions transferred from gas cell to the end of the gas filled RFQ mass filter system.

In this spectrum the major peaks correspond to molecules found in the gas cell or along the RFQ mass filter system. The largest has a mass of 149 a.m.u. and is likely originating from pump oil. This is a known impurity molecule, often found in vacuum pumping systems. Other mass peaks are additional impurities that range in mass from about 50 to 300 a.m.u.

The 149 a.m.u. mass peak shown on the TOF spectrum is used as a calibration peak to perform the following test. The RF potential amplitude applied on the rods of sector 2 is kept at a constant value of V = 225 Vp-p and the DC offset at U = 16 V. The RF frequency,  $\omega$ , is scanned and the maximum and minimum frequencies at which half of the mass 149 peak amplitude is lost are noted. These two frequencies limit the stability range of the 149 a.m.u. mass peak. One can then find the associated a and q values from equations 2.4.12 and 2.4.13 respectively. This procedure is repeated for various DC

offsets (U) between the rods of sector 2. The results are shown in table 5.2. A plot of the calculated a and q values that delimit the stability region follows in figure 5.9.

Table 5.2: RF frequencies at which half of the calibration peak's amplitude is lost for various U values and calculated a and q values. The RF amplitude is V = 225 Vp-p.

Talloud O Value of the Color of								
U (Volts)	ω <sub>min</sub> (kHz)	a <sub>min</sub>	$q_{ m min}$	ω <sub>max</sub> (kHz)	a <sub>max</sub>	<b>q</b> <sub>max</sub>		
16.0±0.5	338.0±1.0	0.14±0.04	1.01±0.04	480.0±1.0	0.07±0.04	0.50±0.04		
20.0±0.5	343.0±1.0	0.17±0.04	0.98±0.04	429.0±1.0	0.11±0.04	0.63±0.04		
22.0±0.5	346.0±1.0	0.19±0.04	0.96±0.04	405.0±1.0	0.14±0.04	0.70±0.04		
24.0±0.5	350.0±1.0	0.20±0.04	0.94±0.04	389.0±1.0	0.16±0.04	0.76±0.04		
25.0±0.5	350.5±1.0	0.21±0.04	0.94±0.04	385.5±1.0	0.17±0.04	0.77±0.04		
26.0±0.5	351.0±1.0	0.22±0.04	0.93±0.04	377.8±1.0	0.19±0.04	0.81±0.04		
27.0±0.5	352.0±1.0	0.22±0.04	0.93±0.04	368.5±1.0	0.20±0.04	0.85±0.04		
28.0±0.5	353.5±1.0	0.23±0.04	0.92±0.04	362.0±1.0	0.22±0.04	0.88±0.04		
28.5±0.5	355.4±1.0	0.23±0.04	0.91±0.04	357.0±1.0	0.23±0.04	0.90±0.04		

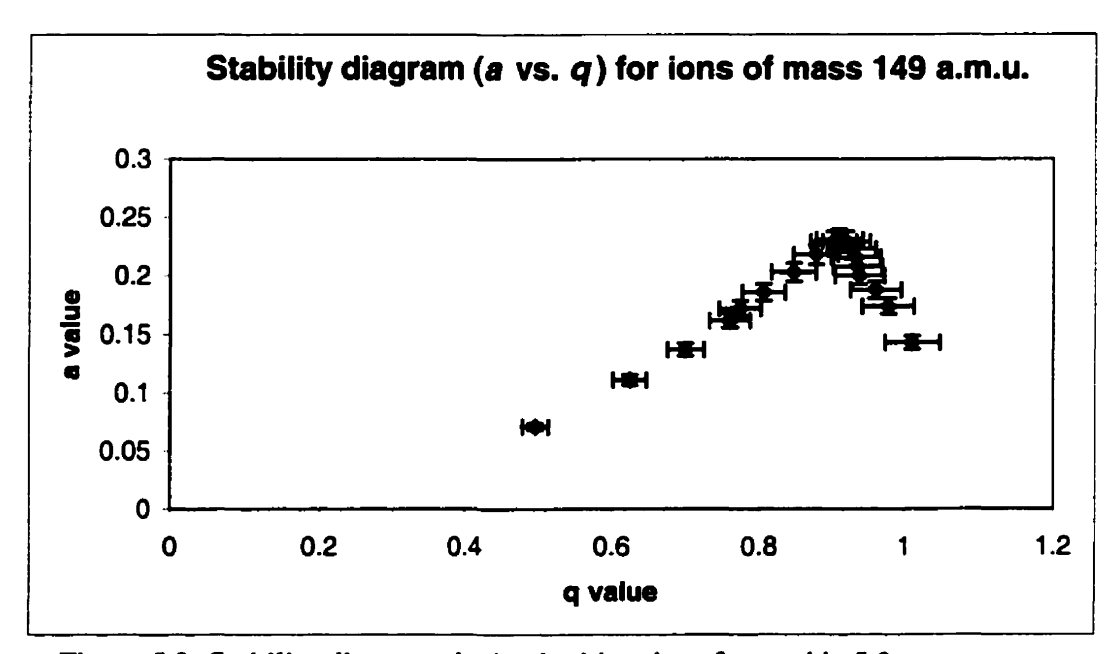


Figure 5.9: Stability diagram obtained with values from table 5.2.

From the above graph, one can see that although the peak a value agrees within experimental error with the expected value, the q value at the peak of the stability diagram,  $0.91 \pm 0.04$  differs by 29% from the theoretical q value of 0.706 obtained from

solving the Mathieu equation. This can be due to having a lower RF voltage amplitude applied to the rods than the one that is actually measured. Some intensity could be lost especially towards the middle of the sector. Other possibilities include the effect of the addition of gas in our system or imperfections in the shape of the rods.

### 5.2.3 Mass Distribution of <sup>252</sup>Cf Fission Fragments.

From the previous calibration, it is now known how changing the parameters can influence the mass filter's acceptance range. It is possible to tune the system such that only certain fission fragments from the <sup>252</sup>Cf fission source are allowed to be transferred. This is performed in the following experimental study. The mass filter parameters are set to a certain resolution only letting pass through a mass range of < 10 a.m.u. by using U = 27.5 V and V = 225 Vp-p. Varying the RF frequency  $\omega$  on the rods enables scanning for radioactivity along different mass regions. For example, the previous calibration indicates that at an RF frequency of 356 kHz, only masses of 149±5 a.m.u. are stable in the mass filter and are subsequently transmitted to the end of the RFO mass filter system. Since the points (a,q) that are lying in the stable region of the stability diagram are proportional to 1/mω<sup>2</sup>, raising this frequency will let through ions of lower mass. Similarly, lowering the frequency will favor the transmission of heavier ions. A number of discrete RF frequencies each corresponding to different mass stabilities are applied to the rods and the resulting transmission is measured with the silicon detector at the end of the RFQ mass filter system. The amount of activity measured for each mass region determines the mass distribution of the fission fragments of the <sup>252</sup>Cf source which can

then be compared with the expected distribution. Figure 5.10 shows the results of this study.

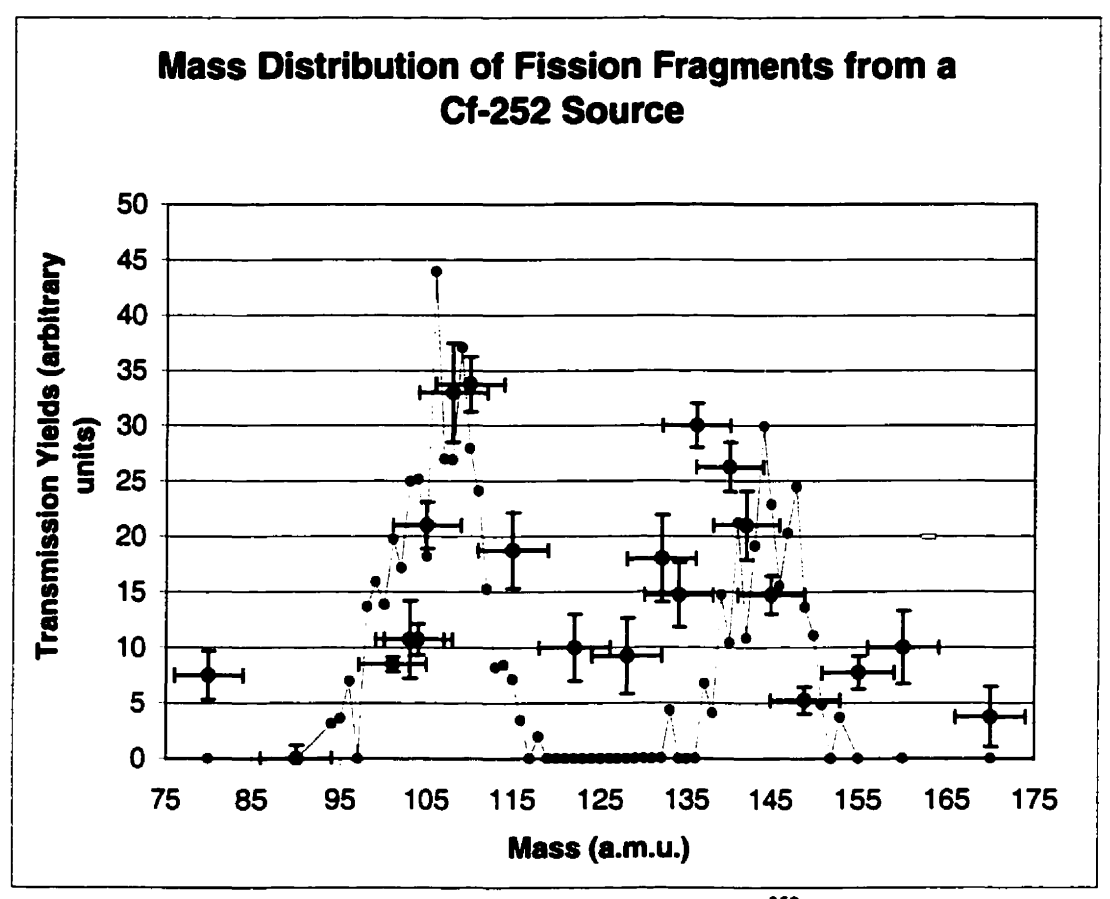


Figure 5.10: Mass distribution of fragments from the <sup>252</sup>Cf source. A calibration of the system is previously made to find the relationship between the RF frequency applied to the rods and the filter's mass allowance. The solid line represents the expected distribution of the fission fragments.

As one can see in the above figure, two major peaks appear for masses near 105 a.m.u. and 145 a.m.u., in agreement with the theoretically expected yields.

#### 5.2.4 Summary of Sector 2 Tests

Studies of sector 2 indicate that a low DC gradient along the rods and a small potential difference from the last segment to the exit nozzle are needed in order to maximize the transfer efficiency. Transmission is better when a pressure of 82 mtorr is used as compared to 14 mtorr. The mass filter properties are determined and agree with what is seen in the simulation. It is possible to selectively transport ions of a small given mass range through the gas filled RFQ mass filter system to find the mass distribution of the fission fragments from the <sup>252</sup>Cf source.

#### 5.3 Sector 3 of the Gas Filled RFQ Mass Filter System

As discussed in section 4.3, the third sector of the gas filled RFQ mass filter system is characterized by being much longer than the other two sectors, and having a lower pressure of about  $2x10^{-4}$  torr, resulting in an ion mean free path of 39 cm. The other distinctive feature is the linear trap found at the end of the sector to cool, accumulate, and later eject the ions. The various operation parameters of sector 3 are described and experimentally investigated in the following sections. First, the potential gradient applied on the rods is optimized. Then, tests to establish the capture and ejection parameters of the linear trap are performed.

#### 5.3.1 DC Potential Gradient

A DC potential gradient between the first segment and the last segment of the rods needs to be applied to guide the ions forward. The following test is conducted to find the effect of varying this DC gradient. While keeping all other operation parameters of the gas

filled RFQ mass filter system constant, the DC potential gradient along the rods of sector 3 is varied. Here the linear trap is used to capture and pulse out the transmitted ions and the resulting yields are measured with the silicon detector after sector 3. Figure 5.11 shows a plot of the results of this study.

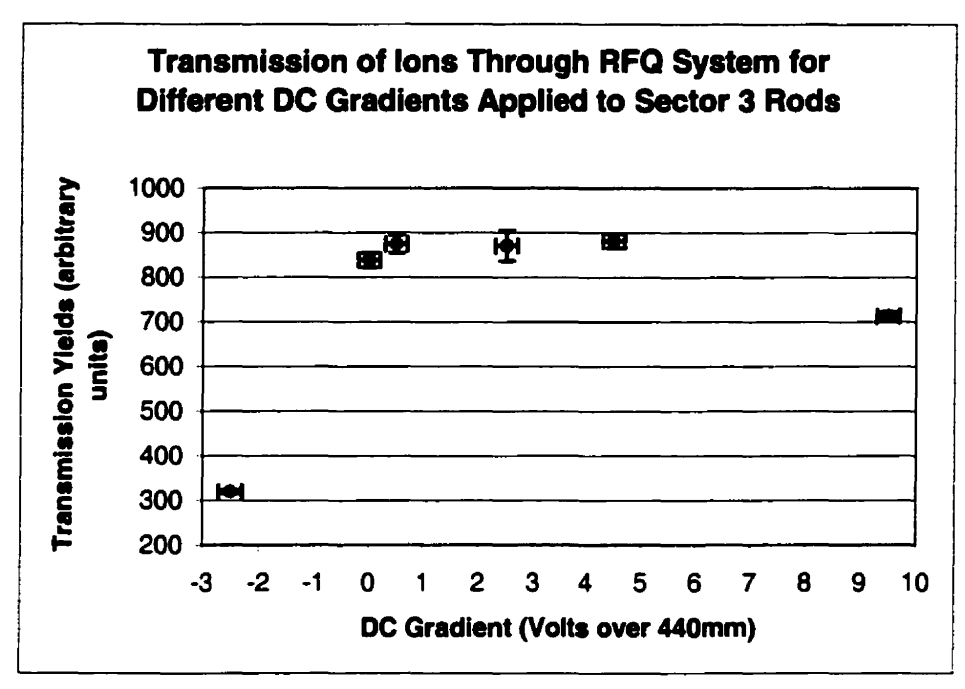


Figure 5.11: Effect of DC gradient along sector 3 rods on ion transmission.

From the graph, one sees that the transmission efficiency remains more or less constant if the DC gradient is in the 0 V to 5 V range (0 V/m to 11 V/m). Negative gradients are detrimental to transfer since the ions are guided in the opposite direction. A larger positive DC gradient of +9.5 V over 440 mm (21.6 V/m) is also shown to decrease the transmission yields. In this case the ions gain too much energy and the linear trap can not capture the ions which end up hitting the last exit plate. This effect is also noticed in simulation results (section 4.3.2).

#### 5.3.2 Linear Trapping

As described in section 4.3 the last three segments of sector 3 are used as a linear trap to capture, accumulate, and cool the ions before they are ejected into the transfer line to the CPT mass spectrometer. Here a number of operation parameters have to be considered. The depth of the trap, the ejection pulse amplitude, the pulse width, and the rate at which this pulse is applied are all studied. These factors not only affect transmission efficiency but also determine the energy spread and the time-of-flight (TOF) spread of the ejected ions.

The effect of varying the depth of the linear trap is first investigated. The potential difference between the three rod segments creates an approximately harmonic potential well into which ions fall, get trapped and cooled. The trap depth is varied while keeping all other parameters constant, and it is found that a depth of a few volts is sufficient to trap the ions. A larger potential difference does not increase the trapping efficiency but if the trap depth is increased to over 20 V, the transfer efficiency starts to decrease rapidly, as seen with the simulation (see table 4.3).

Once the ions are confined and cooled inside the trap, an ejection pulse is applied to transmit the trapped ions to the mass spectrometer. As previously described, this ejection pulse basically consists of the fast, simultaneous application of an additional positive DC potential to S1, and an additional negative potential to S3 and the last plate. The pulse amplitude, pulse width (duration of pulse application), and rate at which this pulse is applied can each be varied.

The effect on transmission of the width of the ejection pulse is assessed in the following study. Ions are sent in the gas filled RFQ mass filter system and captured in

the linear trap. An 85 V ejection pulse with variable pulse width is then applied at a rate of 20 Hz. Transmission yields are compared with the use of a silicon detector after the linear trap, and results are plotted in figure 5.12.

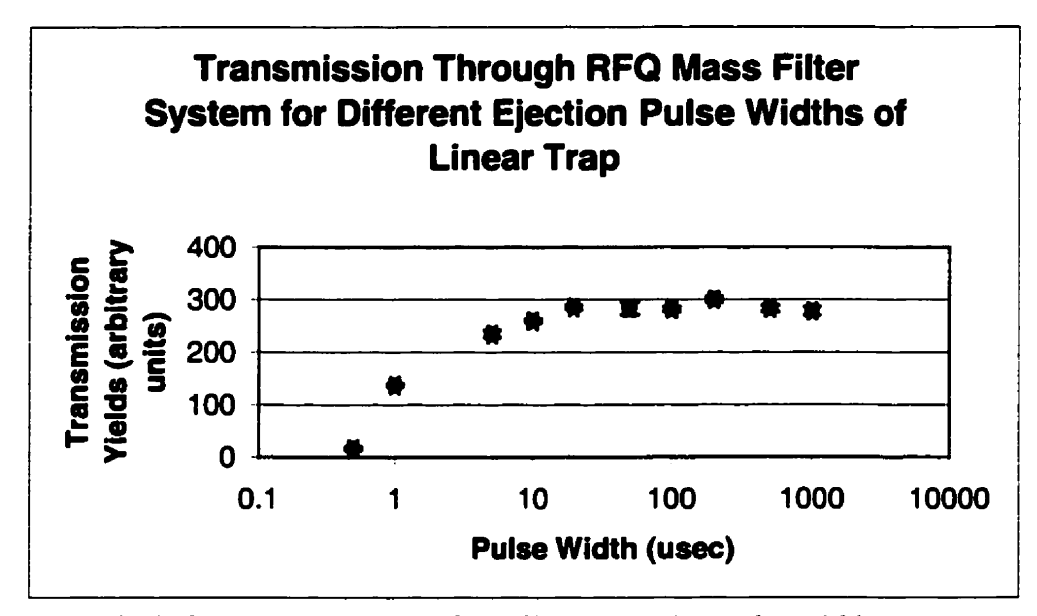


Figure 5.12: Transmission yields for different ejection pulse widths.

The above figure shows that pulses shorter than 7  $\mu$ s do not efficiently eject all the ions from the trap. This agrees with the simulation results. The transfer then remains roughly constant as the pulse width is increased up to  $1000~\mu$ s.

In a subsequent study, the effect of varying the ejection pulse's potential amplitude is examined while keeping all other parameters fixed. One should note that when it is stated that a pulse amplitude is of 100 V, this actually means that a pulse of +100 V is applied to S1 simultaneously with a pulse of -100 V to S3 and the last plate. Results are plotted in figure 5.13.

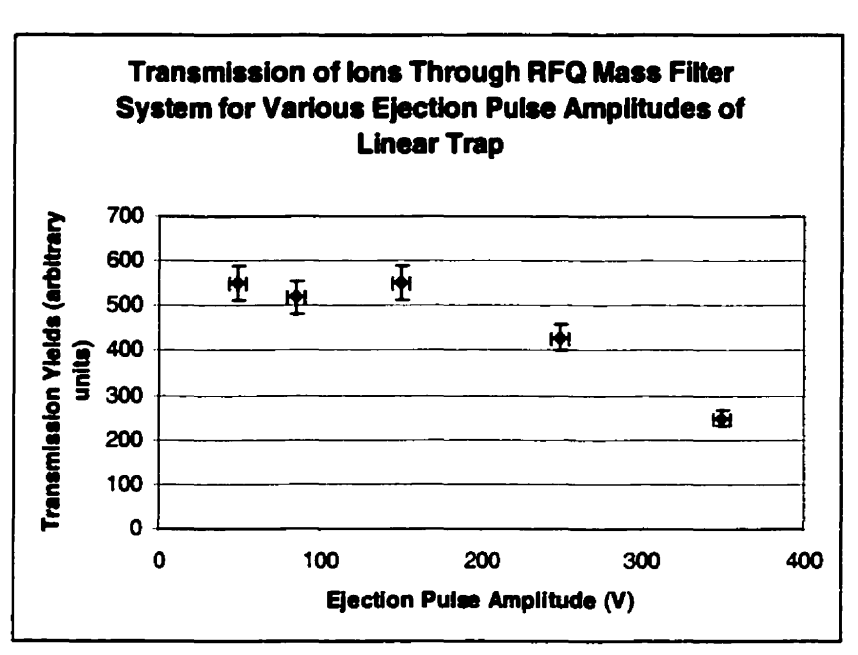


Figure 5.13: Transmission efficiency as a function of linear trap ejection pulse amplitude.

From this test one can conclude that the pulse amplitude does not have a significant effect on the overall transfer efficiency, as long as it is kept within the reasonable range of 50 V to 150 V. At higher potentials of 250 V and 350 V, ion losses are seen. The simulation shows that greater ejection pulse amplitude reduces the TOF spread of ions after ejection. This can be experimentally confirmed by looking at the MCP detector placed after the linear trap while varying the amplitude at which the linear trap's ejection pulse is applied. This test is performed, and TOF spectra are taken for a 10 µs wide pulse for pulse amplitudes of 50, 85, 100, 150, 200, and 300 volts. Resulting spectra are seen in figure 5.14.

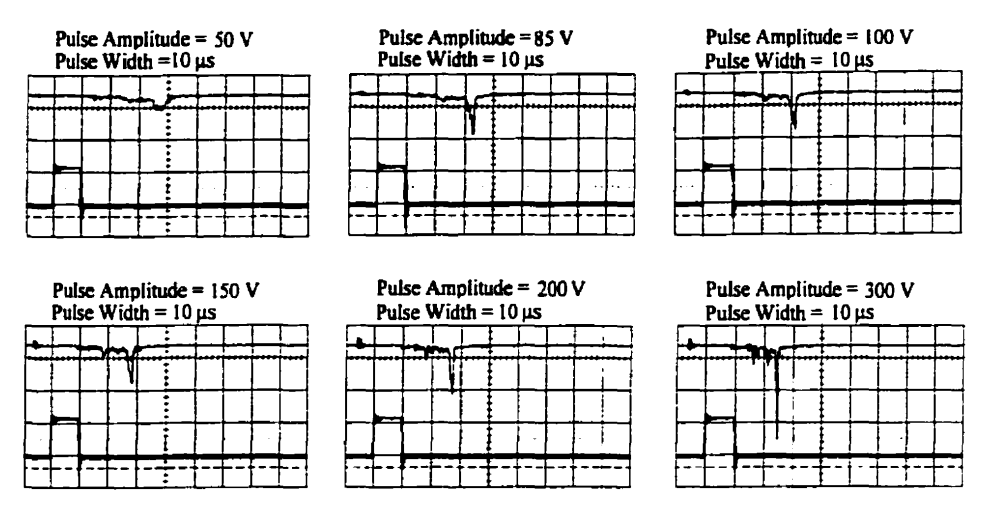


Figure 5.14: Comparison of time-of-flight spreads of mass peaks for various pulse amplitudes as seen on the MCP at the end of the RFQ mass filter system. The pulse width is kept at a constant  $10~\mu s$ .

From the above spectra one clearly sees that the TOF spreads become narrower for larger ejection pulse amplitudes.

Finally, the rate of application of the pulse of the linear trap is studied. As with previous tests, the pulse rate is varied while keeping all other parameters constant, and the silicon detector is used to compare transfer efficiencies. Results are plotted in figure 5.15.

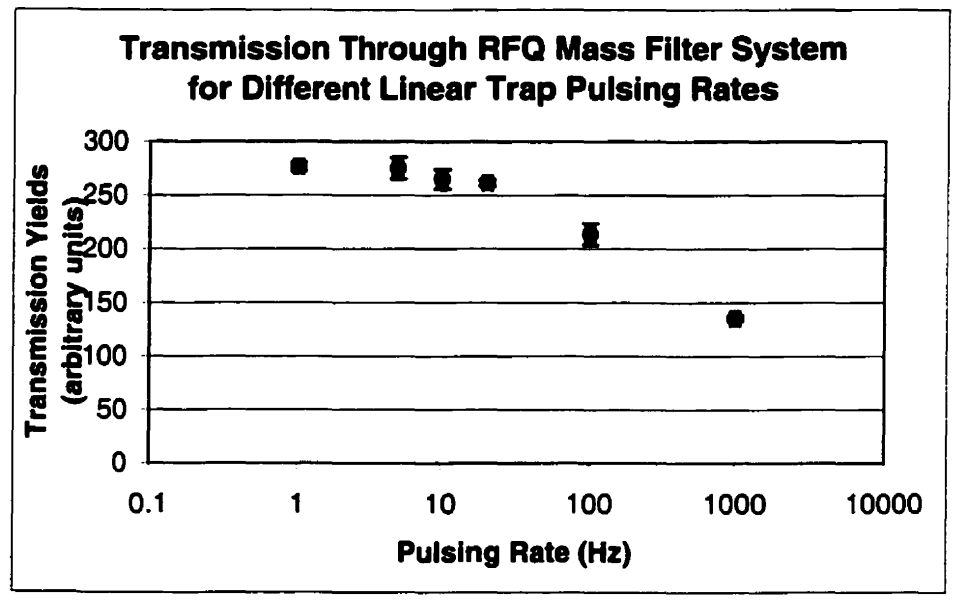


Figure 5.15: Effect of ejection pulse rate on transmission efficiency.

Ejection rates below 20 Hz are shown to result in better transfer efficiency. The transmission starts to drop rather dramatically for rates of 100 Hz and 1000 Hz. One can conclude that ions need to remain in the trap long enough to be properly cooled before being ejected. Also, faster rates can decrease the amount of ions that get into the trap since the ions that are arriving at the trap will not be able to enter it while the pulse is being applied.

Once the capture and ejection parameters are optimized, the total trapping efficiency can be estimated by comparing the transmission yields of the gas filled RFQ mass filter system that is operated with the linear trap to the transmission yields without using the trap. The latter is simply executed by keeping the DC potentials on segments S1, S2, and S3 of the linear trap as a linearly decreasing slope. Ions will just be guided towards the last plate's exit aperture without being trapped. By performing this test, the trapping efficiency is typically observed to be as high as 90±5 %.

#### 5.3.3 Summary of Sector 3 Tests

The DC potential gradient is best kept in the 0 V to 5 V over 440 mm (0 V/m to 11 V/m) range for good transfer efficiency. The linear trap parameters are studied. Results show that the trap depth needs to be of a few volts for proper trapping. The ejection pulse subsequently applied to eject the trapped ions gives the optimal transmission efficiency when its width is over 7  $\mu$ s, its rate is equal to or under 20 Hz and its amplitude is from 50 V to 150 V. In addition, it is found that increasing the pulse amplitude reduces the TOF spread of ions ejected from the trap. The linear trap's efficiency is over 90±5 %.

#### 5.4 Conclusion of Gas Filled RFQ Mass Filter Tests

The experimental tests performed on the three sectors of the gas filled RFQ mass filter system are generally in good agreement with the results obtained from the SIMION simulation. This reinforces the notion that the simulation is an adequate model of the system. Parameters of the three sectors are tested and optimized for better transfer efficiency and a list of these results is given in table 5.3.

Table 5.3: Summary of gas filled RFQ mass filter system optimal parameters.

	5.5.5 definitely of Eastined Re & mass inter sy	The special parameters.		
Sector	Parameter	Operation Values		
1	ΔV DC between gas cell exit plate and 1 <sup>st</sup> rod segment	-4 V to 4 V		
1	DC gradient along rods	-4 V to 6 V over 160 mm (-25 V/m to 37.5 V/m)		
1	ΔV DC between last rod segment and nozzle	1.5 V to 4.5 V		
1	RF potential	> 300 Vp-p @ 788 kHz		
2	DC gradient along rods	0 V to 2.5 V over 200 mm (0 V/m to 12.5 V/m)		
2	ΔV DC between last rod segment and nozzle	0 V to 1 V		
2	RF potential	250 Vp-p @ 550 kHz		
3	DC gradient along rods	0V to 5V over 440 mm (0 V/m to 11 V/m)		
3	RF potential	350 Vp-p @ 650 kHz		
3	Linear trap depth	2 V		
3	Linear trap ejection pulse width	≥ 7µs		
3	Linear trap ejection pulse amplitude	50 V to 150 V		
3	Linear trap ejection pulsing rate	≤ 20 Hz		
2 3 3 3 3 3	RF potential DC gradient along rods  RF potential Linear trap depth Linear trap ejection pulse width Linear trap ejection pulse amplitude	0 V to 1 V  250 Vp-p @ 550 kHz  0V to 5V over 440 mm (0 V/m to 11 V/m)  350 Vp-p @ 650 kHz  2 V  ≥ 7μs  50 V to 150 V		

It is noticed that the range of DC potentials applied to the rods of sector 1 can be much greater than that of sector 2 and 3. An explanation for this lies in the fact that the gas flow from the gas cell plays a more dominant role in sector 1's transfer conditions. The RF potentials quoted in the table are ones that give best transfer efficiencies of the fission fragments of the <sup>252</sup>Cf source which range in mass from 90 a.m.u. to 155 a.m.u.

These values have to be adjusted according to the stability equations if ions of a different mass range need to be transported.

For a device as complex as the gas filled RFQ mass filter system, the variable parameter space is large and practically impossible to investigate fully. While the parameters of table 5.3 are optimal in a given situation, other combinations might also be effective since many parameters are likely interrelated.

The overall efficiency of the system can be estimated from comparing the yields of the silicon detector placed at the end of the gas filled RFQ mass filter system to ones obtained from a similar detector placed right at the exit of the gas cell. A fair estimate is a total transfer efficiency of  $56 \pm 5$  %.

## Chapter 6

## The On-Line Transfer of <sup>120</sup>Cs

The first on-line mass measurement of a radioactive isotope with the CPT mass spectrometer was performed in August and September 2000. The ions produced from a fusion evaporation reaction were successfully transported to the mass spectrometer with the gas filled RFQ mass filter system. This chapter will briefly describe each step of this experiment while emphasizing the importance of the RFQ mass filter system in mass measurement studies.

#### 6.1 The Reaction

The experiment started with a 235 MeV <sup>60</sup>Ni beam hitting a natural Copper target (69% <sup>63</sup>Cu and 31% <sup>65</sup>Cu) in the target chamber area seen in figure 3.2. Products emerging from this reaction and their expected cross sections were obtained from a Pace calculation and the main ones are listed in table 6.1.

Table 6.1: Expected reaction products from fusion evaporation of a <sup>60</sup>Ni beam on

a natural Co target.

<b>A</b> =	113	114	115	116	117	118	119	120	121	122	123
Ва											
Cs											
Хe						-0. V (0.	(Z):Z			2.96 mb	
1			3.56 110			i Vije Mbasa					
Те	236 nb.			8.97 mb							
	+										
	Half- life :	> 1 hr									

The experiment's aim was a measurement on the radioisotope <sup>120</sup>Cs having an expected cross section of 46.48 mb and a half life of 57 seconds. The isotopes produced in this reaction entered the gas-filled Enge magnetic spectrograph where they were separated from the scattered beam and focused onto the entrance window of the gas cell. Here they were thermalized and acquired a charge state of +1. These positive ions were then extracted into the three sectors of the gas filled RFQ mass filter system.

## 6.2 Transfer of Radioisotopes in the Gas Filled RFQ Mass Filter System

The transfer of radioisotopes in the RFQ mass filter system was done successfully by using the parameters found to be optimal in off-line studies. In particular the mass filter properties of sector 2 were used for the two following purposes. First, a verification that the reaction products lied in the expected mass range was needed to confirm that impurities in the system weren't bound to the products to form more massive molecules. In addition the mass filter was used to filter out unwanted ions before they reached the

linear trap at the end of sector 3 where saturation is often a problem while performing online experiments.

#### 6.2.1 Mass Distribution of Products

The mass distribution of the reaction products was found by using sector 2 in mass selective mode, i.e. with  $U \neq 0$ . A calibration of the mass filter was performed to know the mass range of ions let through the filter for different applied DC and RF potentials. This was done by looking at the time-of-flight (TOF) spectra obtained from the MCP detector at the end of the RFQ mass filter system. The first calibration test involved varying the U value on sector 2 rods, while keeping the RF potential at 230 Vp-p with a frequency of 394 kHz. The other parameters of the gas filled RFQ mass filter system were kept constant, and the resulting TOF spectra are shown in figure 6.1.

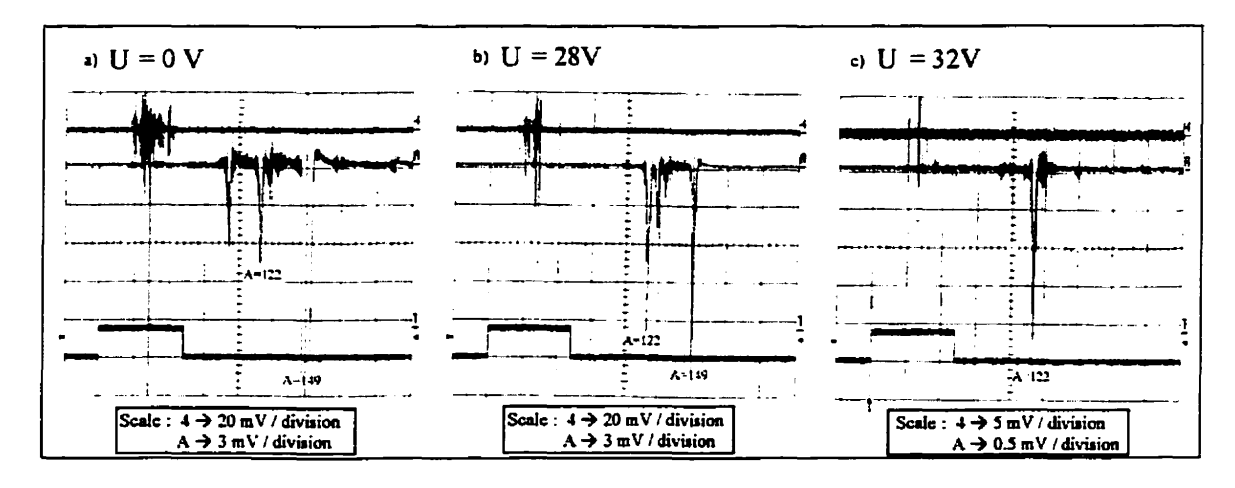


Figure 6.1: TOF spectra for different DC offsets (U) on sector 2 rods; a) no offset on the rods; b) 28 V offset; c) 32 V offset. The RF amplitude and frequency was kept at 230 Vp-p @ 394 kHz in the three spectra. The scales are indicated under each spectrum. The lower TOF (A) distribution is simply a time average of the top distribution (#4).

From the above spectra, one sees that with U = 0 V, a wide range of masses were detected. Indeed the signal was spread across masses ranging from about 70 a.m.u. to 500

a.m.u. Increasing U to 28 V and 32 V narrowed this region. At U = 28 V, ions of masses from about 122 a.m.u. to 149 a.m.u. were successfully transferred through the mass filter system and at U = 32 V, only a few peaks around the mass 122 a.m.u. region were observed. These results gave a good indication of the mass filter system's resolution parameters. At a given resolution, the RF frequency on sector 2's rods could then be modified to scan across different mass regions. This was done in the following test, where U was kept at 28 V and the RF frequency was varied from 380 kHz to 450 kHz. The resulting TOF spectra are shown in figure 6.2.

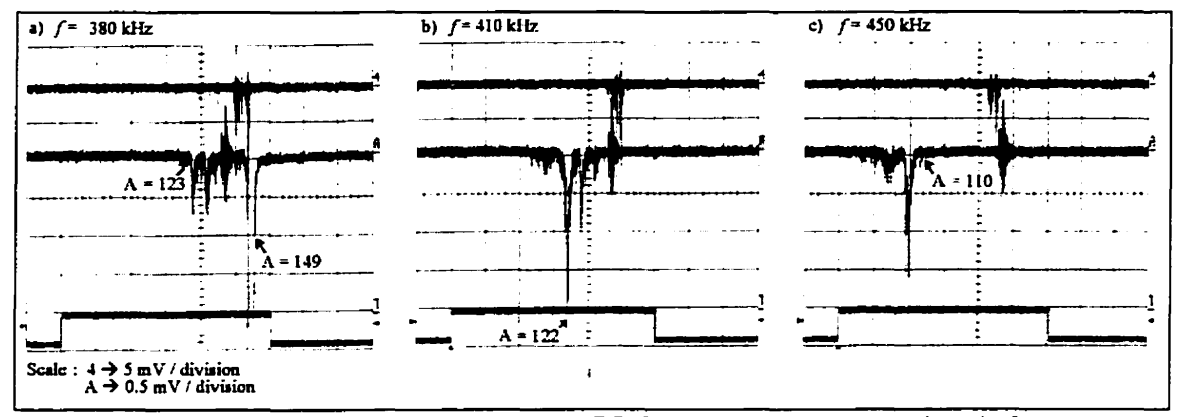


Figure 6.2: TOF spectra for different RF frequencies on sector 2 rods for a mass filter with U = 28 V and V = 230 Vp-p; a) the RF frequency was 380 kHz; b) the RF frequency was 410 kHz; c) the RF frequency was 450 kHz. The bottom TOF (A) distribution is a time average of the top TOF (4) distribution.

One now sees from the above spectra that the mass spread of the transmitted ions shifted towards lower masses when the RF frequency was increased. At U = 28 V, our mass filter was estimated to let through a range of masses about 15 a.m.u. wide. With this calibration it was then known which frequencies would let ions of a given mass pass through the filter. The silicon detector at the end of the RFQ mass filter system was used to confirm that the ions transported were indeed the desired radioisotopes. For an RF

amplitude of V = 230 Vp-p and a DC offset of U = 32 V (about 5 a.m.u. wide mass filter acceptance), the RF frequency was scanned over a wide range of values. The resulting transmission was assessed with the silicon detector located at the end of the gas filled RFQ mass filter system. Figure 6.3 shows a plot of the results.

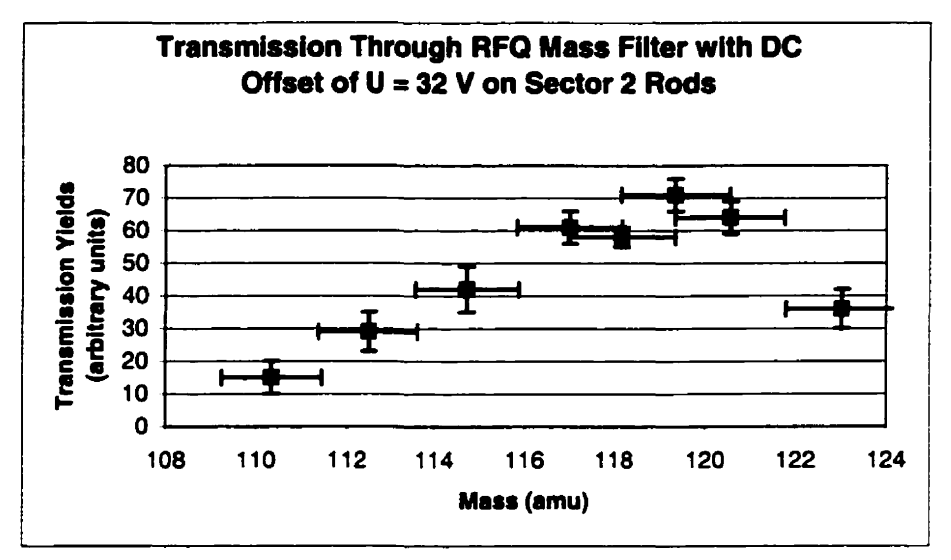


Figure 6.3: Mass distribution of ions transmitted through gas filled RFQ mass filter system with U=32 V on sector 2 rods.

As seen in the above graph, most radioactive ions were detected within the expected mass range of about 116 to 123 a.m.u.

#### 6.2.2 Adding Mass Selectivity to Prevent Saturation of Linear Trap

When doing on-line experiments, there is an enormous amount of ionization in the gas cell due to the intensity of the scattered incident beam which can enter it. These ions end up saturating the linear trap at the end of sector 3. Consequently, fewer of the desired reaction products can get trapped. A solution is to filter out some of these unwanted ions before they enter the trap by using sector 2 as a mass selective filter. To confirm this effect the following experiment was conducted. The U value was varied while keeping the other parameters constant for optimal transfer, and the transmission efficiency was

once again monitored with the silicon detector at the end of the RFQ mass filter system.

Results are plotted in figure 6.4.

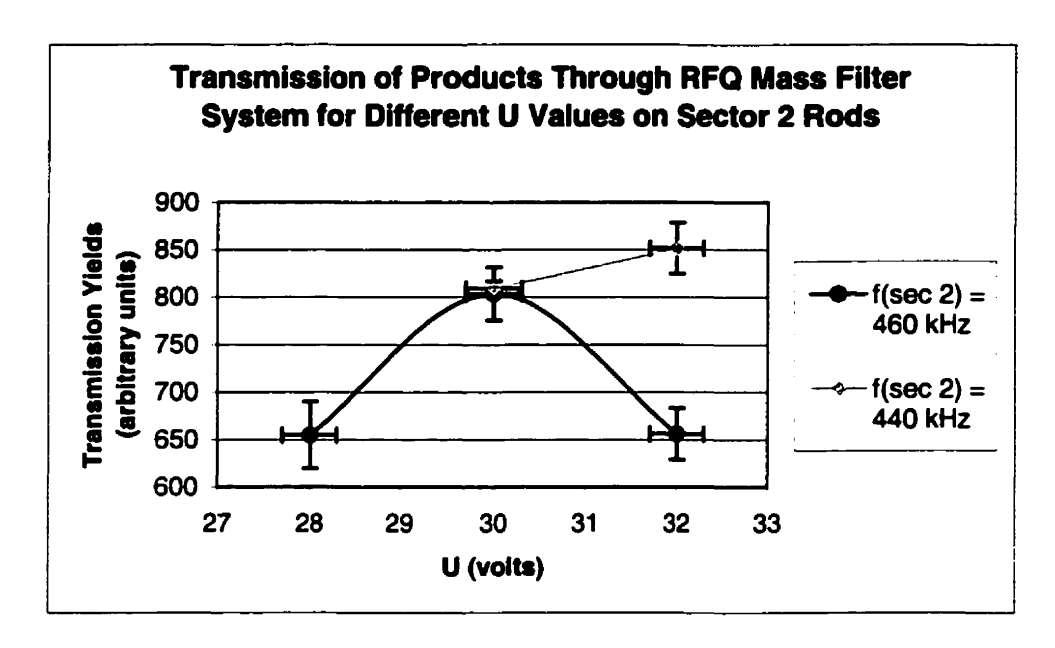


Figure 6.4: Ions transmitted for different U values at RF frequency of 460 kHz and 440 kHz applied to the rods of sector 2. The solid lines are just used to guide the eye.

This graph shows that when the mass allowance of our filter was reduced by raising U, the number of transferred radioactive reaction products increased. For an applied RF frequency of 460 kHz, the transmission yields went down when a U of 32 V was applied. This indicated that this frequency wasn't properly tuned for the masses intended to be let through the filter. Indeed, lowering the frequency to a more adequate value of 440 kHz increased the transmission yields.

#### 6.3 Transfer to CPT and Results

After tuning the gas filled RFQ mass filter system to enable the best possible transfer efficiency, the reaction products were sent to the Canadian Penning Trap (CPT) mass spectrometer as described in section 3.1.6. The Paul trap accumulated and cooled ions of

a few mass units around 120 a.m.u. and these were transferred to the Penning Trap. A mass measurement on  $^{120}$ Cs was performed resulting in a mass of 119 920 640  $\pm$  27  $\mu$ a.m.u., in agreement with the accepted value of 119 920 678  $\pm$  11  $\mu$ a.m.u. Further mass measurements on other isotopes from different fusion reactions are currently being explored.

#### 6.4 Conclusion of On-Line Experiments

Products created from a fusion reaction were efficiently transported by the gas filled RFQ mass filter system to the CPT mass spectrometer where the precise mass measurement of <sup>120</sup>Cs was made. The operation parameters of the gas filled RFQ mass filter system were set to the previously determined optimal transfer parameters from off-line tests. The mass filter properties of sector 2 were used to confirm that the radioactive products lied in the expected mass region. The mass filter was also used to selectively transport ions within a small mass range to avoid saturating the linear trap at the end of the RFQ mass filter system. Now that the transfer of radioactive products through the whole experimental system has been established, the mass measurements of radioisotopes emerging from other fusion reactions can be achieved.

## Chapter 7

#### **Conclusion**

The gas filled RFQ mass filter system is an effective tool for the transport of radioactive ions from a high pressure of about 150 torr to high vacuum environments with pressures close to 10<sup>-4</sup> torr. Because of the electrical fields created by the application of DC and RF potentials, ions are radially stable in the rod structure and guided forward while a differential pumping system gradually gets rid of the gas. The gas filled RFQ mass filter system installed at ANL is divided into three sectors, each having particular purposes and different characteristics.

The first sector captures the ions ejected from a higher pressure gas cell. Placing the rods of the sector closer to the gas cell and increasing the RF potential amplitude applied to the rods helps in transferring ions into the sector. Unfortunately, the pressure in this region limits the RF amplitude that can be applied since these values approach the ones where the helium gas breaks down at minimal applied voltages (Paschen curves), causing electrical discharges in the system [Mee53]. To avoid this, the pressure in sector 1 could be better controlled and modified by either improving the pumping system

or changing the exit aperture size of the gas cell. Both the simulation and the off-line experiments indicate that the gas flow in this region takes the leading role in guiding the ions forward. The DC potential differences along the sector's rods are therefore less important. Because of the short mean free path of ions in sector 1, their trajectories get sufficiently damped and the ions can easily enter the small 2 mm aperture at the end of the sector. Making the above modifications to the pumping system and therefore changing the pressure would affect this feature so this also needs to be put into consideration.

The second sector has a lower pressure of 80 mtorr and the gas flow is less important. This makes the DC potential gradient along the rods more critical for guiding the ions forward. A small gradient of 0 V to 2.5 V is found to be adequate for proper transmission. Moreover, the simulation indicates that a higher pressure of 120 mtorr would increase the transfer efficiency but this has yet to be tested experimentally. The relatively stable gas pressure and flow conditions make it possible for this sector to be used as a mass selective filter to only transfer the ions of a given mass region. This feature is mostly useful for on-line experiments, where it becomes necessary to get rid of the large amount of impurities before they can saturate the system.

The desired ions subsequently enter the third sector, kept at a pressure of about  $2x10^{-4}$  torr. This sector is of greater length to compensate for the large mean free path of ions due to low gas pressures. In addition, at its end is found a linear trap to capture and further cool the incoming ions. Here they are accumulated and ejected out in bunches into the transfer line to the CPT mass spectrometer. The simulation and experimental results indicate that certain trapping parameters are needed in order to efficiently capture and

eject the ions in the linear trap. The DC potential gradient along the rods is best kept between 0 V and 5 V, and a linear trap potential well depth of 2 V to 8 V results in the adequate trapping of ions. Once the ions are confined and sufficiently cooled in the trap, an ejection pulse of 50 V to 150 V in amplitude, at least 7  $\mu$ s wide, and having a repetition rate equal to or under 20 Hz sends the ions from the trap to the mass spectrometer with over 90% efficiency as long as the gas pressure is not reduced below  $2x10^{-4}$  torr.

The optimized gas filled RFQ mass filter system is presently in use as part of the experimental set-up for on-line mass measurement studies at Argonne National Laboratory. It has demonstrated its ability to efficiently transport reaction products from the gas cell to the mass spectrometer. In August and September of 2000, a mass measurement of <sup>120</sup>Cs created in the fusion reaction of a <sup>60</sup>Ni beam on a natural Cu target was executed. This was the first measurement of a radioactive isotope with the CPT mass spectrometer, and measurements of other isotopes are currently under way.

#### **References**

- Bec89 St. Becker, G. Bollen, F. Kern, H. –J. Kluge, R. B. Moore, G. Savard, L. Schweikhard, H. Stolzenberg, and the ISOLDE Collaboration, CERN EP89-126 (1989).
- Cap96 R. M. Caprioli, A. Malorni, G. Sindona(editors), Selected Topics in Mass Spectrometry in the Biomolecular Sciences, Kluwer Academic Publishers, Dordrecht, (1996).
- Dah95 D. A. Dahl, SIMION 3D Version 6.0 User's Manual, Idaho National Engineering Laboratory, Idaho Falls, (1995).
- Daw76 P. H. Dawson(editor), Quadrupole Mass Spectrometry and Its Applications, Elsevier, Amsterdam (1976).
- Den71 D. R. Denison, "Operating parameters of a quadrupole in a grounded cylindrical housing", J. Vac. Sci. Technol., 8 (1971) 266.
- Fuk00 H. Fukutani, First Measurements of Atomic Masses with the Canadian Penning Trap (CPT) Mass Spectrometer, Master Thesis, University of Manitoba, (2000).
- Gul86 S. L. Gulick, Ion Injection into Radio Frequency Quadrupole Field Devices, Master Thesis, McGill University (1986).
- Her00 F. Herfurth, J. Dilling, A. Kellerbauer, G. Bollen, S. Henry, H.-J. Kluge, E. Lamour, D. Lunney, R. B. Moore, C. Scheidenderger, S. Schwarz, G. Sikler, J. Szerypo, "A linear radiofrequency ion trap for accumulation, bunching, and emittance improvement of radioactive ion beams", Elsevier preprint, (2000).

- liv91 A. Iovonen, K. Morita, K. Riikonen, R. Saintola, K. Valli, "Focusing ions by viscous drag and weak electric fields in a ion guide", Nucl. Inst. And Meth., A307 (1991) 69.
- Kim97 T. Kim, Buffer Gas Cooling of Ions in a Radio Frequency Quadrupole Ion Guide, Ph.D. Thesis, McGill University (1997).
- Klu92 H. –J. Kluge, G. Bollen, "Ion traps recent applications and developments", Nucl. Inst. and Meth., B70 (1992) 473.
- Klu93 H. –J. Kluge, G. Bollen, In Proceedings of the Workshop on Traps for Antimatter and Radioactive Nuclei, TRIUMF, Vancouver, BC, February 25-27, (1993).
- Leo94 W. R. Leo, Techniques for Nuclear and Particle Physics Experiments, Springer-Verlag, Berlin (1994).
- Lun99 M. D. Lunney, R. B. Moore, "Cooling of mass-separated beams using a radiofrequency quadrupole ion guide", Int. J. Mass Spectrom., 190/191 (1999) 153.
- Mar98 P. Martinez, Ion Accumulation in a Paul Trap for the Canadian Penning Trap Mass Spectrometer, Master Thesis, McGill University, (1998).
- Mas88 E. A. Mason and E. W. McDaniel, *Transport Properties of Ions in Gases*, Wiley, New York (1988).
- Mee53 J. M. Meek and J. D. Craggs, *Electrical Breakdown of Gases*, Clarendon Press, Oxford, (1953).
- Pau89 M. Paul, B. G. Glagola, W. Henning, J. G. Keller, W. Kutschera, Z. Liu, K. E.
   Rehm, B. Schneck, R. H. Siemssen, "Heavy Ion Separation with a Gas-Filled Magnetic Spectrograph", Nucl. Instr. and Meth., A277 (1989) 418.
- Pau58 W. Paul, H. P. Reinhard and U. von Zahn, Z. Phys., 152 (1958) 143.
- Sam71 D. G. Samaras, *Theory of Ion Flow Dynamics*, Dover Publications, Inc., New York, (1971).
- Sav97 G. Savard, "Ion trap technology at accelerator facilities", Nucl. Instr. and Meth., B 126 (1997) 361.
- Sca91 F.Scarlassara, B. G. Giagola, W. Kutschera, K. E. Rehm, A. H. Wuosmaa, "Nuclear charge separation of low-energy medium-mass ions with a gas-filled magnetic spectrograph", Nucl. Instr. And Meth., A309 (1991) 485.
- Von56 U. von Zahn, Kiplomarbeit, University of Bonn, (1956), quoted in Pau58.